LU-TP 21-11

The Angantyr Model For Simulating Heavy-Ion Collisions

Harsh Shah

Supervisor: Prof. Leif Lönnblad

LUND
UNIVERSITY

A thesis presented for the degree of Licentiate

Theoretical Particle Physics
Lund University
Sweden

Date: 2021 May

CONTENTS

1

INTRODUCTION

This thesis is about an extension of Pythia (PYTHIA8) [1] event generator, primarily used to simulate *pp* collision events, to simulate heavy-ion (HI) collision events. An important question, which has motivated this study is whether a HI collision is an accumulation of many nucleon-nucleon collisions or there is indeed a transition from a hadronic[1] state to a new state of matter; a hot plasma of free *partons*[2], a Quark Gluon Plasma (QGP). The hot plasma of free partons is thought to exist in the early universe after (few microseconds of) the Big Bang [2]. Therefore, if such a new state of matter can be created in the HI collision experiments then it is important to verify and validate its existence. For this purpose, we have to verify the observations which are used to support the existence of the hot plasma, because those observations should not be explained by theoretical models which do not consider the creation of the hot plasma. In this thesis, we tested the limits of a phenomenological model to reproduce HI collision observables without assuming the creation of the hot plasma.

A heavy ion (heavy nucleus) can be imagined as a bag containing protons and neutrons, and a collision of two such bags leads to simultaneous collisions of many sub-nucleonic particles[3]. These sub-collisions involve a large amount of kinetic energy, and as a result the total number of produced particles in a HI collision is an order of magnitude higher than in a *pp* collision.

1 Baryons (e.g. protons and neutrons) and mesons (e.g. pions) are collectively called hadrons. Baryons have three quarks (or three anti-quarks) and mesons have a quark and an anti-quark in their sub-structure.

2 Quarks and gluons are collectively called partons.

3 Protons and neutrons consist of three valence quarks and depending on the collision energy-momentum exchange an incoming particle may also interact with a sea (anti-)quark or a gluon from the target nucleon.

HI collision experiments at Relativistic Heavy Ion Collider (RHIC) and Large Hadron Collider (LHC) have observed a number of phenomena with names like *strangeness enhancement*, *near side ridge*, *jet quenching*, and *quarkonia suppression*. These observations have been accepted as the signatures of the new state of matter, which was thought to be created only in HI collisions.

Recently, the LHC experiments with *pp* collisions at $\sqrt{s} = 7$ TeV and 13 TeV show that the high multiplicity *pp* events have *near side ridge* [3] and *strangeness enhancement* [4]. These new results from the LHC do not only blur the boundary between HI collisions and *pp* collisions physics, but also raise doubts about phenomenological understanding of the observations made in the HI collision experiments.

Observations of enhancement or suppression in the multiplicity of specific types of particles and long range collectivity among produced hadrons are difficult to explain by perturbative Quantum Chromo Dynamics[4] (pQCD) first principles, and we require phenomenological models to investigate such observations. Since phenomenological models are developed based on theoretical understanding and the free parameters of the theories are tuned to the experimental data, they act as the bridge connecting theory predictions and experimental observations. These models provide finite values for various calculations using random number generators (for computational purposes) and are known as event generators or Monte-Carlo (MC) models. In this thesis we used the Pythia event generator.

The observations made in HI collision experiments are widely explained using MC models developed with an assumption that a hot plasma of free partons is created in the HI collision. On the other hand, Pythia is a MC model which simulates collision events of smaller systems like *pp*, with an assumption of colour strings interacting at zero temperature in vacuum.

The LHC results of *strangeness enhancement* and *near side ridge* in *pp* collisions are reproduced neither by Pythia-like event generators nor by hydrodynamics based event generators. It is important to note that the final state hadrons emerge from the colour string fragmentation mechanism (which is based on the Lund String Model[5]) in Pythia. Moreover, the entire collision simulation in Pythia is performed without any prior assumption of the creation of a thermalised medium

4 QCD is a quantum field theory, and it is used to describe interactions through colour charge exchange between partons.

(the QGP). On the other hand, the idea of a medium creation and its thermalisation is the basis of conventional HI event generators. These LHC results of *pp* collisions are similar to some of the HI observations, and if they are produced due to the same underlying physics, then these results should be consistent with either of the phenomenological approach. Hence, questions like "*How do we explain such unexpected observations in pp collisions?*", "*Is there a boundary distinguishing HI collisions from pp collisions?*", and "*Can all relativistic hadronic collisions be explained using the same phenomenological approach?*" are necessary to be addressed for better understanding of the results from the collider experiments.

The hydrodynamics-based HI event generators require a certain amount of the number density of produced partons to be achieved by the colliding systems. Hence, hydrodynamics-based models can not reproduce observables for collisions with low number density of produced partons (which are majority of *pp* and *ee* collisions). On the other hand, we can modify the colour strings interaction mechanism in a microscopic event generator. As an example, in the Pythia event generator, the string-string interactions can be modified in the high string density environment, which can explain the new observations in high multiplicity *pp* collisions [6, 7].

If a HI collision is indeed a sophisticated superposition of multiple *pp* like collisions, then the reproduction of HI observables is possible using the string interaction modifications with the Angantyr model, and we can have *one model to rule them all*.

2

HEAVY-ION PHYSICS

Lattice[1] QCD calculations show that at the extreme temperature, the QCD system in equilibrium has the number of the degrees of freedom close to a system of free partons. It means, there is a phase transition[2] from confined hadronic matter to a deconfined system of free partons. Moreover, Lattice QCD calculations also show that at around 300 MeV temperature, the QCD matter can have an energy density close to 12 GeV/fm^3.

If a new state of the QCD matter is created in a HI collision, then the system must have a temperature of a few trillion Kelvin[3] ($\geq$ 175 MeV). A rough estimate based on *PbPb* head-on collisions at $\sqrt{s_{NN}}$ = 2.76 TeV shows that the average energy density due to the total transverse energy deposited in the pseudo-rapidity[4] interval $\eta \in$ [-0.5, 0.5] between two colliding nuclei at time 1fm/c after the collision is approximately[5] 11 GeV/fm^3. The above estimate of energy density is closer to the Lattice QCD prediction for the matter density and the extreme tem-

1 A non-perturbative QCD treatment is performed on a lattice of discrete lattice points in a finite space-time volume.

2 The QCD phase transition is analogous to the phase transition of water to vapour at 373 Kelvin and one atmospheric pressure. But while water-to-vapour is a first-order phase transition, the QCD phase transition is a continuous cross-over at zero baryon potential.

3 In the natural units, $1\frac{eV}{k_B} \approx 1.16 \times 10^4$K, where k_B is the Boltzmann constant

4 The pseudo-rapidity (η) is used to define the angular position of the referred particle with respect to the beam axis. It is represented as $\eta = \frac{1}{2}\ln\left(\frac{|\mathbf{p}|+\mathbf{p_z}}{|\mathbf{p}|-\mathbf{p_z}}\right)$, where $\mathbf{p}$ is three momentum and p_z is momentum of the particle in the direction of the beam axis.

5 If particle masses are neglected compared to their energy then $y \approx \eta$, and from the relation $y = tanh^{-1}\beta_L$, where β_L is the longitudinal velocity. $\beta_L \in$ [-0.46, 0.46] for the given η interval. For the approximate total transverse energy of 1.65 TeV[8], the radius of the Pb nucleus, which is $7fm$, and the separation between two Pb nuclei at 1fm/c time after a collision is 0.92 fm. If we assume approximately a cylindrical system then the energy density with complete overlap between two Pb nuclei is 1.65 TeV/$(\pi * (7\text{fm})^2 * 0.92\text{fm}) \approx 11$ GeV/fm^3.

perature at the QCD phase transition. Hence, it is not completely unreasonable to expect that a QGP may be formed in HI collisions.

The QGP formation can be possible either during the early stage of the universe (when the temperature was extreme) or in the core of the neutron stars (where the temperature is low, but the matter density is approximately 3-5 times larger than the nuclear density). Unfortunately, neither of these possibilities can be tested experimentally to verify the theoretical predictions about the QCD phase transition and creation of the QGP.

HI collisions can in the laboratory (the particle colliders) create an environment similar to the few microseconds old universe. Therefore, the HI physics research is motivated to collide heavy-ions at relativistic energies to explore the possibility of the QCD phase transition and the QGP creation. As an example, the QCD phase diagram with temperature vs baryon chemical potential is explored in Au-Au collisions by varying collision energies ($\sqrt{s_{NN}}$ = 7 - 200 GeV) in experiments at the Relativistic Heavy-Ion Collider (RHIC).

The fluctuations in the amount of energy deposited are due to the event-by-event fluctuations of the geometric overlap between two colliding heavy ions, which is the prominent characteristic of HI collisions. The fluctuations in the energy deposition are the direct consequence of the fluctuations in the number of nucleon-nucleon collisions in HI collisions. The majority of nucleon-nucleon collisions do not exchange a large amount of transverse momentum (p_T), only a small fraction of hard nucleon-nucleon collisions produce particles with large p_T in HI collisions. These high p_T particles undergo interactions with particles produced in other nucleon-nucleon collisions and lose their energy to the medium. The energy loss results in suppressed signals for the energy deposition in the detectors (more details are in the section "jet quenching"), which is very unlikely to happen in collisions of smaller systems e.g. *ee*, *pp* etc.

The hadronisation of produced partons, and the properties of the partons, which travelled through the QGP medium, are other concepts which are yet to explore properly in the HI collisions. HI collisions modify the flavour (types of quarks) production rate compared to *pp* collisions. The hadronisation in collisions like $e^+e^- \longrightarrow q\bar{q}$ is well understood. The produced quarks form jets[6], which are well described and reproduced by the *Lund String Model* [5] implemented in the

6 A jet is a collimated spray of hadrons.

Pythia event generator. In HI collisions, the observed relative production rate of the identified hadrons requires a better understanding of the hadronisation mechanism.

One of the differences between HI collisions and *pp* collisions is that the QGP is expected to exist only in the HI collisions. But the new LHC results (mentioned in the previous chapter) from *pp* collisions indicate that there may be new hadronisation mechanisms when large amount of kinetic energy is involved in the collisions irrespective of the colliding system sizes. An improved hadron production mechanism, the rope hadronisation model [6, 7] in Pythia, was developed as a first attempt to address a shortcoming of Pythia's default hadronisation mechanism. Following this attempt, we also require to scrutinise the interpretations of the hadron production mechanism in the HI collisions.

2.1 WHAT DOES A HEAVY-ION COLLISION LOOK LIKE?

A relativistic accelerated nucleus looks like a longitudinally Lorentz contracted flat disc[7], and two such Lorentz contracted nuclei collide in a HI collision (Figure 1). The overlap of the colliding discs is defined by the impact parameter (**b**), the distance between the centres of the two nuclei at the time of the collision. The complete overlap ($\mathbf{b} = 0$) represents a head-on collision, and the smaller the overlap between the nuclei, the larger the impact parameter (**b**). Even at the fixed **b**, the radii of the nucleons and the positions of the nucleons inside the nuclei vary event-by-event, which contributes to fluctuations in the interaction probability.

In experiments, **b** can not be controlled and measured directly, and it has to be estimated using some observables, which are assumed to correlate with the collision geometry. The event multiplicity (number density) is an observable which strongly correlates with **b**. Therefore, by measuring the multiplicity of produced hadrons in the central (or forward) region, we can indirectly estimate **b**. HI collision events are studied based on this estimate, and the events are separated into percentile bins of the total charged multiplicity, which is called the event *centrality*. The least percentile values ($\sim 0 - 5\%$) represent central (or higher multiplicity) collisions, while the gradual increase in the percentile refers to more peripheral

7 The thickness of the disc depends on the relativistic γ factor as $2\mathbf{r}/\gamma$; $\gamma = \frac{1}{\sqrt{1-v_z^2/c^2}}$, where **r** is the nucleus's radius, v_z is the velocity along the beam axis and c is velocity of light in vacuum.

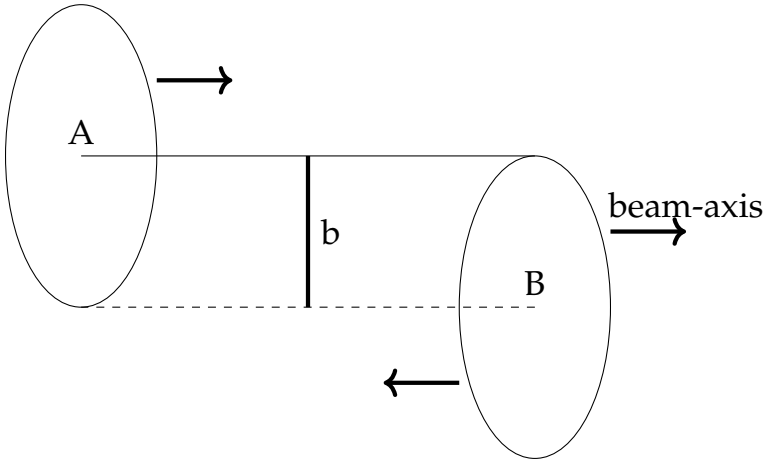

Figure 1.: A schematic representation of a HI collision at an impact parameter (**b**) between two Lorentz contracted nuclei marked as **A** and **B**; and their relative directions of motion are shown with arrows.

(or lower multiplicity) collisions. The centrality based analysis is used to compare central HI collisions with peripheral HI collisions, and to compare results from HI collisions with proton-proton collisions.

Nucleons within the overlapped area often participate in the collision, and those interacting nucleons are called *participants*. Nucleons outside of the overlapped area usually do not collide, and they continue to travel in the respective beam's direction after the collision, and they are called *spectators*. One can not directly measure the number of participants (N_{part}) and number of nucleon-nucleon binary collisions (N_{coll}) in a HI collision. Therefore, one has to estimate N_{part} and N_{coll} using phenomenological models, and the Glauber model [9, 10] is widely used for this purpose. A correlation between the Glauber calculated N_{part}, and the observed event multiplicity is assumed. For example, the highest ($\sim 0-5\%$) centrality bin of the event multiplicity distribution is assumed to correspond to a certain interval of **b**, and based on that impact parameter interval the corresponding average N_{part} or N_{coll} are generated using the Glauber model.

Nucleons are assumed to travel in a straight line without deflection at relativistic velocity, so the participants can interact with multiple nucleons inside the target while penetrating through the incoming nucleus. Experimental analysis shows that the rate of hard interactions is proportional to N_{coll}, while the charged particles multiplicity scales better with N_{part} [11]. This correlation implies the need for sophisticated handling of N_{part}.

Once N_{part} is obtained the evolution of the HI collision event is conventionally described by hydrodynamics based models. The N_{part} is also important for these models because it is used to calculate the kinetic energy, the energy density for the given centrality and the system property like entropy density (s) to model the post collision scenario. The free parameters like temperature and ratio of the viscosity and the entropy density (η/s) are then tuned to the experimental data of HI collisions.

2.2 HYDRO-DYNAMICAL APPROACH

Conventionally, the QGP production and expansion is described by the macroscopic theory of microscopic interactions. Properties of a macroscopic system depend on the initial condition, interactions of constituent particles, conservation laws and external constraints[8]. A hydrodynamic model of the QGP evolution in space-time can be constructed based on estimates of the equilibrium properties of the QGP, using models inspired by the kinetic theory of gases, distribution functions and transport theory. The details of the relativistic hydrodynamic model building are out of scope in this thesis. But I will discuss here a simplified picture of various stages of the HI collisions starting from the instant of collision till the free propagation of final state particles from the hydrodynamic point of view. The HI events have four stages in the hydro-dynamical picture: a) Pre-equilibrium stage, b) Expansion of the QGP, c) Freeze-out stage, and d) Final state hadron scattering.

Pre-equilibrium stage is just after a HI collision when the QGP is just formed and it is in a non-equilibrium state. The partons are correlated strongly, and they are continuously interacting with each other, while the system is expanding and achieving equilibrium. The time taken to achieve local equilibrium is called the thermalisation time of the medium, which is assumed to be within the time scale of 1 fm/c in the medium rest frame.

The momenta of partons generate a pressure gradient during the **expansion stage**. Hence, depending upon the magnitude of the pressure gradient, different regions of the QGP medium expand at different rate. The medium expansion reduces the system density and the system cools down, and as the energy density of the

8 Density, temperature, entropy etc. are characteristics of such macroscopic systems.

system reduces below a critical density, $\rho_{crt} \approx 1GeV/\text{fm}^3$ [12], partons start to hadronise. A mixed state of hardons and the free partons coexist during the initial stage of the hadronisation, but the mixed phase vanishes during the transition from QGP to hadron gas and the system is left with hadrons only.

The **hadron scattering** and the **freeze-out stage** are connected to each other. The freeze-out stage is sub divided into *chemical freeze-out* and *kinetic freeze-out*[9]. The produced hadrons initially undergo inelastic scatterings and keep the expanding system in equilibrium. The chemical freeze-out point have been reached when the probability of inelastic collisions reduce to almost zero. Prior to the chemical freeze-out, hadrons are producing new hadrons through inelastic scatterings, but after the chemical freeze-out only elastic scatterings occur and the types of hadrons remain constant. As the system expands further, inter-hadronic distances grow larger than the strong interaction range, and the probability of elastic collisions gradually reduces. At this stage, it is not possible to maintain the thermal equilibrium, and the system reaches the kinetic freeze-out phase. The hydrodynamic picture can not survive anymore. Hadrons travel freely in the vacuum after the kinetic freeze-out, until they decay into more stable particles or hit the detectors.

Hydrodynamic models describe observables of the HI collisions by separating events into the above mentioned four stages. The initial conditions like the start time (a relaxation time required to pass after the collision), temperature, initial number density, and the cut-off conditions like freeze-out temperatures, are crucial to obtain relevant results for hydro-phenomenology [14].

2.3 NON-THERMAL MODELS

Unlike hydrodynamic models, there are microscopic models which do not consider temperature or thermalised medium creation in the particle collisions. All conventional general purpose event generators for *pp*-like collision systems, such as Pythia, HERWIG [15], and SHERPA [16] etc., belong to this category. The Angantyr model is developed as an extrapolation of Pythia for HI collision sim-

9 Both of these freeze-outs are assumed to occur at certain fixed temperatures ($T_{chemical} > T_{kinetic}$) for all quark flavours. From the freeze-out stage Cooper-Frye prescription [13] is used to obtain invariant distribution of particles.

ulations without considering a QGP production. Therefore, the Angantyr model is also a non-thermal model for HI event simulation. In non-thermal models, the post-collision scenario is described based on partonic scattering and radiations in a vacuum. Moreover, unlike hydrodynamic models, where a collision event has four discrete stages, in non-thermal models, the event evolves continuously with various stages, but without any thermalised medium creation.

The final state observables in high multiplicity *pp* collisions show signatures of *strange- ness enhancement* and a *near side ridge* similar to the HI collisions. String fragmentation is the primary technique for hadron production in Pythia event generator. A model to explain these new observations by modifying the colour string interactions has been included in Pythia. Colour strings in the default Pythia do not interact among themselves except during the colour reconnection stage[10], but in the light of the new LHC results, an idea emerged that the accumulation of many colour strings due to high parton density can modify the effective string tension in high multiplicity events.

Strings usually stretched longitudinally, but they also have width, and there may be some overlap between two neighbouring strings in the dense environment of the high multiplicity events. This idea is now implemented in Pythia as *rope hadronisation* [6, 7] and *string shoving* [17, 18] mechanisms for *pp* events.

The string shoving mechanism gives ridge like effects in *pp* collision simulations. Here, the transverse push to the near-by colour strings in the outward direction is generated due to the colour field of neighbouring strings. So far it handles only low p_t strings in Pythia with an assumption that all strings are parallel to each other and to the beam axis as well. In recent paper [18], non-parallel strings are also included to perform the string shoving mechanism.

The rope hadronisation is a new model in Pythia. According to this model, the string density will modify the effective string tension (κ) in Pythia. This

10 Partons are connected with colour strings in Pythia and they undergo rearrangement of colour strings. The reconnection of colour strings is performed by the colour reconnection model in Pythia. This process reduces the total string length and re-connects near-by partons with each other by colour strings, and later these colour strings break to produce hadrons according to the string fragmentation mechanism.

modification affects the relative yield of strange quarks, because during the string fragmentation the relative strangeness production probability depends on κ as:

$$\rho \propto exp\left(\frac{-\pi(m_s^2 - m_u^2)}{\kappa}\right) \tag{1}$$

where ρ is the relative production probability of strange quarks of mass m_s over up quarks of mass m_u. The increment in the value of κ increases the strangeness production probability (ρ), and κ is modified due to the colour rope formation. This way, Pythia can reasonably reproduce strangeness enhancement as a consequence of higher string density in the high multiplicity pp events. The same ideas may be implemented in the Angantyr model for HI events to explain similar observations of HI collisions without assuming the QGP.

2.4 HI COLLISION OBSERVABLES

The observations of *jet-quenching* and *collective flow* at RHIC and LHC are the two most important observations from the HI collision experiments. Jet quenching is the consequence of multiple interactions between the coloured medium and the partons produced with high transverse momentum in HI collisions. The collective flow of hadrons was predicted in the ideal hydrodynamic models, and its observation at RHIC supported the claim of a QGP formation [19] in HI collisions.

HI collision observables are often compared with pp collision observables to study and investigate differences (or similarities) between these colliding systems. These comparisons are performed by analysing the nuclear modification factor R_{AA}. For example, a transverse momentum dependant $R_{AA}(p_T)$ is:

$$R_{AA}(p_T) = \frac{\frac{d^2N_{AA}}{d\eta dp_T}}{\langle N_{coll}\rangle \frac{d^2N_{pp}}{d\eta dp_T}} \tag{2}$$

Here the numerator is the differential particle yield in HI collisions and the denominator is the average number of nucleon-nucleon collisions ($\langle N_{coll}\rangle$) (obtained from a Glauber model) in HI collisions multiplied with the differential particle yield in pp collisions. This is a general representation of R_{AA} and it can be modified according to the study-specific observables. The suppression ($R_{AA} < 1$) or enhancement ($R_{AA} > 1$) will reflect nucleus induced effects or effects due to a QGP formation in HI collisions (because so far the QGP is believed to be created

only in HI collisions.). For example, R_{AA} below unity means hadron production in HI collisions is suppressed compared to pp collisions. R_{AA} is also studied for jets [20, 21] to understand medium effects on jets, jet quenching, at different centrality, and to explore the possibility of jet quenching in the high multiplicity *pp* collisions.

2.4.1 *Collective flow*

Strong azimuthal correlations are observed among particles widely separated in the rapidity[22, 23] in HI collisions. These correlations are stronger than one can expect from a mere superposition of many *pp* collisions, but the correlations are expected if some kind of plasma formed, which can have a collective outward flow of the matter due to its fluid-like properties. These correlations indicate that they may have originated in the early stage of the collision, and their study may provide indirect information about the earliest stage of the collision.

The arrangement of nucleons inside the overlapped region of the colliding nuclei defines anisotropy in their spatial distribution (Figure 2). The spatial anisotropy of participants results in an asymmetry in the collision geometry, and that is assumed as the origin of anisotropy in the momentum distribution of the produced particles.

The Fourier transformed multiplicity as a function of azimuthal angle (with respect to the reaction plane) gives an indirect insight into the initial state properties of the collision.

$$E\frac{d^3N}{d^3p} = \frac{d^2N}{p_T dp_T dy}\frac{1}{2\pi}\Big[1 + \sum_{n=1}^{\infty} 2v_n \cos n(\phi - \Psi_{RP}^n)\Big] \tag{3}$$

Here the quantities p_T, y, ϕ and Ψ_{RP}^n are transverse momentum, rapidity[11], the azimuth angle of the produced particles, and the reaction plane angle w.r.t. x-axis respectively. The reaction plane angle (Ψ_{RP}^n) (figure 2) for n^{th} harmonic is not an experimentally known quantity. It is derived through the estimated plane having maximum number of transversely distributed final state particles event-by-event.

11 The rapidity (y) is defined as $y = \frac{1}{2}ln\frac{E+p_z}{E-p_z}$, where E and p_z are the energy and the longitudinal momentum. The rapidity (y) can be exchanged with pseudo-rapidity (η) for mass-less or ultra-relativistic particles, which then gives azimuth angle (θ) for those particles because $\eta = -ln(tan\frac{\theta}{2})$.

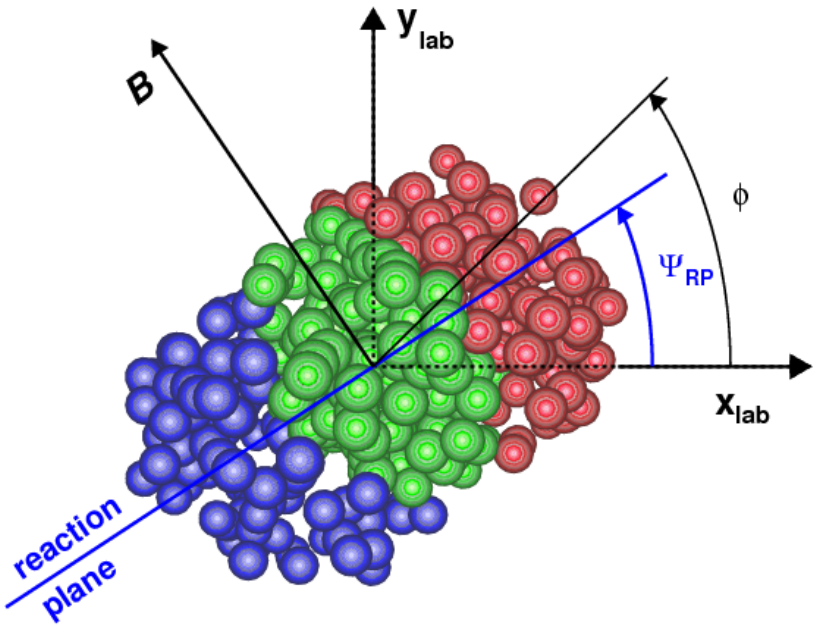

Figure 2.: A schematic representation of a HI collision, where the beam axis is perpendicular to the page. Blue and red spheres represent nucleons from two colliding nuclei. Green spheres represent nucleons participating in the collision. The blue solid line and Ψ_{RP} define reaction plane (formed by the beam axis and the impact parameter axis) and angle of the reaction plane with respect to the x-axis (lab-frame) respectively. The image is from [24].

This estimated reaction plane contains the impact parameter (which is obtained from a Glauber model) and the beam axis.

In the absence of fluctuations, the complete overlap ($\mathbf{b} = 0$) of colliding nuclei produce particles moving outward with isotropic momentum vectors, and all flow coefficients $v_n = 0$. The collisions do not always occur without fluctuations and the overlap of the colliding nuclei also vary event-by-event, and the flow coefficients v_n may be non-zero quantities. Non-vanishing v_n coefficients represent contributions from various modes of the generated anisotropy in the non-central HI collisions (usually an almond-shaped collision geometry; Figure 2). The first two coefficients of the cosine function are v_1 (directed flow) and v_2 (elliptic flow), and the second order coefficient v_2 is the most sensitive observable for the almond shaped collision geometry.

The differential v_n coefficients can be determined by the event plane method [25]. The v_n coefficients are obtained as a function of p_T and rapidity (y), and they are averaged over all events in the given p_T and rapidity bin:

$$v_n(p_T, y) = \langle e^{in(\phi - \Psi^n_{RP})} \rangle = \langle \cos n(\phi - \Psi^n_{RP}) \rangle = \frac{\int \frac{d^3N}{p_T dp_T dy d\phi} \cos n(\phi - \Psi^n_{RP}) d\phi}{\int \frac{d^3N}{p_T dp_T dy d\phi} d\phi} \tag{4}$$

Another method to obtain v_n coefficients is multi-particle correlation technique. The two-particle correlation is the simplest case of the multi-particle cumulants method [26, 27], where azimuthal correlations between particle pairs are obtained independent of the reaction plane angle (Ψ^n_{RP}). For example, the $v_n\{m\}$ coefficients of m-particle correlation can be defined from the cumulats $c_n\{m\}$. For $m = 2$, it is:

$$v_n\{2\} = \sqrt{c_n\{2\}} = \sqrt{\langle \{ e^{in(\phi_1 - \phi_2)} \} \rangle} = \sqrt{\langle \{ \cos n(\phi_1 - \phi_2) \} \rangle} = \langle v_n^2 \rangle + \delta_n \tag{5}$$

where $\{..\}$ represents average over all particles in an event and $\langle .. \rangle$ represents average over all events. Here ϕ_1 and ϕ_2 are the azimuthal angles of the paired particles, $c_n\{2\}$ refers to the two-particle cumulant, which provides $\langle v_n^2 \rangle + \delta_n$, where δ_n refers to the contribution from the *non-flow* components. The non-flow is correlation due to jets and resonance particles decay, and these correlations are assumed to be short-ranged. The non-flow contributions have to be minimised by various techniques or by excluding jetty events from the flow analysis. Hence, often a rapidity gap ($\Delta y > 1$) between paired particles is introduced when calculating the cumulant to reduce the non-flow contributions.

It is assumed that the non-flow contribution is smaller than the flow component, so the measured distribution of $v_n\{2\}$ with two-particle cumulants is primarily due to the flow ($\langle v_n^2 \rangle$) component only. The assumption of dominating flow component in two-particles correlation holds true only if $v_n\{2\} >> 1/\sqrt{N}$ [26], where N is the event multiplicity. Non-flow contribution scales with $1/N^{2m-1}$ for multi-particle cumulants $c_n\{2m\}$ [26], where $2m$ is the number of particles in the cumulant.

Higher order multi-particle cumulants (e.g. $c_n\{4\}$, $c_n\{6\}$ etc.) are calculated to reduce uncertainty and non-flow contribution, because the lower order multi-particle cumulants are subtracted from the higher order multi-particle cumulants. For example :

$$v_n\{4\}^4 = -c_n\{4\} = 2\langle v_n^2 \rangle^2 - \langle v_n^4 \rangle \tag{6}$$

$$v_n\{6\}^6 = \frac{1}{4} c_n\{6\} = \langle v_n^6 \rangle - 9\langle v_n^4 \rangle \langle v_n^2 \rangle + 12\langle v_n^2 \rangle^3 \tag{7}$$

Here, $\langle v_n^2 \rangle$, $\langle v_n^4 \rangle$, and $\langle v_n^6 \rangle$ represent two-particle, four-particle, and six-particle flow components. In the above two equations, it is evident that the lower ordered multi-particle components are subtracted while calculating the higher order multi-particle cumulants.

The initial state fluctuations play a major role in the anisotropic flow study, and therefore spacial and geometrical fluctuations are studied theoretically as the *eccentricity* analysis. A one-to-one correlation between eccentricity and flow coefficients is also observed in models. Some references for more detailed discussions of event-by-event fluctuations and anisotropic flow are obtained in [28, 29, 30].

2.4.2 *Jet quenching*

A di-jet event consists of observation of two high energetic collimated sprays of hadrons at approximately 180° angular separation (in azimuth) in the detector. The g + g $\longrightarrow$ g + g scattering is the most dominant partonic interaction in the high energy collisions, and they emerge as jets in the detectors. The time scale of partonic interactions is inversely proportional to the energy scale of the partons. Therefore, hard interactions with the exchange of large transverse energy occur during the earliest stage of the collision, even before a thermalised QGP formation.

In the HI events, jets often propagate through the so-called QGP medium and lose some energy due to the jet-medium interactions, which suppress the signal of an expected jet in the opposite direction of a leading jet. This phenomenon of suppressed or missing sub-leading jet is called *jet quenching*. It was first observed in HI collisions at RHIC and now also at LHC, but so far no jet quenching is observed in *pp* collisions.

The energy loss depends on the colour charge, the mass of the travelling parton, and the colour charged medium density. The hard gluons travel through the medium and loose energy to the medium either in the form of medium induced radiation or through the elastic scattering with medium partons. The former is the dominant mode of energy loss in the case of high p_T partons [31, 32]. The energy loss is proportional to the path travelled by the parton inside the medium, and the jet quenching analysis provides insight into the medium size and the QGP medium lifetime.

If jet quenching occurs due to the coloured medium interacting with the high energy partons, then there must not be any energy loss for the colourless particles travelling through the medium e.g. photons, $W^{\pm}$and Z^0. Figure 3 shows the nuclear modification factor as a function of p_T for colourless particles, which have their values close to one, and suppressed nuclear modification factors for coloured particles for *PbPb* collisions.

For charged hadrons R_{pA} is consistent with unity for $p_T > 2GeV$ (blue points in the left window of figure 3), hence suppression in R_{AA} can not be an initial state effect, but it must be a final state effect similar to the jet quenching. If the suppression in the R_{AA} would have been an initial state effect then the similar trend should be observed in R_{pA} for high p_T particles as well. The suppression in the charged hadrons yield can be related to the energy loss for jets passing through the coloured medium and losing their energy to the medium particles. Analogically, instead of losing energy, the high p_T charged hadrons may decay within the medium after multiple re-scatterings. Heavy mesons of weakly bound quark-antiquark pairs break their bonds, and the quarks and anti-quarks rebound with different flavoured anti-quarks or quarks from the medium partons. Such effects require a larger volume of the coloured medium, which is more likely to be created in the final state of AA type collisions than the final state of pA type collisions.

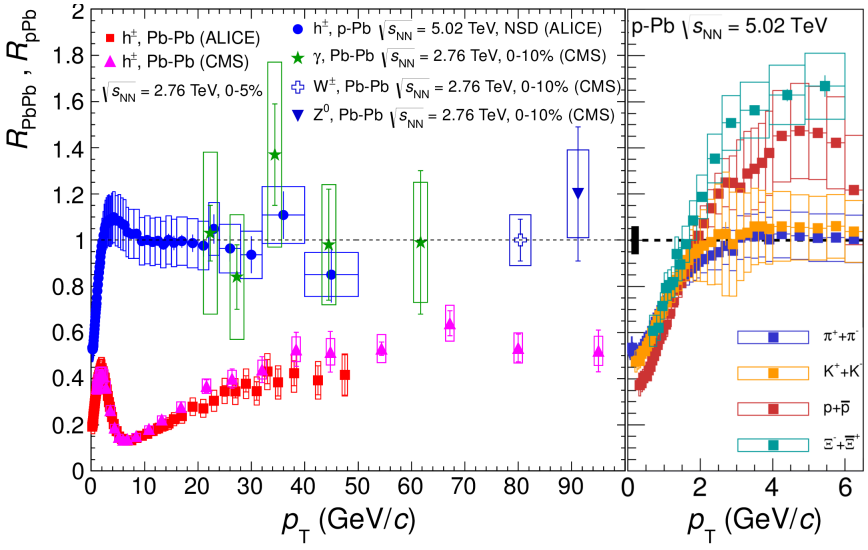

Figure 3.: p_T dependent R_{AA} distribution for gauge bosons and charged particles for pPb and PbPb collisions. Right side of the histogram shows R_{pPb} distribution of identified particles in the low-p_T range. The histogram is taken from ref. [33].

2.4.3 *Other observables*

Other interesting observations related to the flavour production are the strangeness enhancement and the quarkonium suppression.

Strangeness enhancement was proposed to be observed in relativistic HI collisions [34, 35] when compared to pp collisions. This was observed first in NA35, and later at RHIC, and LHC HI experiments. The supporting argument is that the QGP temperature is of the order of the strange quark mass (m_s), and because of that the s and $\bar{s}$ production should be enhanced even though the bare mass of the strange quarks is higher than the u and d quark masses; $m_s >> m_{u,d}$. The abundance of gluons produced in HI collisions are the primary source of strangeness through $s\bar{s}$ pair production. On the other hand, in Pythia, modification of colour string interactions in high multiplicity events is proposed as the underlying mechanism for the observed strangeness enhancement.

The Quarkonium sector is explored in HI collisions to study production and suppression of the heavy quark flavours. The quarkonia is a $q\bar{q}$ state where q represents either the charm or the bottom quark. The top quark is excluded here; due to very short lifetime of top quarks the $t\bar{t}$ mesons can not be formed. The suppression of the heavy bound state J/ψ ($c\bar{c}$) in HI collisions has been predicted

in theory [36] as a sign of QGP formation. The argument is that the screening of the quarkonium potential in the QGP will melt different quarkonium states at different temperatures. Predictions for quarkonium suppression therefore make it interesting to measure quarkonium production. J/ψ suppression in $PbPb$ collisions is observed in the NA50 experiment at the SPS [37], at RHIC [38], and at LHC [39].

Quarkonium production is a hard interaction event, and it is safe to argue that most of the quarkonium would have been produced in the collision before the QGP formation. The quarkonium study provides unique observables as perturbative probes to study the production of heavy-quark pairs in the medium, and as probes to understand the non-perturbative mechanism of heavy hadron bound state production. Quarkonium can be studied for all three types of hadronic collision systems i.e. pp, pA and AA collisions. pp collisions give an insight into quarkonium production in the vacuum, pA collisions can reveal effects of the cold nuclear matter, and AA collisions can provide insight (if there is any) of the medium effect on the quarkonium production.

3

EVENT GENERATORS

Event generators or Monte-Carlo models are simulation programs developed based on theoretical understanding of the experimental observations in particle physics. Particle physicists use them to analyse experimental data, to understand detector efficiencies, to distinguish signal and background events during the data analysis, and to verify theory predictions.

3.1 *pp* EVENT GENERATORS

Pythia, HERWIG [15] and SHERPA [16] are widely used event-generators for *pp* like small system collisions. All three models can reproduce a wide range of observables with a detailed picture of the collision. These event generators are called multi-purpose event-generators. They have their own set of modules to reproduce various stages of a *pp* event. Every module is developed to mimic specific physics mechanisms of the collision event, some of them are:

- Parton Distribution Functions (PDFs) of the beams
- Multi-parton interactions (MPIs)
- Initial and final state radiation
- The beam remnants
- Hadronisation and decay of unstable hadrons

A good reference about the finer details of different modules of these event-generators is [40] and references therein.

The work in this thesis is based on the Pythia event generator, which has been proven as an excellent phenomenological model to explain most of the *pp* physics

observations with good precision. The core idea in Pythia's phenomenology for event simulation is based on the colour string evolution and the string fragmentation to produce final state hadrons. The proton contains many partons and multiple partons can participate in the collision from each colliding proton. As a result, there are many produced partons and many colour strings in the space between the two beam remnants in Pythia's *pp* collision events due to the multiple parton interactions (MPIs).

The produced partons are colour connected by colour strings stretched between them and also between produced partons and the beam remnants; quarks are connected to one string and gluons are connected to two strings[1].

The colour flow and the number of strings are modified by Pythia's colour re-connection model in such a way that it conserves the total colour charge, but it reduces the total string length. As a result, the number of produced hadrons is reduced after the colour re-connection. The colour re-connection model allows Pythia to reproduce the observations of the charged multiplicity distribution and the average transverse momentum distribution as a function of the charged multiplicity ($\langle p_t \rangle$ (N_{ch})). The produced hadrons can interact with each other due to hadronic scattering [41], a new development, which is recently added to Pythia.

But when it comes to explaining new high multiplicity *pp* collision observations at LHC, Pythia can not reproduce enhanced strangeness production, near side ridge effects, and flow like behaviour with good accuracy. There is a new model [17, 18] in Pythia, which modifies the string tension in high multiplicity *pp* events and improves Pythia's description of these new results; I have provided a short overview of this new model in the non-thermal model's section of the previous chapter.

3.2 HI EVENT-GENERATORS

HIJING [42], AMPT [43], and EPOS [44] are widely used event generators for HI collisions. Unlike other hydrodynamics based simulations, these models simulate complete HI events. Here below is a short overview of these three event generators. It is for the sake of completeness and to provide an abstract idea of the

1 The colour strings represent colour flux tubes, (anti-)quarks carry an (anti-)colour charge, while a gluon carries both a colour and an anti-colour charge.

event simulation methods of these well known HI models before discussing the Angantyr model.

Glauber modelling

A realistic calculation to obtain N_{coll} and N_{part} requires information about the position of the nucleons inside the colliding nuclei. N_{coll} is the number of inelastic nucleon-nucleon sub-collisions, and N_{part} is the number of nucleons which have had at least one inelastic sub-collision. The Glauber model [9, 10] provides an arrangement of nucleons inside the nucleus according to the Woods-Saxon distribution of nucleon density:

$$\rho(r) = \frac{\rho_0}{1 + exp((r - R)/a)} \tag{8}$$

Here **r** is the distance of a nucleon from the centre of the nucleus in 3-dimension, R is the radius of the nucleus, and a is called thickness parameter.

The probability to find a given nucleon at some transverse position **s** inside the projectile nucleus is $T_{proj}(\mathbf{s}) = \int \rho_{proj}(\mathbf{s}, z)dz$. The interaction probability between the nucleons from the projectile and the target can be calculated from the nuclear overlap function T(**b**) for the given impact parameter (**b**) of the collision:

$$T(\mathbf{b}) = \int T_{proj}(\mathbf{s})T_{tar}(\mathbf{s} - \mathbf{b})d^2\mathbf{s} \tag{9}$$

where, the collision occurs at impact parameter **b**, "**s**" is the position of a projectile nucleon from the centre of the nucleus and "$\mathbf{s} - \mathbf{b}$" is the relative position of a target nucleon in the incoming nucleus. The overlap function is normalised as $\int d^2\mathbf{b}T(\mathbf{b}) = N_{proj}N_{tar}$ by integrating over all impact parameters, where N_{proj} and N_{tar} are number of nucleons in the projectile and the target nucleus respectively.

A Glauber model provides N_{coll} and N_{part} according to the geometric overlap between two colliding nuclei for the given impact parameter **b**, and the nucleon-nucleon inelastic interaction cross section σ_{inel}^{NN}. The overlap function describes the combined density of colliding nucleons in the projectile and the target nuclei, in a HI collision with impact parameter **b**. For the given σ_{inel}^{NN} the average number of nucleon-nucleon interactions is given by $T(\mathbf{b})\sigma_{inel}^{NN}$.

All HI event generators use a Glauber calculation to obtain N_{coll} and N_{part}. The significant difference among the HI event generators occurs in the process of their

treatment of the underlying scatterings. In the Angantyr model, we included the fluctuations both in the positions of the nucleons in the nuclei and the fluctuations in the nucleon-nucleon cross section, as discussed further in section 3.2.4, and distinguishing the type of collisions while obtaining N_{coll} and N_{part}.

3.2.1 *HIJING*

The Heavy Ion Jet INteraction Generator (HIJING) [45, 46] model has two primary components: *mini-jets* and *soft interactions*. In HIJING parton interactions are classified into semi-hard or soft. A semi-hard process has at least one pair of jets with $p_T > p_0$. Partonic interactions with $p_T < p_0$ are treated non-perturbatively and characterised by soft parton cross section (σ_{soft}).

HIJING uses Pythia for the kinematics of jet pairs and associated initial and final state radiations, and for hadronisation of partons according to the Lund string fragmentation model. HIJING has impact parameter dependent parton structure function to study the effects of nuclear shadowing on the observables, where the shadowing effects due to gluons and quarks are not distinguished from each other. The jet quenching in HIJING is modelled for moderate and high p_T observables, and it is based on assumed energy loss per unite distance ($\frac{dE}{dx}$) of the particles travelling through the medium.

3.2.2 *AMPT*

The AMPT (A Multi-Phase Transport) model [43] is primarily used to study the flow (collectivity) in HI collisions at RHIC and now also at LHC. It has four components: 1) Initial states, 2) Parton cascade, 3) Hadronisation, and 4) Hadron cascade. It has two modes of event simulation: 1) Default mode and 2) String melting mode. The string melting mode is developed assuming a QGP formation.

The AMPT uses the initial particle distribution from HIJING. The model performs parton-parton scattering according to the Zang Parton Cascade (ZPC) [47] model. For hadronisation, in the default mode the AMPT uses Lund string model, and in the String Melting mode it uses the quark coalescence model. The AMPT string melting model assumes production of quarks and anti-quarks only, which

allows it to have consistent recombination into hadrons by the coalescence model. The coalescence allows every $\bar{q}$ and q to choose partners from surrounding quarks and anti-quarks based on their separation from each other, but a parameter r_{BM} controls the relative formation of baryons over mesons. The ART(A Relativistic Transport[2]) model [48] performs the final state inelastic and elastic scattering of the produced hadrons in both modes.

3.2.3 *EPOS*

EPOS is a semi-hydrodynamic event generator. Hydrodynamic interactions are restricted as a part of the *core* and hydro-independent interactions are part of the *corona*. The separation of the core and the corona is based on string density at some proper time τ_0; the core is the region with string density higher than a certain value ρ_0, and the corona is the region with lower string density [49]. The model treats scatterings according to a Gribov-Regge theory [50] of parton ladders stretched between two colliding nucleons. These parton ladders include initial evolution of partons from projectile and target nucleons. In the core the parton density is high and the model generates MPIs in this region, which leads to the higher number of parton ladders. The low density of partons suppresses MPIs in the corona region.

The hadronisation in the core is performed using a statistical model. The corona is the region at large rapidity or low density, and here hadronisation is done similar to Pythia's string fragmentation mechanism. The primary difference between the string fragmentation mechanisms in Pythia and EPOS is in their treatment of the beam remnants. In Pythia, the two beam remnants are connected through the strings extended by the produced partons, but EPOS treats beam remnants individually and independently from the produced partons.

Unlike HIJING and AMPT, EPOS can also generate *pp* events in addition to the HI events. The core appears only if the local density of strings is higher than ρ_0. Hence, for the high multiplicity *pp* collision events, at mid-rapidity particles are produced through the core, otherwise, they all are produced according to the normal string fragmentation.

2 The extended ART generates secondary interactions of all produced hadrons except D, D_s, J/ψ, B and Y hadrons.

3.2.4 *Angantyr*

We wanted to test the limits of an extrapolation based on *pp* collision dynamics to describe the observed HI data without considering any thermalised QGP medium during the event simulation. The Angantyr model is a generalisation of the previous work [51] done for pA to AA interactions, without assuming a QGP formation. This new model has improved mechanism for sub-collisions (nucleon-nucleon collisions) in pA and AA events.

The multiplicity distribution in *pPb* collisions shows that the projectile proton participates in multiple sub-collisions with nucleons from the target Pb nucleus. Moreover, the asymmetric multiplicity distribution as a function of pseudo-rapidity in pA collisions discards the possibility of a mere superposition of many independent *pp*-like collisions to generate a HI event. Hence, if one wants to stack multiple *pp* events to generate a HI event, it will require a sophisticated superposition of several *pp*-like collisions.

The nucleons called "participants" above, and are calculated using the Glauber model, are also called "wounded nucleons". This terminology is e.g. used in the old FRITIOF model [52, 53], which assumed that the event multiplicity is approximately proportional to the number of such wounded nucleons.

Glauber's original calculation did not include effects of fluctuations in the scattering process. They have later been shown to be quite important. Fluctuations in the nucleon positions within a nucleus is accounted for by MC simulations. Gribov pointed out that it is important to account for diffractively excited nucleons as intermediate states in multiple NN sub-collisions [54]. In Angantyr we use the Good-Walker formalism [55] to describe diffraction as a result of fluctuations in the projectile and target wave functions.

The discrimination of the collision types when calculating the number of binary collisions is essential for a realistic simulation of HI events, because different types of collisions produce different multiplicity distribution in different pseudo-rapidity ranges. We modified the old FRITIOF model to distinguish wounded nucleons as diffractively or non-diffractively wounded. This modification improved the classification of the wounded nucleons in different collision types (inelastic collisions: non-diffractive, single or double diffractive collisions) in the Angantyr model.

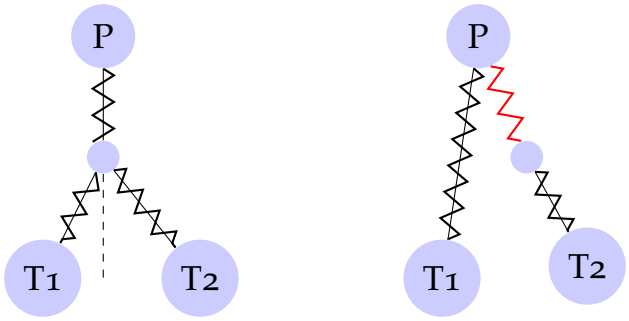

Figure 4.: (Left) A schematic diagram of a projectile particle colliding with two target particles represented with a triple cut-Pomeron vertex. The cut-Pomeron vertex represents non-diffractive interaction between the participants.
(Right) A schematic diagram of a projectile particle colliding with a target particle (T1) with a cut-Pomeron exchange (non-diffractive) interaction, and it is interacting with a target (T2) via a Pomeron exchange (single-diffractive) interaction.
(A cut-Pomeron is represented as a zigzag with a straight line, and an uncut-Pomeron is represented as a zigzag.)

After obtaining the number of wounded nucleons and types of sub-collisions, the interactions are ordered based on the impact parameter between colliding nucleons. The sub-collisions are generated using Pythia's machinery as described in sections 3 and 4 of the paper [56].

The event-by-event fluctuations are simulated by fluctuating nucleon radii, which in turn influences the nucleon opacity and the interaction cross-sections at a given impact parameter. Also at fixed impact parameter, the final state event multiplicity fluctuates in HI collisions, and in the event simulation, we have to reproduce these fluctuations.

Secondary non-diffractive events

During a HI event simulation with the Angantyr model, a crucial part is when the Glauber calculation predicts multiple non-diffractive (ND) interactions between a projectile nucleon and several target nucleons or vice-versa. This is also the part in Angantyr model, where I worked the most, so I am taking an opportunity to go in more details of the physics description in the text below.

A schematic diagram of a three-particle interaction (a collision between a projectile and a nucleus with two nucleons) is shown in figure 4 (Left), where a projectile (P) is interacting with two target nucleons (T1 and T2). The diagram shows a triple cut-Pomeron[3] vertex to represent ND interactions between the projectile and two target nucleons.

Pythia is fundamentally a $2 \rightarrow n$ type event-generator, which can have beams of electrons and/or protons only. We aim to use Pythia's machinery to extrapolate the *pp* collision dynamics for HI collisions. Hence, in the case of a three particle collision (figure 4), where the projectile is colliding with two target nucleons, we opt for simulating two collisions of two particles in such a way that the projectile is the participant in both collision events. The simulation of two ND events, in this case, is a non-trivial task because not only the vertex position of the triple cut-Pomeron can vary in rapidity, but also the momentum fraction shared between the two cut-Pomerons from the targets can vary.

A simple solution is to ignore the ND interaction between the projectile and the target nucleon, which has larger impact parameter and only simulate the ND interaction with smaller impact parameter. The effect of such a hard vetoing on allowed interactions will reduce N_{coll} and N_{part}, and the reduction will directly affect the final state particle production in HI events. Figure 21 of our paper [56] shows the contributions of diffractive and multiple ND interactions for *pPb* and *PbPb* events, and it reflects that a large number of multiple ND interactions occur in the simulation of both types of events. Therefore, the simple solution of ignoring ND interactions for larger impact parameter, if either of the participant nucleons is already identified as a participant in another ND interaction with smaller impact parameter, will reduce the final state particle production excessively.

We handle such situations by modifying the tags of collision types, and we re-tag the interaction with smaller impact parameter as the primary ND collision. Once the primary ND collision is fixed, the other ND collision is re-tagged as the secondary ND collision. In a situation like figure 4, the impact parameter between

3 A cut-Pomeron diagram represents a non-diffractive interaction between interacting particles, while a single uncut Pomeron exchange is argued for the observed rapidity gaps in a diffractive scattering in *pp* collisions. The Pomeron is proposed in the Regge theory (which is a predecessor of the QCD.) to explain hadronic cross-section at high energy. The Pomeron is treated as a mediator particle with quantum numbers of the vacuum. It has neither an electric charge nor a colour charge. A good reference for more details about the Pomerons in the Regge theory is [57].

the projectile (P) and the target nucleon (T1) is smaller than the impact parameter between the projectile (P) and the target nucleon (T2). Therefore, the interaction between the projectile (P) and the target (T1) is the primary ND (figure 4 (Right)), and it is generated using Pythia's default ND mechanism.

Now, we have to handle the interaction between the projectile (P) and the target (T2), which is the secondary ND. The secondary ND sub-event is simulated with a new modified mechanism, which is detailed in section 5 of the paper [56]. In a nutshell, a modification is performed in such a way that the rapidity span filled with the produced particles in the modified high-mass single-diffractive (SD[4]) collision should look similar to an ND collision in the same rapidity range.

At this stage, it is important to note that this is a non-trivial attempt to include secondary ND collisions in the HI event simulations driven by technical limitations, and we are not advertising that this is the only way to handle the multiple ND collisions involving the same participants. We want to come up with a mechanism, which uses Pythia's event generation set-up and allow us to simulate secondary ND events. The secondary ND collision can be mimicked if we use the high-mass SD mechanism in Pythia because a ND like interaction is simulated between the Pomeron and the proton, where the proton, which emits the Pomeron, remains intact but loses momentum.

Pythia's high-mass SD events are simulated with a Pomeron emission from the projectile and the interaction will occur between the Pomeron and the incoming target or vice-versa. The rapidity gap (Δy) in the diffractive event depends on the diffractive mass (M_{diff}) for the given centre of mass energy ($\sqrt{s}$) as $\Delta y = ln(s/M^2_{diff})$. The particles are produced in the rapidity range between the Pomeron-proton interaction vertex and the remnants of the target proton. In this region the high-mass SD event on average looks similar to the ND event (Figure 5 in the paper [56]).

4 The diffractive scatterings in Pythia are simulated according to non- perturbative soft Pomeron exchange. The diffraction in Pythia is separated into soft and hard diffraction. The soft diffraction is further sub-divided into low-mass and high-mass diffraction based on the diffractive mass (M_{diff}) of the event. The diffractive event is classified as low-mass diffraction if $M_{diff} \leq 10GeV$, otherwise it is classified as high-mass diffraction in Pythia. The high-mass diffractive events are simulated using MPIs and Pomeron PDFs, which are similar to those in the non-diffractive event simulation in Pythia.

Now, in the situation of figure 4 the projectile is interacting with both the targets. The projectile proton is replaced with a Pomeron for the secondary ND collision. We modified the Pomeron PDF so that it looks like a re-scaled proton PDF, and the secondary ND proton-proton collision is simulated as a modified Pomeron-proton collision, while regular diffractive events are generated according to the default Pomeron-proton collision set-up in Pythia.

After generating the primary ND event, the energy-momentum of the beam remnants are tracked. The energy-momentum conservation is checked while generating the secondary ND using the new mechanism, and if the event does not conserve the energy-momentum then it is vetoed. The diffractive mass (M_{diff}) of a diffractive event depends on the momentum of the emitted Pomeron, and we can produce the Pomeron at different energy in the event simulation. We tested the influence of the energy-momentum conservation by allowing few retrials of generating previously vetoed secondary events by reproducing them. If the Pomeron has lower energy than the previously vetoed event, then it is likely to be accepted. The result of our test is shown in figure 25 of the paper [56], but in the default set-up, only one attempt to generate a secondary ND event for the given nucleon is allowed.

After generating all sub-collisions, the final state partons are stacked together by shifting the collision points of the participating nucleons with respect to the impact parameter of the nucleus collision. The production vertices of partons are shifted according to the relative shift in the positions of the collision points of the participating nucleons inside the nucleus at the time of the collision. The colour strings produced in the nucleon-nucleon collisions undergo colour re-connection (CR) within the same sub-collision event, and there is no colour flow between two sub-collisions. Later, these strings hadronise by string fragmentation, every string breaks independently, and the produced hadrons are assumed to travel freely without any further interactions, and later unstable hadrons decay into stable particles. Hence, in the current version, final state hadrons do not show long-range collectivity, and they also do not interact among themselves.

The Angantyr model at its current stage can reproduce final states multiplicity and momentum distribution quantitatively in different centrality bins for HI events. The model can be used to study effects of the initial state fluctuations and non-flow contributions in HI collisions. We have compared Angantyr gener-

ated multiplicity distributions with other HI event-generators and we are able to reproduce competitive results.

3.3 OUTLOOK

We have developed a model based on pp collision dynamics, and it generates events which reproduce features of HI events. As shown in the results section of our paper, the model reproduces pp, pA, and AA multiplicity distributions as functions of pseudo-rapidity in different centrality bins. The momentum distribution is also reproduced without any additional re-tuning to HI data.

Along with the Angantyr model, a model is developed, which treats collective effects in pp collisions caused by string interactions through the rope hadronisation and the string shoving mechanisms. These effects are not yet included in Angantyr, and we can not reproduce flow observables in HI events with the Angantyr model at this stage.

The CR model can not generate long-range collectivity among produced hadrons due to its short-range. The CR is so far applied only among colour strings evolved from the same sub-collision, and there are no interactions among near-by strings from different sub-collisions. We are keen to introduce collectivity among the final state hadrons in HI events by modifying the CR mechanism in Pythia in such a way that the CR shall depend on the spatial parameters, independent of the origin of the colour string in the collision. One approach is to study the effects of a CR model which accommodates partons from different sub-collisions while generating HI events using the Angantyr model. Since the CR process restructures the orientation of the colour flow, it may produce effects similar to collectivity in the HI collisions.

The Angantyr model with string shoving and rope hadronisation may explain the strangeness enhancement and the flow like effects as the result of increased effective string density and modification in the colour re-connection, without considering the creation of a thermalised medium in the event simulation. The phenomenological understanding of jet quenching and quarkonium suppression through the Angantyr model is another field yet to be explored.

At last, apart from providing an alternative phenomenological explanation to HI collision observations, the Angantyr model also opens a door with a new set of questions e.g. what are the signature observations to support or disfavour either of the phenomenological scenarios for the HI collision? Is a thermalised medium created at all in the HI collisions? Is there a similarity between the string picture and the hydrodynamic description of particle production and the transport mechanism?

MY CONTRIBUTION

I tested available single-diffractive interaction models of Pythia and modifications in the Pomeron PDFs to obtain an acceptable tune, to be used to simulate secondary non-diffractive interactions. Later, this is used in the Angantyr model to generate secondary non-diffractive collisions in pA and AA event simulations. I am responsible for generating histograms for the section 5 and the first draft of the section 5, which was later heavily edited by Leif.

BIBLIOGRAPHY

[1] T. Sjöstrand et al. "An Introduction to PYTHIA 8.2". In: *Comput. Phys. Commun.* 191 (2015), p. 159. DOI: 1410.3012.

[2] J. C. Collins and M. J. Perry. "Super dense matter: Neutrons or asymptotically free quarks?" In: *Physical Review Letters* 34 (1975), pp. 1353–2356.

[3] V. Khachatryan et al. (CMS collaboration). "Evidence for collectivity in pp collisions at the LHC," in: *Phys. Lett.B.* 765.193 (2017). arXiv: 1606.06198.

[4] J. Adam et al. (ALICE collaboration). "Enhanced production of multi-strange hadrons in high-multiplicity proton-proton collisions". In: *Nature Phys.* 13.535 (2017). arXiv: 1606.07424.

[5] B. Andersson et al. "Parton Fragmentation and String Dynamics". In: *Phys. Rept.* 97 (1983), pp. 31–145.

[6] Christian Bierlich et al. "Effects of Overlapping Strings in pp Collisions". In: *JHEP* 03 (2015), p. 148. DOI: 10.1007/JHEP03(2015)148. arXiv: 1412.6259 [hep-ph].

[7] Christian Bierlich. "Rope Hadronization and Strange Particle Production". In: *EPJ Web Conf.* 171 (2018), p. 14003. DOI: 10.1051/epjconf/201817114003. arXiv: 1710.04464 [nucl-th].

[8] A. Toia [ALICE collaboration]. In: *J. Phys.* G38.124007 (2011). arXiv: 1107.1973.

[9] R. Glauber. "Cross Sections in Deuterium at High Energies". In: *Physical Review* 100.1 (1955), pp. 242–248.

[10] Michael L. Miller et al. "Glauber Modeling in High Energy Nuclear Collisions". In: *Ann.Rev.Nucl.Part.Sci.* 57 (2007), pp. 205–243. DOI: 10.1146/annurev.nucl.57.090506.123020.

[11] B. Alver et al. "Phobos results on charged particle multiplicity and pseudorapidity distributions in Au+Au, Cu+Cu, d+Au, and p+p collisions at ultra-relativistic energies". In: *Phys. Rev.* C83 (2011), p. 024913. arXiv: 1011.1940.

[12] Tetsuo Hatsuda, Kohsuke Yagi, and Yasuo Miake. "Quark-Gluon Plasma: From Big Bang to Little Bang". In: Cambridge University Press, 2008. Chap. 3, p. 49.

[13] F. Cooper and G. Frye. In: *Phys. Rev.* D10 (1974), p. 186.

[14] Peter F. Kolband and Ulrich Heinz. "Hydrodynamic description of ultrarelativistic heavy-ion collisions". In: (2003). DOI: 0305084[nucl-th].

[15] J. Bellm et al. "Herwig 7.0/Herwig++ 3.0 release note". In: *Eur. Phys. J.* C76.196 (2016). DOI: 1512.01178.

[16] T. Gleisberg et al. "Event generation with SHERPA 1.1". In: *JHEP* 02.007 (2009). DOI: 0811.4622.

[17] Christian Bierlich, Gösta Gustafson, and Leif Lönnblad. *A shoving model for collectivity in hadronic collisions*. 2016. arXiv: 1612.05132 [hep-ph].

[18] Christian Bierlich et al. "Setting the string shoving picture in a new frame". In: (Oct. 2020). arXiv: 2010.07595 [hep-ph].

[19] M. Gyulassy and L. McLeran. In: *Nucl. Phys. A* 30.750 (2005).

[20] G. Aadet al.(ATLAS Collaboration). "Measurements of the Nuclear Modification Factor for Jets in PbPb $\sqrt{s_{NN}}$ =2.76TeV with the ATLAS Detector". In: *Phys. Rev. Lett.* 114.072302 (2015).

[21] David d'Enterria. "Jet quenching". In: *Landolt-Bornstein* 23 (2010), p. 471. DOI: 10.1007/978-3-642-01539-7_16. arXiv: 0902.2011 [nucl-ex].

[22] S. Chatrchyan et al. [CMS collaboration]. In: *Eur. Phys. J.* C72.2012 (2012). arXiv: 1201.3158.

[23] K. Aamodt et al. [ALICE collaboration]. In: *Phys. Lett.* B708.249 (2012). arXiv: 1109.2501.

[24] Fufang Wen et al. "Event-shape-engineering study of charge separation in heavy-ion collisions". In: *Chin. Phys.* C42.1 (2018), p. 014001. DOI: 10.1088/1674-1137/42/1/014001. arXiv: 1608.03205 [nucl-th].

[25] Arthur M. Poskanzer and S.A.Voloshin. "Methods for analyzing anisotropic flow in relativistic nuclear collisions". In: *Phys. Rev. C* 58 (1998), pp. 1671–1678.

[26] Nicolas Borghini, Phuong Mai Dinh, and Jean-Yves Ollitrault. "Flow analysis from multiparticle azimuthal correlations". In: *Phys. Rev. C* 64.054901 (2001).

[27] Ante Bilandzic, Raimond Snellings, and Sergei Voloshin. "Flow analysis with cumulants: Direct calculations". In: *Phys. Rev. C* 83.044913 (2011).

[28] U. Heinz and R. Snellings. In: *Ann. Rev. Nucl. Part. Sci.* 63.123 (2013).

[29] C. Gale, S. Jeon, and B. Schenke. In: *Int. J. Mod. Phys. A* 28.1340011 (2013).

[30] P. Huovinen. In: *Int. J. Mod. Phys. E* 22.1330029 (2013).

[31] R. Baier et al. "Angular dependence of the radiative gluon spectrum and the energy loss of hard jets in QCD media". In: *Phys. Rev.* C60.064902 (1999). DOI: 10.1103/PhysRevC.60.064902.

[32] C.A . Salgado and U.A . Wiedemann. "Medium modification of jet shapes and jet multiplicities". In: *Phys. Rev. Lett.* 93.042301 (2004). DOI: 10.1103/PhysRevLett.93.042301.

[33] Panagiota Foka and Maĺgorzata Anna Janik. "An overview of experimental results from ultra-relativistic heavy-ion collisions at the CERN LHC:Hard probes." In: *Rev. Phys.* 1 (2017), pp. 172–194.

[34] J. Rafelski and B. Müller. In: *Phys. Rev. Lett.* 48.1066 (1982).

[35] P. Koch, B. Müller, and J. Rafelski. In: *Phys. Rept.* 142.167 (1986).

[36] T. Matsui and H. Satz. "J/ψ Suppression by Quark-Gluon Plasma Formation". In: *Phys. Lett. B* 178 (1986), pp. 416–422. DOI: 10.1016/0370-2693(86)91404-8.

[37] B. Alessandroet al. NA50Collaboration. "A new measurement of J/ψ suppression in Pb-Pb collisions at 158-GeV per nucleon". In: *Eur. Phys. J.* C39 (2005), pp. 335–345. arXiv: hep-ex/0412036 [[nucl-ex]].

[38] A. Adareet al. PHENIXCollaboration. "J/ψ suppression at forward rapidity in Au+Aucollisions at $\sqrt{s_{NN}}$=200 GeV". In: *Phys. Rev.C84(2011) 054912,* 84.054912 (2011). arXiv: 1103.6269 [[nucl-ex]].

[39] B. Abelevet al ALICECollaboration. "J/ψ Suppression at Forward Rapidity in Pb-Pb Collisions at $\sqrt{s_{NN}}$=2.76 TeV". In: *Phys. Rev. Lett.* 109.1 (2012). arXiv: 1202.1383 [[hep-exp]].

[40] Andy Buckley et al. “General-purpose event generators for LHC physics”. In: *Phys. Rept.* 504 (2011), pp. 145–233.

[41] Torbjorn Sjostrand and Marius Utheim. *A Framework for Hadronic Rescattering in pp Collisions*. 2020. arXiv: hep-ph/2005.05658v1.

[42] X.-N. Wang and M. Gyulassy. “HIJING: A Monte Carlo model for multiple jet production in pp, pA and AA collisions”. In: *Phys. Rev. D* 44.3501 (1991).

[43] Z.-W. Lin et al. “A Multi-phase transport model for relativistic heavy ion collisions”. In: *Phys. Rev.* C72.064901 (2005). DOI: nucl-th/0411110.

[44] T. Pierog et al. “EPOS LHC: Test of collective hadronization with data measured at the CERN Large Hadron Collider”. In: *Phys. Rev.* C92.034906 (2015). DOI: 1306.0121.

[45] X. N. Wang. In: *Phys. Rep.* 280.287 (1997). DOI: 10.1016/S0370-1573(96)00022-1.

[46] Wei-Tian Deng, Xin-Nian Wang, and Rong Xu. “Hadron production in p+p, p+Pb, and Pb+Pb collisions with the hijing 2.0 model at energies available at the CERN Large Hadron Collider”. In: *Phys. Rev. C* 83.014915 (2011). DOI: 10.1103/PhysRevC.83.014915.

[47] Bin Zhang. “ZPC 1.0.1: A Parton cascade for ultrarelativistic heavy ion collisions”. In: *Comput. Phys. Commun.* 109 (1998), pp. 193–206. DOI: 10.1016/S0010-4655(98)00010-1. arXiv: nucl-th/9709009.

[48] B. -. Li and C. M. Ko. “Formation of superdense hadronic matter in high energy heavy-ion collisions”. In: *Physical Review C* 52.4 (1995), pp. 2037–2063.

[49] Klaus Werner. “Core-corona separation in ultra-relativistic heavy ion collisions”. In: *Phys. Rev. Lett.* 98 (2007), p. 152301. DOI: 10.1103/PhysRevLett.98.152301. arXiv: 0704.1270 [nucl-th].

[50] H.J. Drescher et al. “Parton based Gribov-Regge theory”. In: *Phys. Rept.* 350 (2001), pp. 93–289. DOI: 10.1016/S0370-1573(00)00122-8. arXiv: hep-ph/0007198.

[51] Christian Bierlich, Gösta Gustafson, and Leif Lönnblad. “Diffractive and non-diffractive wounded nucleons and final states in pA collisions”. In: *JHEP* 10 (2016), p. 139. DOI: 10.1007/JHEP10(2016)139. arXiv: 1607.04434 [hep-ph].

[52] Bo Andersson, G. Gustafson, and B. Nilsson-Almqvist. "A Model for Low p(t) Hadronic Reactions, with Generalizations to Hadron - Nucleus and Nucleus-Nucleus Collisions". In: *Nucl. Phys.* B281 (1987), pp. 289–309. DOI: 10.1016/0550-3213(87)90257-4.

[53] Hong Pi. "An Event generator for interactions between hadrons and nuclei: FRITIOF version 7.0". In: *Comput. Phys. Commun.* 71 (1992), pp. 173–192. DOI: 10.1016/0010-4655(92)90082-A.

[54] V.N. Gribov. "Glauber corrections and the interaction between high-energy hadrons and nuclei". In: *Sov. Phys. JETP* 29 (1969), pp. 483–487.

[55] M. L. Good and W. D. Walker. "Diffraction dissociation of beam particles". In: *Phys. Rev.* 120 (1960), pp. 1857–1860.

[56] Christian Bierlich et al. "The Angantyr model for Heavy-Ion Collisions in PYTHIA8". In: *JHEP* 10 (2018), p. 134. DOI: 10.1007/JHEP10(2018)134. arXiv: 1806.10820 [hep-ph].

[57] Eugene Levin. *An Introduction to pomerons*. 1998. arXiv: hep-ph/9808486 [hep-ph].

Part I

APPENDIX

A

THE ANGANTYR MODEL OF HEAVY IONS IN PYTHIA8

Published for SISSA by Springer

Received: *June 29, 2018*
Revised: *September 29, 2018*
Accepted: *October 8, 2018*
Published: *October 22, 2018*

The Angantyr model for heavy-ion collisions in Pythia8[1]

Christian Bierlich, Gösta Gustafson, Leif Lönnblad and Harsh Shah

Deptartment of Astronomy and Theoretical Physics,
Sölvegatan 14A, S-223 62 Lund, Sweden

E-mail: Christian.Bierlich@thep.lu.se, Gosta.Gustafson@thep.lu.se, Leif.Lonnblad@thep.lu.se, Harsh.Shah@thep.lu.se

Abstract: We present a new model for building up complete exclusive hadronic final states in high energy nucleus collisions. It is a direct extrapolation of high energy pp collisions (as described by Pythia), and thus bridges a large part of the existing gap between heavy ion and high energy physics phenomenology. The model is inspired by the old Fritiof model and the notion of wounded nucleons. Two essential features are the treatment of multi-parton interactions and diffractive excitation in each NN sub-collision. Diffractive excitation is related to fluctuations in the nucleon partonic sub-structure, and fluctuations in both projectile and target are here included for the first time. The model is able to give a good description of general final-state properties such as multiplicity and transverse momentum distributions, both in pA and AA collisions. The model can therefore serve as a baseline for understanding the non-collective background to observables sensitive to collective behaviour. As Pythia does not include a mechanism to reproduce the collective effects seen in pp collisions, such effects are also not reproduced by the present version of Angantyr. Effects of high string density, shown to be able to reproduce e.g. higher strangeness ratios and the ridge in pp, will be added in future studies.

Keywords: Heavy Ion Phenomenology, Phenomenological Models

ArXiv ePrint: 1806.10820

[1]Work supported in part by the Swedish Research Council, contracts number 2016-03291, 2016-05996 and 2017-0034, in part by the European Research Council (ERC) under the European Union's Horizon 2020 research and innovation programme, grant agreement No 668679, and in part by the MCnetITN3 H2020 Marie Curie Initial Training Network, contract 722104.

https://doi.org/10.1007/JHEP10(2018)134

Contents

JHEP10(2018)134

JHEP10(2018)134

1 Introduction

At hadron collider experiments at RHIC and LHC, protons as well as large nuclei, are collided, and the results are interpreted to obtain better knowledge about the dynamics of the fundamental interactions at high energies. The strong nuclear force plays a central role, but the studies of proton-proton (pp) collisions and heavy ion collisions respectively, are often carried out in quite different ways.

In the case of pp collisions, so-called "general purpose Monte Carlo event generators", such as Sherpa [1], Herwig 7 [2] and Pythia8 [3], have been established as cornerstones in aiding our understanding. These event generators have over the last three decades succeeded in simultaneously simulating the dynamics of strong and electroweak processes from very high momentum transfer scales where perturbation theory is applicable, down to scales around Λ_{QCD}, where one must rely on models inspired by analogies to electrodynamics or results from lattice QCD. This has resulted in a remarkably precise description of the majority of observations in proton-proton collisions, which both further experimental and theoretical developments often rely heavily upon.

In high energy heavy ion collisions, the landscape is quite different. Here efforts are more often directed towards signals for the formation of the Quark-Gluon Plasma (QGP), and studies of its properties. The existence of such a phase is demonstrated in lattice calculations and it is presumed to have existed in the hot, early Universe. In this area event generators also exist, but are usually more "special purpose" than "general purpose", each attempting to describe a specific array of observations ascribed to the formation of a QGP. Event generators generating full exclusive events also exist, and the ones most frequently used in analyses investigating particle production mechanisms are, arguably, EPOS-LHC [4], AMPT [5] and HIJING [6]. At least for the bulk event properties, these three generators have for many years defined the "golden standard" for Monte Carlo comparisons to experimental data. In section 8 we outline some of the main similarities and differences between these models and our own.

Several features, which in heavy ion physics are interpreted as a QGP effect, are also observed in pp collisions at the LHC, which may indicate that the dynamics at play in these

two types of collision systems are in fact very similar. Two typical examples are enhanced strangeness [7] and the formation of a "ridge" [8]. This immediately raises a challenge for the general purpose pp event generators and their underlying models. If a QGP is indeed formed even in pp collisions, then the effects of such a formation should be included. On the other hand, if the flow-like effects in pp collisions have a different, non-thermal, origin, then it might be possible to capture the general features of nuclear collisions by adding a nuclear structure "on top" of existing pp models.

In the present paper we will primarily address the second of these possibilities, presenting a model, henceforth called "Angantyr", which is an extrapolation of pp dynamics to collisions with nuclei with a minimum of adjustable parameters. In this way it forms a bridge between heavy ion and high energy hadron phenomenology. Angantyr is a generalisation to AA collisions of the model for pA scattering in ref. [9], which was able to reproduce general features in pA collisions, like multiplicity as a function of (measured) centrality, rapidity distributions, and to a certain degree also $p_\perp$ distributions. Like Pythia8 and the model in ref. [9], Angantyr does not include an assumption of a hot thermalised medium. The model can therefore serve as a baseline for understanding the non-collective background to observables sensitive to collective behaviour.

Before discussing the generalisation to heavy ion collisions, we want to discuss some features of *high energy pp scattering*, which are important for this generalisation.

First, as will be discussed in more detail below, diffractive excitation is important. At high energies the real part of the pp amplitude is small, and usually neglected in applications to collisions with nuclei. Diffraction (elastic scattering and diffractive excitation) is then the shadow of absorption into inelastic (non-diffractive) channels. Absorption is here specified by colour exchange between projectile and target, while diffraction corresponds to colour neutral (Pomeron) exchange. In the Good-Walker formalism diffractive excitation is then part of the diffractive beam, when the projectile mass eigenstate (the proton) is a (coherent) linear combination of scattering eigenstates with different absorption probability. These eigenstates have in refs. [10, 11] been interpreted as different parton cascades.

Secondly multiple partonic sub-collisions are very important at high energies. Here we use the scheme from ref. [12], as implemented in Pythia8, to describe inelastic non-diffractive events. Hard scattering is also seen in diffractive events, and here we use the Ingelman-Schlein formalism [13], which is also included in the Pythia8 package.

A generalisation of the formalism for pp collisions to an event generator for pA *and* AA *collisions* will have *four separate components*:

(i) It is necessary to determine nucleon positions within the colliding nuclei. Here a number of MCs are already available to generate nucleon distributions, see e.g. refs. [14–17].

(ii) One has to calculate the number of interacting nucleons and binary NN collisions. This is generally performed using the Glauber formalism [18, 19]. This formalism is based on the eikonal approximation in impact parameter space, where the projectile nucleon(s) are assumed to travel along straight lines and undergo multiple sub-collisions with nucleons in the target. The importance of including diffractive excitation was early pointed out by Gribov [20], but has often been neglected also in recent applications (see e.g. the review

JHEP10(2018)134

by Miller et al. [19]).[1] As mentioned above, diffractive excitation is a consequence of fluctuations in the nucleon substructure. An important point is then that a nucleon in the projectile is fixed in the same state during its passage through the target nucleus. (And similarly the state of a target nucleon is fixed through the projectile nucleus.)

Fluctuations in the *projectile* proton in pA collisions was studied by Heiselberg et al. [21], for estimates of the number of individual NN sub-collisions. This formalism was further developed in several papers (see refs. [22–25] and further references in there). It is often referred to as the "Glauber-Gribov" colour fluctuation model (GGCF or just GG), and is used in several experimental analyses, e.g. in refs. [26, 27].

As discussed in ref. [9], taking averages over target nucleon states is enough for calculations of cross sections and the number of wounded nucleons in pA collisions, *provided* diffractively excited nucleons are also counted as wounded nucleons. For a generalisation to AA collisions it is, however, necessary to take into account individual fluctuations in both projectile and target nucleons. As far as we know, Angantyr is the first model where this condition is satisfied.

(iii) One must estimate the contribution to the final state from each interacting nucleon. The Angantyr model is here inspired by the old Fritiof model for pA and AA collisions [28, 29] and the notion of "wounded" nucleons.[2] Białas, Bleszyński, and Czyż [30] showed that the production of soft particles is determined by the number of wounded (or participant) nucleons, rather than the number of individual NN sub-collisions. (The latter was later seen to be correlated to hard processes, like production of high $p_\perp$ particles or vector bosons.) In the early Fritiof model [28] it was assumed that an interacting nucleon suffers a longitudinal momentum exchange with a distribution $\sim dQ/Q$, leading to an excited mass $\sim dM^2/M^2$. When hadronising like a colour string this gives *on average* a triangular distribution in rapidity. This behaviour was also later obtained by Białas and Czyż in an analysis of dAu collisions at RHIC [31].

The Fritiof model did not explicitly include diffractive excitation. We note, however, that if the mass distribution for diffractive excitation can be approximated by $dP \propto dM^2/M^2$, then the contribution from a diffractively excited nucleon is very similar to the contribution from an average wounded nucleon in the Fritiof model or from the analysis in ref. [31]. The wounded nucleons in Fritiof can therefore effectively represent both non-diffractively and diffractively wounded nucleons.

(iv) At high energies, the *hard* partonic sub-collisions (scaling with NN sub-collisions rather than wounded nucleons) play a very essential role. It is therefore necessary to account for those specifically in events with multiple NN collisions, e.g. when one projectile nucleon interacts with several target nucleons (or *vice versa*). In ref. [9] we introduced the concept of *primary* and *secondary absorptive* interactions, when a projectile nucleon is interacting absorptively with more than one target nucleon. The corresponding NN parton-level event could be generated using the full multi-parton interaction (MPI) machinery in Pythia8, for both absorptive and diffractive interactions. To generate fully

[1] As an example, in many analyses the NN interaction has been approximated by a "black disk model", where diffractive excitation of individual nucleons is completely neglected.

[2] This is also the case for the HIJING model.

JHEP10(2018)134

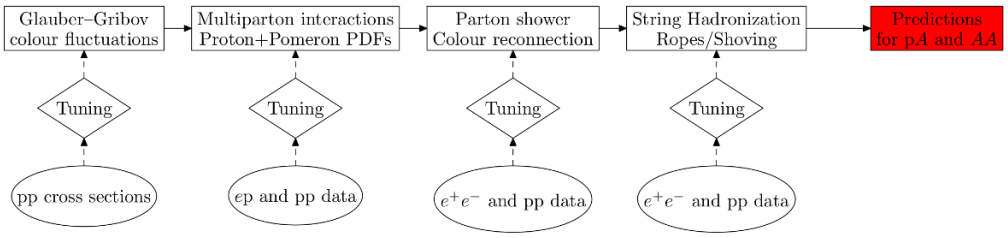

Figure 1. Flowchart showing the programmatic structure of Angantyr. In order to make predictions for heavy ion collisions, several parts of a normal PYTHIA8 simulation needs to be modified, and tuned accordingly. In the flowchart we illustrate how each separate part is tuned to either e^+e^-, ep or pp data, while no tuning is done to heavy ion data.

exclusive final states in AA collisions, we then have to calculate all sub-collisions between a nucleon μ in the projectile and nucleon ν in the target, study the number of multiple sub-interactions for all nucleons μ and ν, and here separate diffractive from non-diffractive (absorptive) interactions. This process is fully described in section 3.

We now return to the question of QGP formation. In the current version of Angantyr the generated partonic states are hadronised using the string fragmentation model in PYTHIA8, without including any final-state collective effects. In this way the model can be used as a starting point for implementing and analysing new models for collectivity. As an example we showed [32] that an enhanced strangeness production can be expected in (high multiplicity) pp collisions, due to overlapping colour strings forming "ropes", in agreement with experimental observations [7]. Furthermore we demonstrated in refs. [33, 34] that the enhanced density also ought to give an outward pressure, which may explain the observed flow-like effects in pp scattering.

In the present version of the model we limit ourselves to general features like distributions of particle density in rapidity and $p_\perp$, postponing a discussion of flow-like effect to a coming publication. We would like to emphasise, however, that the model can still be used as an important tool for understanding non-flow effects on experimental observables designed to measure flow and other collective behaviours.

In figure 1 we show how the structure described above is put together and tuned in the concrete simulation. Since all parts of the simulation; GG colour fluctuations to generate the number of sub-collisions, the PYTHIA8 MPI model, the parton shower and the hadronisation model rely on a number of parameters, these parameters need to be tuned, and a large part of this paper describes how this procedure is carried out. We want to emphasise from the beginning that all parts are tuned to data from collisions of smaller systems, e^+e^-, ep and pp, and no tuning is done to heavy ion data. The results can thus be regarded as real predictions depending only on the chosen extrapolation procedure, and not a specific choice of parameters.

The layout of the paper follows the workflow of the generation procedure as shown in figure 1, and implemented in PYTHIA8. In section 2 we discuss how to calculate the number of wounded nucleons and the number of individual NN sub-collisions. Here we include fluctuations both in the distribution of nucleons in the nuclei and in the individual nucleon

JHEP10(2018)134

states, both for nucleons in the projectile nucleus and in the target nucleus. We note that a projectile (target) nucleon is fixed in the same diffractive eigenstate through the passage through the target (projectile) nucleus. If it is then not absorbed, it may end as diffractively excited, when projected to the system of mass eigenstates. Then in section 3 we discuss how to generate the parton-level sub-events for the different kinds of sub-collisions, and in section 4 we describe the procedure for stacking these sub-events together into complete exclusive hadronic final-states in AA. In section 5 we then make a digression to discuss the details of the generation of secondary absorptive sub-collisions, before we present some sample results in section 6. In section 7 we discuss model uncertainties, especially related to our treatment of secondary absorptive sub-collisions. Finally we discuss differences and similarities between our approach and other heavy ion event generators in section 8, before presenting some conclusions and an outlook in section 9.

2 Nucleon-nucleon sub-collisions in pA and AA

In high energy pp collisions the real part of the amplitude A is small. If this can be neglected, we can define the real quantity

$$T \equiv \mathbb{I}\mathrm{m}\{A\} = 1 - S. \tag{2.1}$$

If diffractive excitation also can be neglected, the elastic cross section is just the shadow of the absorption, which in impact parameter space is determined by the probability $1 - S^2$. The inelastic cross section is then simply the difference between the two. The elastic, total, and inelastic pp cross sections are then given by $d\sigma^{NN}_{\mathrm{el}}/d^2b = T(\mathbf{b})^2$, $d\sigma^{NN}_{\mathrm{tot}}/d^2b = 2T(\mathbf{b})$, and $d\sigma^{NN}_{\mathrm{abs}}/d^2b = 2T(\mathbf{b}) - T^2(\mathbf{b})$ respectively.

The formulations of high energy nucleus collisions in terms of individual nucleon-nucleon interactions was carried out by Glauber in a pioneering paper in ref. [18]. In this paper several kinds of fluctuations were neglected. As pointed out by Gribov, and discussed in the introduction, diffractive excitation of individual nucleons is essential, both for cross sections and for final state properties. The Glauber theory is formulated in impact parameter space, where cross sections can be directly interpreted as probabilities. It is then most convenient to include diffractive excitation using the Good-Walker formalism [35], as the result of fluctuations in the nucleon wave functions. In this section we shortly discuss the Glauber and Good-Walker formalisms for estimating scattering cross sections and distributions of wounded nucleons and NN sub-collisions. The discussion of effects on the properties of exclusive final states will be presented in section 3.

2.1 Glauber formalism

The Glauber formalism is based on the eikonal approximation in transverse coordinate space. Here the projectile nucleon(s) travel along straight lines, and undergo multiple sub-collisions with small transverse momenta. Multiple interactions correspond to a convolution of the individual S-matrices in transverse momentum space, which in transverse coordinate space simplifies to a product.

JHEP10(2018)134

We let $\mathbf{b}_\mu$ and $\mathbf{b}_\nu$ denote the set of positions in impact parameter space for the nucleons in the projectile and target nucleus respectively, and $\mathbf{b}$ the separation between the centres of the colliding nuclei. The S-matrix for scattering between nucleus A and nucleus B is the given by

$$S^{AB}(b) = \prod_{\mu=1}^{A}\prod_{\nu=1}^{B} S^{(N_\mu,N_\nu)}(b_{\mu\nu}). \tag{2.2}$$

Here $\mathbf{b}_{\mu\nu} = \mathbf{b}_\mu + \mathbf{b} - \mathbf{b}_\nu$ is the relative separation between the two colliding nucleons N_μ and N_ν. For pA collisions the product over μ contains only the projectile proton with $b_\mu = 0$.

As mentioned above, fluctuations were neglected in Glauber's original paper. In the *optical limit*, with a smooth distribution of nucleons in the nuclei, and where the size of the nuclei are large compared to the range of the NN interaction, the resulting nucleus-nucleus cross sections can be calculated analytically.

2.2 Fluctuations

2.2.1 Nucleus geometry

The simplest way to include fluctuations in the nucleon positions, $\mathbf{b}_\mu$, within a nucleus, is to randomly distribute the A nucleons in three-dimensional space according to a Woods-Saxon distribution. More advanced models include correlations in form of a hard repulsive core (e.g. [14, 15]), or a more sophisticated description of the two- (or three-) particle correlations between the nucleons within the nucleus [16, 17]. Fluctuations in the geometry is taken into account, when new nucleus states are generated for each new event.

2.2.2 Fluctuations in the individual *NN* interactions, and the Good-Walker formalism

We here shortly describe the Good-Walker formalism for diffractive excitation, assuming for simplicity first that a fluctuating projectile collides with a non-fluctuating target. For a projectile particle with an internal substructure, it is possible that the mass eigenstates differ from the elastic scattering eigenstates. We denote the mass eigenstates Ψ_i, with the projectile in the ground state (e.g. a proton) denoted Ψ_0, while Φ_l are the eigenstates to the scattering amplitude T, with $T\Phi_l = t_l\Phi_l$. The mass eigenstates are linear combinations of the scattering eigenstates, $\Psi_i = \sum_l a_{il}\Phi_l$. The scattering can now be regarded as a measurement, where the projectile "has to choose" one of the eigenvalues t_l, with probability $|a_{0l}|^2$.

The elastic amplitude for the ground state projectile is then given by $\langle\Psi_0|T|\Psi_0\rangle = \sum_l |a_{0l}|^2 t_l \equiv \langle T\rangle$, where $\langle T\rangle$ is the expectation value for the amplitude T for the projectile. The elastic cross section is then given by

$$d\sigma_{el}/d^2b = \langle T(b)\rangle^2. \tag{2.3}$$

We here work in impact parameter space, and the amplitude depends on b. The total diffractive scattering σ_{diff} (including the elastic) is the sum of transitions to all states Φ_l:

$$d\sigma_{\text{diff}}/d^2b = \sum_l \langle\Psi_0|T|\Phi_l\rangle\langle\Phi_l|T|\Psi_0\rangle = \langle\Psi_0|T^2|\Psi_0\rangle, \tag{2.4}$$

JHEP10(2018)134

where we have used the fact that Φ_l form a complete set of states. Subtracting the elastic cross section we then get the cross section for diffractive excitation, which thus is given by the fluctuations in the scattering amplitude:

$$d\sigma_{\mathrm{D}}/d^2b = \langle T^2\rangle - \langle T\rangle^2. \tag{2.5}$$

In a nucleon-nucleon collision both the projectile and the target are fluctuating, leading to single diffractive excitation of the projectile or the target, as well as to double diffraction. The different cross sections are then given by

$$\begin{aligned}
d\sigma^{NN}_{\mathrm{tot}}/d^2b &= \langle 2T(\mathbf{b})\rangle_{p,t} \\
d\sigma^{NN}_{\mathrm{abs}}/d^2b &= \langle 2T(\mathbf{b}) - T^2(\mathbf{b})\rangle_{p,t} \\
d\sigma^{NN}_{\mathrm{el}}/d^2b &= \langle T(\mathbf{b})\rangle^2_{p,t} \\
d\sigma^{NN}_{\mathrm{Dt}}/d^2b &= \left\langle \langle T(\mathbf{b})\rangle^2_p \right\rangle_t - \langle T(\mathbf{b})\rangle^2_{p,t} \\
d\sigma^{NN}_{\mathrm{Dp}}/d^2b &= \left\langle \langle T(\mathbf{b})\rangle^2_t \right\rangle_p - \langle T(\mathbf{b})\rangle^2_{p,t} \\
d\sigma^{NN}_{\mathrm{DD}}/d^2b &= \langle T^2(\mathbf{b})\rangle_{p,t} - \left\langle \langle T(\mathbf{b})\rangle^2_p \right\rangle_t - \left\langle \langle T(\mathbf{b})\rangle^2_t \right\rangle_p + \langle T(\mathbf{b})\rangle^2_{p,t}\,.
\end{aligned} \tag{2.6}$$

Here $\langle\cdots\rangle_p$ and $\langle\cdots\rangle_t$ are averages over projectile and target states respectively, and subscripts Dt, Dp and DD stand for single diffractive excitation of the target, the projectile, and double diffraction respectively. We note here that while the total cross section depends only on the average of $T(b)$, all other cross sections include also average of T^2 over projectile and/or target states. However, if wounded target nucleons include also diffractively excited nucleons, we see that the corresponding cross section for a wounded target nucleon, $\sigma^{NN}_{\mathrm{Wt}} \equiv \sigma^{NN}_{\mathrm{abs}} + \sigma^{NN}_{\mathrm{Dt}} + \sigma^{NN}_{\mathrm{DD}}$, can be written

$$d\sigma^{NN}_{\mathrm{Wt}}/d^2b = \left\langle 2\,\langle T(\mathbf{b})\rangle_t - \langle T(\mathbf{b})\rangle^2_t \right\rangle_p = 1 - \left\langle \langle S(\mathbf{b})\rangle^2_t \right\rangle_p. \tag{2.7}$$

2.2.3 Fluctuations in collisions with nuclei

The expression for the amplitude $T(\mathbf{b}) = (1 - S(\mathbf{b}))$ in eq. (2.6) can be directly inserted into the amplitude for collisions with nuclei in eq. (2.2) (as before we neglect the real part of the amplitudes). The scattering probability can be regarded as a measurement, after which a projectile nucleon is in one of the eigenstates to the amplitude T, and thus also to the probability for colour connection (the absorption probability) $2T - T^2$. Thus all nucleons are frozen in the same state during the scattering process. (We here neglect the modification when one or a few partons have changed colour in the first encounter.) As a consequence the average of the AA amplitude in eq. (2.2) will include also higher powers of T. However, for pA collisions the multiple sub-collisions imply that the total and wounded nucleon cross sections contain higher moments with respect to *projectile* fluctuations, but still only the average over the uncorrelated *target nucleon* states. We also note that these moments should be taken for fixed impact parameters. Thus, to calculate the ratios of e.g.

JHEP10(2018)134

the *integrated* elastic and total cross sections, it is also necessary to know the b-distribution of the amplitude.

To visualise the effects of fluctuations and diffractive excitation we can study a simple example with a proton colliding with two target nucleons, with and without fluctuations. We assume in both cases that the inelastic NN cross section (including diffractive excitation) is $d\sigma_{\rm inel}^{NN}/d^2b = 3/4$.

Case 1: no fluctuations. The NN amplitude and S matrix are $T^{\rm NN} = 1/2$ and $S^{\rm NN} = 1 - T^{\rm NN} = 1/2$. The inelastic cross section when hitting *two* target nucleons is then from eqs. (2.2), (2.7) given by $d\sigma_{\rm inel}/d^2b = 15/16$, ($\sigma_{\rm D} = 0$).

Case 2: with fluctuations. We neglect the fluctuations in the target, and assume that the projectile state is given by $\Psi_0 = (1/\sqrt{2})(\Phi_1 + \Phi_2)$. The states Φ_1 and Φ_2 are here diffractive eigenstates with eigenvalues $t_1 = 0$ and $t_2 = 1$. From eq. (2.6) we get for collision with *one* target nucleon $d\sigma_{abs}/d^2b = 1/2$ and $d\sigma_D/d^2b = 1/4$. For *two* target nucleons we get actually the same result. If the projectile is in state Φ_1 it misses both targets, and if in state Φ_2, it is absorbed already in the first one. Thus the inelastic cross section is only 3/4 (1/2 for absorption and 1/4 for diffractive excitation) compared to 15/16 in the non-fluctuating case.[3]

2.3 From cross sections to probabilities

The absorptive cross section in impact parameter space shown in eq. (2.6) is the average of the expression $2T_{i,k}(\mathbf{b}) - T_{i,k}^2(\mathbf{b}) \equiv 1 - S_{i,k}^2(\mathbf{b})$, where $T_{i,k}$ is the scattering amplitude (and $S_{i,k}$ the S-matrix) for a projectile proton in state i colliding with a target in state k. This expression is always ≤ 1, and it can be directly interpreted as the probability for an absorptive interaction between the projectile and the target. (Such an interpretation is not possible in transverse momentum space, where the cross section has the dimension of momentum to the fourth power.)

We note, however, that neither the elastic cross section nor diffractive excitation is the average of an expression depending on only i and j. (The elastic cross section can be written $\sum_{i,j,k,l} T_{i,k}T_{j,l}$.) When the interaction is driven by absorption, elastic scattering and diffractive excitation is the result of interference between waves, which missed the absorbing target. The cross section for this diffractive scattering is also bounded by 1, and together with absorption it gives a total cross section bounded by 2. A consequence of this feature is that to properly generate events including diffractive excitation for AA collisions in an event generator, it is necessary to, for every projectile nucleon, μ, in state i calculate the average of the amplitude $T_{i,k}(b_{\mu\nu})$ over all states of each target nucleon, ν, for all impact parameters $b_{\mu\nu}$ (and similarly all averages over projectile states i for every target state j). This would give a very slow program, and in section 2.5 we show how to obtain a good approximation.

In pA collisions the picture is, however, much simplified. From eq. (2.7) we note that although the wounded nucleon cross section $d\sigma_{\rm Wt}^{NN}/d^2b$ contains one piece from absorption

[3]This case is actually essentially the "fluctuating gray disk model" discussed in section 2.4.2 and used in analyses of RHIC data by PHENIX.

JHEP10(2018)134

and one piece from diffraction, the sum is always bounded by 1. The question whether a target nucleon ν will be a wounded target (with this definition) in a sub-collision with a projectile in state i can only be answered by yes or no. Therefore the answer yes must have the probability given by the cross section in eq. (2.7). This is used e.g. in applications of the Glauber-Gribov model described in section 2.4.2.

2.4 NN scattering models used in Glauber calculation Monte Carlos

2.4.1 Non-fluctuating models

The simplest approximation for the NN amplitude is the "*black disk model*", where the target acts as a black absorber. This model has been frequently used in experimental analyses (see e.g. the review in ref. [19]). It is then assumed that two colliding nucleons are interacting, if their separation in impact-parameter is smaller than some radius R. The cross sections are here given by $\sigma_{\text{inel}} = \sigma_{\text{el}} = \sigma_{\text{tot}}/2 = \pi R^2$. As there are no fluctuations, the cross section for diffractive excitation is zero. It is then obvious that the model cannot reproduce the experimental results, which satisfy $\sigma_{\text{el}}^{NN} \approx \sigma_{\text{D}}^{NN} \approx \sigma_{\text{tot}}^{NN}/4$. (Here σ_{D}^{NN} denotes the sum of single and double diffractive excitation.) In the literature it is common to set $2\pi R^2 = \sigma_{\text{tot}}^{(\text{exp})}$, which reproduces the experimental total cross section, but neither the elastic nor the inelastic cross section (when the latter includes diffractive excitation). In later studies it has become more common to choose $\pi R^2 = \sigma_{\text{inel}}^{(\text{exp})}$, which reproduces the total inelastic cross section, but gives $\sigma_{\text{tot}}^{(\text{model})} = 2\,\sigma_{\text{inel}}^{(\text{model})} \approx 1.5\,\sigma_{\text{tot}}^{(\text{exp})}$.

For most applications in pA and AA, the elastic cross section is not very important, but we note that it could still be reproduced by introducing a grayness or opacity of the collision, assuming that within a radius R the scattering amplitude is a constant a between 0 and 1. R and a can then always be adjusted to reproduce both the total and the elastic cross sections (and thus also the total inelastic cross section). Diffractive excitation would, however, still be absent.

2.4.2 Models including fluctuations

In a variation of the opacity model above, the projectile is instead fully absorbed with probability a. This obviously includes fluctuations and thus also diffraction. With the value $a = 1/2$ we get the cross section ratios $\sigma_{\text{el}}^{NN} = \sigma_{\text{D}}^{NN} = \sigma_{\text{tot}}^{NN}/4$, in reasonable agreement with experiments. As the model describes the combined fluctuations of the projectile and the target, it is here not possible to separate diffractive excitation of the projectile from that of the target or from double diffraction.

In the introduction we mentioned the "Glauber-Gribov" model for pA collisions, developed by Strikman and coworkers [21–25]. It is there assumed that the fluctuations in the *projectile* can be described by a distribution in the quantity $\sigma \equiv \int d^2b\,\langle 2T(\mathbf{b})\rangle_t$ of the form

$$\begin{aligned} P_{\text{tot}}(\sigma) &= \rho\,\frac{\sigma}{\sigma+\sigma_0}\exp\left\{-\frac{(\sigma/\sigma_0-1)^2}{\Omega^2}\right\}, \\ \sigma_{\text{tot}}^{NN} &= \int \sigma P_{\text{tot}}(\sigma)d\sigma. \end{aligned} \tag{2.8}$$

JHEP10(2018)134

(The second relation follows from eq. (2.6).) This formalism, has been used in analyses of pPb data from LHC, e.g. by ref. [26], to estimate the number of wounded or interacting nucleons, which in turn has been used to estimate the centrality for the collision. The quantity σ is then normally rescaled so that the integral in eq. (2.8) gives the inelastic rather than the total cross section. We note that, as the fluctuating quantity σ includes the fluctuations over *projectile* states, but averages over *target nucleon* states, we see from eq. (2.7) that what is counted as wounded nucleons includes diffractively excited nucleons.

As discussed in section 2.3, the cross section in eq. (2.7) also determines the probability distribution for wounded nucleons, but we want to emphasise that the differential cross section $\langle T(\mathbf{b})\rangle_t$ is needed for all values of the impact parameter b. In ref. [23] this is assumed to be Gaussian $\propto \exp(-b^2/2B(\sigma))$, with a slope parameter $B(\sigma)$ proportional to σ, in order to satisfy the unitarity constraint $T(b) \leq 1$.

In ref. [9] we investigated the fluctuations in the nucleon cross sections using Mueller's dipole approach to BFKL evolution [36, 37] as implemented in the DIPSY Monte Carlo program [11, 38, 39]. The model is formulated in impact parameter space, and includes also a set of sub-leading corrections beyond the leading-log BFKL approximation. Nonlinear effects are introduced by the "colour swing" mechanism, which suppresses large dipoles, corresponding to $k_\perp$ below a saturation scale. BFKL evolution is a stochastic process, and the result was here that the fluctuations have a longer tail out to large cross sections compared to the distribution in eq. (2.8). Rather than the Gaussian suppression assumed in [21], we found a distribution more similar to a Log-normal for the b-integrated and target-averaged σ:

$$P_{\text{tot}}(\ln\sigma) = \frac{1}{\Omega\sqrt{2\pi}} \exp\left(-\frac{\ln^2(\sigma/\sigma_0)}{2\Omega^2}\right). \tag{2.9}$$

To also describe the b-dependence of $\langle T(b)\rangle_t$, we used a semi-transparent disk approximation with the elastic amplitude

$$\langle T(\mathbf{b},\sigma)\rangle_t = T_0\Theta\left(\sqrt{\frac{\sigma}{2\pi T_0}} - b\right). \tag{2.10}$$

The parameters (Ω and σ_0) in $P_{\text{tot}}(\sigma)$ and T_0 in eq. (2.10) could here be fitted to σ_{tot}^{NN}, σ_{el}^{NN} and σ_{Wt}^{NN} taken from experimental data, to obtain a Glauber-like calculation for pA. Together with the parton-level stacking also proposed in [9] we then also obtained a fair description of e.g. the observable used by ATLAS in [26] for estimating centrality, as well as the corresponding pseudo-rapidity distributions as a function of that centrality.

We note that the stochastic nature of BFKL evolution has also been studied by Iancu, Mueller and Munier in ref. [40]. When the probability for a dipole splitting is small, the mean field approximation in the Balitsky-Kovchegov equation does not properly describe the probability for rare events with large cross section. In ref. [40] they studied the fluctuations in the saturation scale, Q_s, and showed that for asymptotic energies the width of the distribution in $\ln(Q_s)$ is growing proportional to $\sqrt{\bar{\alpha}\ln(s)}$, with a tail to large Q_s-values in qualitative agreement with eq. (2.9).

JHEP10(2018)134

2.5 Nucleon fluctuations in AA collisions

As mentioned in section 2.2.2, to study pA collisions also higher moments over projectile fluctuations are needed. When we now want to generalise the formalism to AA collisions, both projectile and target nucleons are frozen under the collision (but still uncorrelated). This implies that we must be able to calculate not only $\langle\langle T(b)\rangle_t^n\rangle_p$, but any moment $\langle\langle T(b)^{n_p}\rangle_p^{n_t}\rangle_t$. To cope with this situation we need a formalism which can give the amplitude $T_{ik}(b)$ for any combination of projectile state i and target state k.

We noted that the Log-normal distribution in eq. (2.9) is quite similar to a Gamma-function, and for technical reasons and the fact that the sum of two Gamma distributed random variables is also Gamma distributed, we will use that instead to model fluctuations in the radius, r, of a nucleon:

$$P(r) = \frac{r^{k-1}e^{-r/r_0}}{\Gamma(k)r_0^k}. \tag{2.11}$$

We then also use a slightly different elastic amplitude

$$T(\mathbf{b}, r_p, r_t) = T_0(r_p + r_t)\Theta\left(\sqrt{\frac{(r_p + r_t)^2}{2T_0}} - b\right). \tag{2.12}$$

where the opacity of the semi-transparent disk now depends on r_p and r_t:

$$T_0(r_p + r_t) = \left(1 - \exp\left(-\pi(r_p + r_t)^2/\sigma_t\right)\right)^\alpha. \tag{2.13}$$

This introduces two more parameters, σ_t and α, (besides k and r_0 in eq. (2.11)) and this varying opacity makes it possible to get a reasonable fit to all the cross sections in eq. (2.6), as well as the elastic slope parameter $B = -d\ln\sigma_{\text{el}}^{NN}/dt|_{t=0}$, for a wide range of energies. The result for $\sqrt{s_{NN}} = 5\,\text{TeV}$ is shown in table 1.

2.5.1 Determining the interaction of nucleon sub-collisions

We now want to take all pairs of colliding nucleons in an AA collision, and for each of these select which kinds of interactions are possible. At high energies all nucleons are frozen in their (random) states during the passage through the opposite nucleus. The probability for an absorptive interaction between nucleon μ (in a state i with radius $r_{i\mu}$) in the projectile and nucleon ν (in state k with radius $r_{k\nu}$) in the target, is then directly given by eq. (2.6) as $P_{abs} = 2T_{ik} - T_{ik}^2$, with $T_{ik} = T(\mathbf{b}, r_{i\mu}, r_{k\nu})$ given by eq. (2.12). To estimate the probability for a diffractive excitation of a given nucleon is more difficult, as diffractive excitation is part of the shadow scattering caused by absorption, to which all encountered nucleons contribute.

We showed in ref. [9] that for a given state of a projectile nucleon the probability that a given target nucleon is absorptively or diffractively wounded in the interaction is given by the average over the possible states of the target (cf. eq. (2.7)) and that this probability factorises for all nucleons in the target nucleus. However, in AA the symmetry between projectile and target complicates things further, as we need both a specific state and the average over all states for all nucleons.

JHEP10(2018)134

	σ_{abs} (mb)	σ_{Wp} (mb)	σ_{Wt} (mb)	σ_{Dp} (mb)	σ_{Dt} (mb)	σ_{DD} (mb)	σ_{el} (mb)	B (GeV^{-2})
input	47.7	61.5	61.5	6.1	6.1	7.7	18.4	20.8
model	47.8	61.4	61.5	5.7	5.8	7.9	18.7	24.1
generated	47.8	61.3	61.3	11.4	11.4	2.2	—	—

Table 1. Fitting the values of input cross sections for pp collisions at $\sqrt{s} = 5\,\text{TeV}$ and using the resulting fluctuations in a generation and different collision types. B is the elastic slope $-d\log\sigma_{\text{el}}/dt|_{t=0}$. The cross sections used as "input" were taken from the default parameterisation in Pythia8. The line "model" shows the results of a fit to the model in eqs. (2.11)–(2.13). The line "generated" finally shows the result of the approximation discussed in this subsection and in the appendix. The fitting procedure assumed a 5–10% uncertainty on the input values, and the statistical uncertainty on the presented output values are around and below 0.5%.

In Angantyr this is handled by generating two states (one primary, r, and one auxiliary, r') for each nucleon in the nuclei. The primary one is used to calculate the probability of an absorptive NN interaction, while the secondary is used to statistically sample the average state of each nucleon. The algorithm ensures that on average (over the four possible combinations of states in an NN interaction) we get the correct probability of the projectile and target nucleon being absorptively and diffractively wounded.

The technical details of this algorithm is presented in appendix A, while here we will only show that it works as expected. In table 1 we give an example where we have fitted the parameterisation of the fluctuations according to eqs. (2.11)–(2.13) to the default parameterisation of the semi-inclusive cross sections in Pythia8. This default parametrisation [41, 42] does not necessarily agree well with cross section measurements from LHC [43], and it is possible for a user to easily supply their own cross sections as input to the fit. The last line denoted "generated" shows the results from generating NN collisions in Angantyr for $\sqrt{s} = 5\,\text{TeV}$. We see that the absorptive cross section comes out close to the input one, and also the wounded cross sections, σ_{Wp} and σ_{Wt} are reasonably well reproduced. However, we see that the individual diffractive excitation cross sections are not reproduced, nor is the elastic ones. However, for the final states in AA collisions, we are mainly interested in getting the absorptive and wounded cross section right, so even if our procedure probably can be improved, we are quite satisfied with this result.

3 From wounded nucleons to exclusive final states

In the wounded nucleon model, as formulated by Białas and Czyz [31], each wounded nucleon contributes to the final state multiplicity distribution, according to a single nucleus emission function $F(\eta)$, giving a total multiplicity of:

$$\frac{dN_{ch}}{d\eta} = w_p F(\eta) + w_t F(-\eta). \tag{3.1}$$

Here $w_{p|t}$ denotes the number of wounded nucleons from left and right respectively, calculated for a given centrality class, defined by impact parameter. In the wounded nucleon

JHEP10(2018)134

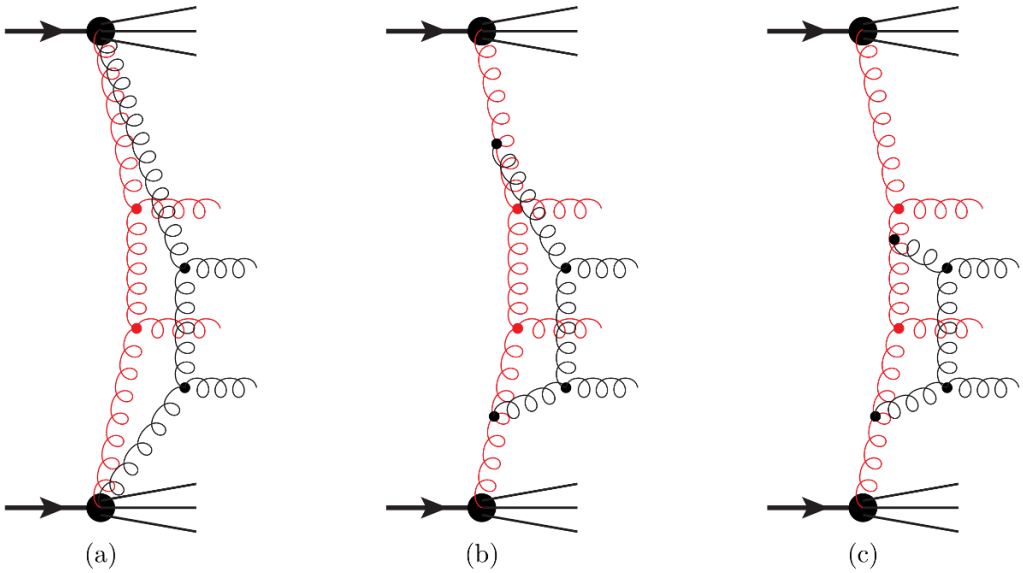

Figure 2. Schematic pictures of multi-parton interactions in a pp collision. The y-axis should be interpreted as rapidity. All initial- and final-state radiation has been removed to avoid cluttering. Each gluon should be interpreted as having two colour lines associated with it, which in the subsequent string hadronisation will contribute to the soft multiplicity. In (a) the colour lines for both sub scatterings stretches all the way out to the proton remnants, while in (b) and (c) the secondary scattering is colour-connected to the primary one.

model, $F(\eta)$ must be extracted from data, and depends on centrality class [44], but a crucial feature of the model is that eq. (3.1) reduces to the pp multiplicity distribution for $w_p = w_t = 1$.

The Angantyr prescription for generating exclusive final states has conceptual similarities with the wounded nucleon model. But instead of extracting an emission function from data, MPI events from Pythia8 are used. We will in this section briefly review the Pythia8 MPI model, and motivate the addition of additional MPIs from multiple wounded nucleons to the model.

3.1 Multiparton interactions in pp collisions

In the Pythia8 MPI model [12], all partonic sub-collisions are to a first approximation treated as separate QCD $2 \to 2$ scatterings.[4] Since the cross section diverges at low $p_\perp$, it is regularised using a parameter $p_{\perp 0}$ which depends on the collision energy, giving:

$$\frac{d\sigma_{2\to 2}}{dp_\perp^2} \propto \frac{\alpha_s^2(p_\perp^2)}{p_\perp^4} \to \frac{\alpha_s^2(p_\perp^2 + p_{\perp 0}^2)}{(p_\perp^2 + p_{\perp 0}^2)^2}. \tag{3.2}$$

This cross section is then folded with parton densities to get a relative probability for each additional sub-scattering. The densities are rescaled according to an overlap function using some assumption about the matter distribution in the colliding protons and an assumed impact parameter.

[4]The MPIs are not fully uncorrelated, as momentum conservation needs to be obeyed, and the parton density corresponding to the extracted parton, is rescaled by a factor $(1 - x)$.

JHEP10(2018)134

In figure 2a there is an illustration of an event with two sub-scatterings (in red and black) which we have assumed are both of the type $gg \to gg$. Note that in the PYTHIA MPI model all incoming and outgoing partons would be dressed up with initial- and final-state radiation, but these have been left out of the figure to avoid cluttering. With completely uncorrelated sub scattering, one would assume the colours of the incoming gluons would also be uncorrelated, and since each gluon carries both colour and anti-colour one would naively think that in the subsequent hadronisation phase, there would be four strings stretched between the proton remnants and giving rise to particle production over the whole available rapidity range. Again to avoid cluttering of the figures, we ask the reader to simply imagine two colour lines (strings) stretched along each gluon and that the vertical axis can be loosely interpreted as rapidity.

Already in the original paper [12] it was realised that it was basically impossible to reproduce data if each sub-scattering was allowed to add particles in the whole available rapidity range. Especially sensitive to this was the multiplicity dependence of the average particle transverse momenta, and to rectify this the MPI model in PYTHIA was modified so that additional sub-scatterings almost always was colour connected to outgoing partons in previous sub-scatterings. This is illustrated in figure 2b and c, where the colour correlation between the two sub-scatterings gives rise to a colour flow *as if* they were (perturbatively) connected. In this way the multiple scatterings can give rise to increased average transverse momentum from the partons coming from extra sub-scattering, without increasing the multiplicity of soft particles due to the strings stretched all the way out to the proton remnants.

3.2 Multi-parton interactions in a pA collision

We now turn to the case of a pA collision and imagine the projectile proton interacting absorptively with two nucleons in the nuclei. To be true to the PYTHIA MPI model we should simply redefine the overlap function using the matter distribution of the two target nucleons. In principle this can surely be done, however, technically we found it almost forbiddingly difficult.

Instead we note that the handling of colour correlations in the pp model would typically result in string topologies corresponding to the sketch in figure 3a. The primary scattering looks like normal scattering between the projectile and one of the target nucleons, while the secondary scattering is now between the projectile and the other target nucleon. Since both target nucleons have been found to be absorptively wounded, the secondary scattering must be colour connected to the second target nucleon, while in the direction of the projectile it looks like a normal secondary scattering.

We also note that we would get the same colour topology, and hence the same distribution of particles, if the second sub-scattering was a separate single (high-mass) diffractive excitation event, which in PYTHIA8 is handled as a Pomeron-proton collision. This is illustrated in figure 3b, where the Pomeron is shown as a green zigzag line. A secondary absorptive wounded nucleon thus contributes to the final state *as if* the final state particles were produced in a single diffractive excitation. This similarity is what we, in the following,

JHEP10(2018)134

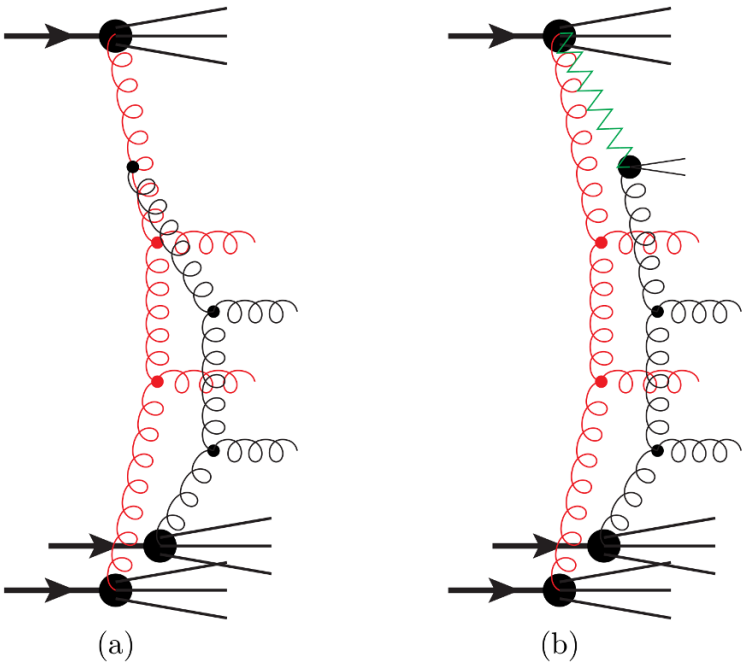

Figure 3. A schematic picture (cf. figure 2) of multiple scattering between one projectile and two target nucleons (e.g. in a pd collisions). In (a) the second interaction is directly colour connected to the first one, while in (b) the second nucleon is only diffractively excited by a Pomeron exchange. Both cases give rise to final string configurations that will contribute in the same way to the final state hadron distribution.

will exploit to build up a final state from primary absorptive interactions and secondary absorptive interactions, the latter being modelled as single diffractive excitation.

The procedure will therefore be to decide which of the two absorptive interactions is to be considered the primary one, and treat this as a completely normal non-diffractive multiple scattering event in Pythia. The secondary scattering will be generated as a single diffractive excitation event in Pythia. Also here there may be additional multiple parton scatterings, but they will be treated as multiple scatterings in the Pomeron-proton system, which is standard in the high-mass diffraction machinery in Pythia.

Referring back to eq. (3.1), this means that we are modelling the single nucleus emission function $F(\eta)$ using high-mass diffractive excitation events. We do not expect them to necessarily look like ordinary diffractive event, but we nevertheless use the diffractive machinery in Pythia8. In section 5 we will describe how we modify this machinery in order to try to fulfil the requirement that $F(\eta) + F(-\eta)$ (i.e. $w_p = w_t = 1$ in eq. (3.1)) would reproduce the distribution in a normal non-diffractive pp event in Pythia8.

The two different sub-events are then merged together so that the elastically scattered proton in the diffractive event is discarded, and the momentum of the Pomeron is instead taken from remnants of the projectile proton.

The assumption in [9] was that the momentum fraction of the Pomeron in such diffractive events can be taken to be distributed approximately as $dx_{\mathbb{P}}/x_{\mathbb{P}}$, which means that

JHEP10(2018)134

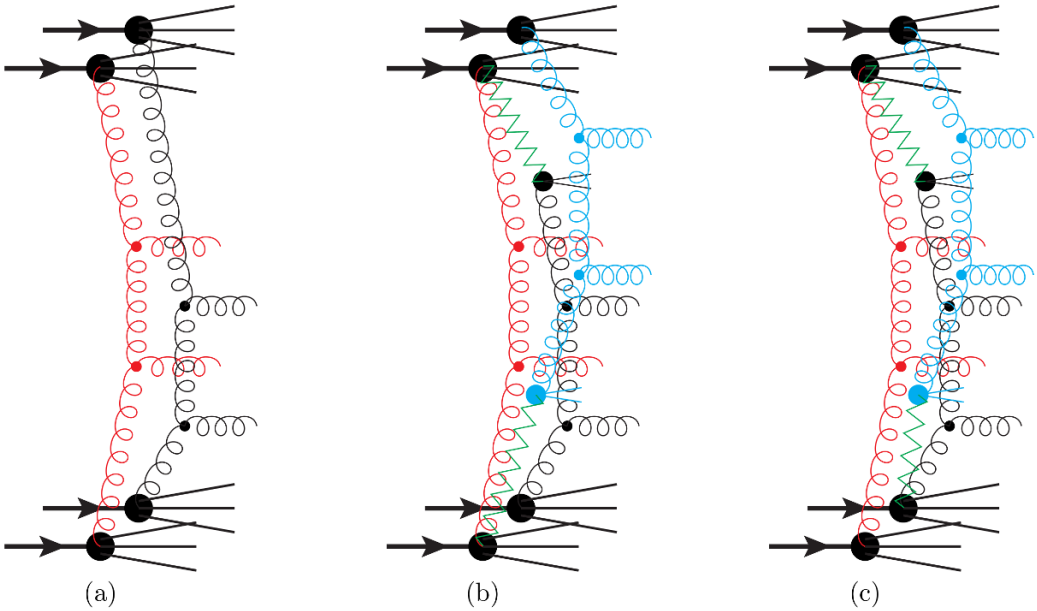

Figure 4. A schematic picture (cf. figure 3) of multiple scatterings between two projectile and two target nucleons in an AA collision. In (a) there are two separate NN collisions, while in (b) and (c) there is one primary sub-collision and two secondary ones.

the mass of the diffractive system is given by dM_X^2/M_x^2. This is approximately what one has found for normal high-mass diffractive events and it is the same assumption as in the old Fritiof model. We do not have a solid explanation why this should be the case. In [9] we gave some handwaving arguments based on AGK cutting rules and the similarity between triple-Pomeron diagrams in diffractive NN scatterings and (doubly) non-diffractive proton-deuterium scattering, but in the end the best argument for this choice is that it seems to work very well.

3.3 Multi-parton interactions in an AA collision

Going one step further in complexity we now consider AA collisions. In figure 4 we illustrate the situation when two nucleons in one nucleus collides with two nucleons in the other, and all four possible NN interactions are absorptive. We find that there is three ways of doing this which are consistent with our pA model. Either, as in figure 4a, we can model it as two primary absorptive interactions, or as one primary and two secondary interactions, where the second of these can either be coupled to the primary interaction (b) or to the first secondary one (c).

All three cases will give us four absorptively wounded nucleons, and in Fritiof and the original wounded nucleon model there would be no distinction between the cases. In the Angantyr model we do, however, want to differentiate between these, and in the following section we will describe a procedure to classify all NN interactions in a AA collisions.

JHEP10(2018)134

4 Generating and combining parton-level NN events

In general, each nucleon in the projectile nucleus may interact with several nucleons in the target nucleus an vice versa. When building up the final state by stacking parton level nucleon-nucleon events we need to concentrate on the most important ones first. This is in line with the general philosophy in PYTHIA8, that harder processes always are considered before softer ones. After having gone through all pairs of projectile-target nucleons and determined their interactions as outlined in the previous section, we therefore order all these interactions in increasing nucleon-nucleon impact parameter, $b_{\mu\nu}$.

We will then go through this list several times, treating one kind of interaction at the time, starting with the absorptive interactions, as they will give the back bones around which we will build up the full event. As soon as an NN interaction has been selected a corresponding sub-event will be generated with the standard PYTHIA8 minimum bias model, and the corresponding nucleons are marked as already interacted. If an NN interaction is found in the list where one of the nucleons has already interacted, this will be labelled *secondary* and the generated sub-event will be added to the sub-event to which the already interacted nucleon belongs, as described in [9] and detailed below.

4.1 Selecting primary absorptive collisions

The first pass over the potential NN interactions, we will only look at absorptive interactions. This will give us a set of N'_{abs} primary absorptive collisions and a set of N''_{abs} secondary ones (where one of the nucleons already has already been absorptively wounded in another interaction).

For each of the primary ones we now generate an inelastic non-diffractive minimum bias event in PYTHIA8, each of which will give a separate sub-events. However, since the procedure takes sub-collisions with small $b_{\mu\nu}$ first, the primary absorptive events should typically be a bit harder and have higher multiplicity than the secondary ones. In [9] this was handled by telling PYTHIA8 to generate $N'_{\text{abs}} + N''_{\text{abs}}$ events, but only keeping the N'_{abs} ones with smallest impact parameter (as reported by PYTHIA8). For the method described here we have instead implemented directly in PYTHIA8 a way to specify by hand which impact parameter you want a given minimum bias event to have, which makes thing a bit more efficient, and also gives a noticeable improvement on the description of some observables, as discussed below in section 6.

Just as in standard PYTHIA8 it is easy to specify signal processes rather than only consider minimum bias events. This may be used to simulate triggers on hard jets more efficiently, or to e.g. produce Z-tagged jets in central AA collisions [45] or top events in pAcollisions [46] or AA. The way this is done is simply to substitute the hardest absorptive primary event with a corresponding signal event, and reweighting the event with a factor

$$w_{\text{signal}} = \frac{(N'_{\text{abs}} + N''_{\text{abs}})\sigma^{NN}_{\text{signal}}}{\sigma^{NN}_{\text{abs}}} \tag{4.1}$$

JHEP10(2018)134

to get the correct cross section. For signal processes with a large cross section the possibility to have additional signal processes in the same event is also taken into account, however for technical reasons at most N'_{abs} signal sub-events can be included in each event.[5]

In the current implementation we assume that minimum bias processes are basically iso-spin invariant, and all such sub-events are generated as pp events in PYTHIA8, flipping by hand the iso-spin of a remnant quark or di-quark afterwards in case the corresponding nucleon was actually a neutron, to conserve total charge. Signal processes are, however, not necessarily isospin invariant. To account for this, we generate pp, pn, np, and nn collisions separately for all signal processes. To decide what type of collision should be generated, all nucleons in the colliding nuclei are marked as either protons or neutrons, under the assumption that neutrons and protons are distributed evenly in the nucleus.

One should note that measurements of proton and neutron distributions in e.g. lead at low energies [47] have indicated that the neutron distribution reaches further out than the proton distribution, giving rise to a "neutron skin" effect. It has been pointed out [48] that this could give rise to effects at the 10% level in selected observables in peripheral PbPb collisions. It has also been pointed out [49] that one could in principle use this effect to design different centrality measures, especially in the case of asymmetrical collision systems. Currently we know of only one very recent Glauber calculation including such effects [50], and in the present version we have left them out entirely.[6]

4.2 Adding secondary absorptive interactions

Once the back-bone sub-events have been generated we go through the list again, this time only looking at the secondary absorptive interactions, in which one of the participating nucleons has already been included in a generated primary absorptive sub-event. As described in [9] we will generate these secondary absorptive sub-collisions as if they were single diffractive excitation events. We here use the standard PYTHIA8 diffraction machinery, but with important modifications detailed in section 5 below.

The final state generated for a given secondary absorptive interaction is then added to a primary absorptive sub-event. The elastically scattered proton is removed and the energy and momentum it had given to the excited nucleon is instead taken from the remnants of the nucleon in the primary sub-events.

It may very well happen that there is not enough energy left in the remnants in the primary sub-event to allow for the addition of a diffractively excited state. In that case it is possible to try again and maybe generate a diffractive event with lower M_X. There is a parameter in the program the limits the number of tries allowed, and if the maximum is passed, the corresponding secondary absorptive interaction is simply discarded (although the corresponding nucleon still has the chance to become wounded in another secondary interaction).

The way secondary nucleon interactions are selected according to the NN cross sections, does not take into account possible effects of energy-momentum conservation, therefore it makes sense to try to take such effects into account in this *a posteriori* way. The

[5] For most use cases this should be adequate, as $\sigma^{NN}_{\text{signal}} \ll \sigma^{NN}_{\text{abs}}$ for most processes of interest

[6] An interested user can, however, plug in their own Glauber MC including neutron skin effects.

JHEP10(2018)134

parameter we introduced should not be taken as the final word in the matter, but at least it allows us to investigate the effects of energy-momentum conservation.

4.3 Adding diffractive interactions

Having taken care of all absorptive interactions we continue with diffractive interactions in much the same way. For each type we again go through the impact-parameter-ordered list of NN interactions twice. In the first round, we only consider *primary* interactions, i.e. where neither of the nucleons have previously been included in a sub-event, and generate a sub-event which could be a single or a double diffractive excitation. These are treated as (soft) diffractive events in Pythia8, as discussed in section 5.

In the second round we also consider *secondary* interactions, where one of the nucleons has already been treated, and an appropriate contribution from the other nucleon (which we will here call a *half* event) is generated and added to the corresponding previous sub-event.

As an example consider an already wounded nucleon in the projectile nucleus, which interacts with a previously unwounded nucleon in the target. The wounded nucleon is already connected to another target nucleon, and cannot be further excited. There are three possibilities for the diffractive interaction:

1. The new interaction is a single diffractive excitation of the *target* nucleon. The interaction is then treated as a normal single diffractive excitation of the target nucleon.

2. The new interaction is a single diffractive excitation of the *projectile* (already wounded) nucleon. In this case the target nucleon is elastically scattered.

3. The new interaction is a double diffractive excitation. In this case the already wounded projectile nucleon is not modified, and the interaction is again treated as a single diffractive excitation of the *target* nucleon.

In a final iteration[7] also purely elastic interactions are considered, and here again the half events are single elastically scattered nucleons. In each case energy and momentum conservation is handled in the same way as for secondary absorptive interaction.

Modulo the effects of secondary interactions being discarded due to energy-momentum conservation, this procedure will correctly handle the probability that a given nucleon is wounded in some way. Note however that, as discussed in section 2.5, although some nucleons in the program are classified as elastically scattered, elastic scattering is not included properly. As elastic scattering is a coherent effect of shadowing due to absorption, the Good-Walker formalism can be used to calculate the cross section for elastic scattering of the incoming *nuclei*, but not for individual nucleons in a nucleus.[8] Diffractive excitation of individual nucleons can, however, be calculated via the trick described in section 2.5.

In the end we have generated a set of parton-level sub-events, which we now can join together in a single parton-level AA event. This event is then handed back to Pythia8 for

[7] Note that central diffraction is not handled properly in the current version of the program.

[8] Naturally electromagnetic interaction, not included here, is responsible for most of the coherent elastic nucleus scattering.

JHEP10(2018)134

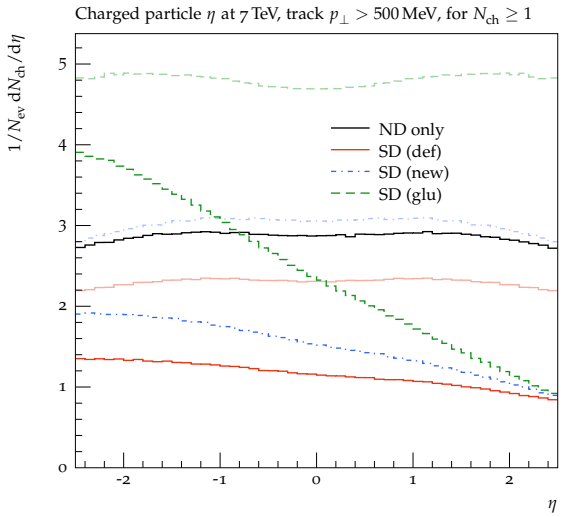

Figure 5. Illustration of the shape of the multiplicity function in eq. (3.1) using the η distribution as measured by ATLAS in [51]. The black and red lines are the shapes of standard non-diffractive and single diffractive events from PYTHIA8 respectively. The green dashed and blue dash-dotted lines are single diffractive events generated by PYTHIA8 using the modifications presented in [9] and the modifications presented in this article respectively. For each single diffractive line there is also a pale line corresponding to adding the mirror image to emulate a non-diffractive distribution à la Fritiof.

hadronisation and decay of unstable hadrons. Finally the non-interacting projectile and target nucleons are bunched together in two remnant nuclei.[9]

5 Modifications of single diffractive to secondary absorptive

In section 3 and in ref. [9] we argued that secondary absorptive interactions will contribute to particle production in the same way as a single diffractive (SD) excitation event (cf. figure 3). Assuming that such SD events produce a simple flat string with mass distributed as dM_X^2/M_X^2, this would naively give a triangular shape of the $F(\eta)$ wounded nucleon emission function in eq. (3.1).

We will use the SD excitation machinery in PYTHIA8, where at high energies the diffractive systems are much more complicated than a single string. As described in more detail below, it models the diffractive excitation as a non-diffractive (ND) interaction between the target nucleon and a Pomeron emitted from the projectile (in the spirit of Ingelman and Schlein [13]), and this is then treated with the full MPI machinery as if the Pomeron was a hadronic object with parton densities. In figure 5 we show the average multiplicity as a function of pseudo-rapidity for ND events, and compare it to SD events from PYTHIA8 using the default settings. Clearly we get a somewhat triangular shape for the SD events (SD(def) in the figure), and adding the multiplicity from target and projectile excitation,

[9]The nucleus remnants are in the event record given the name *NucRem* and PDG-id codes on the form $100ZZZAAA9$, which in the PDG standard corresponds to a highly excited nucleus.

JHEP10(2018)134

we get a shape similar to the ND shape, fully in accordance with eq. (3.1) in the case of $w_p = w_t = 1$.

In ref. [9] we noticed that using the default PYTHIA8 SD machinery for secondary absorptive collisions resulted in too low activity in pA and tried different modifications to increase the multiplicity. One of these modifications included increasing the gluon density in the Pomeron, which is also shown in figure 5 (SD(glu)).

Here we will try to be more systematic in our approach to modify the default PYTHIA8 SD machinery. Looking at figure 3b, it is clear that the rapidity region close to the one close to the direction of the two target nucleons will be our main focus. Here we note that we could equally well have chosen the second nucleon to be in the primary interaction and the first nucleon to be in the secondary, and would then want to have the same distribution of particles. This means that we want the single diffractive event to look as much as possible as a non-diffractive event close to the direction of the two nucleons. We have therefore investigated several different modifications of the SD model and for different diffractive masses we have studied particle distributions in different pseudo-rapidity intervals and compared these with the corresponding particle distributions in the same intervals for ND events.

In the end we settled for a new modification (labelled SD(new) in figure 5), which is the default way of generating secondary absorptive interactions as of version 8.235 of PYTHIA8.[10] To motivate this, we first need to take a closer look at the SD machinery in PYTHIA.

5.1 High-mass diffractive excitation and secondary absorptive

There are more than one way of generating diffractive events in PYTHIA8, but here we will only concern ourselves with the *soft* diffraction used for minimum bias events. Also here there are two treatments depending on the mass, M_X. For low masses, $\lesssim 10\,\text{GeV}$, the excited system is modelled as a simple longitudinally stretched string. In an AA collision, such small excitations will typically be mixed up with the nucleus remnants in the very forward and backward regions and we will here mainly concentrate on high-mass diffraction, which contributes also in the central rapidity region as seen in figure 5.

For high-mass diffraction, PYTHIA treats a proton-Pomeron collision as a normal non-diffractive (ND) hadron-hadron collision and uses the whole MPI machinery with initial- and final-state parton showers. This means that there will be multiple $2 \to 2$ semi-hard partonic scatterings given by

$$d\sigma_{ij}^{\mathrm{p}\mathbb{P}}(p_\perp^2) = \frac{dx_{\mathbb{P}}}{x_{\mathbb{P}}}\frac{dx_1}{x_1}\frac{d\beta}{\beta}F(x_{\mathbb{P}})x_1 f_i^{\mathrm{p}}(x_1,p_\perp^2)\beta f_j^{\mathbb{P}}(\beta,p_\perp^2)d\hat{\sigma}_{ij}(p_\perp^2). \tag{5.1}$$

Here $x_{\mathbb{P}}$ denotes the fraction of the target proton momentum taken by the Pomeron; β is the fraction of the Pomeron momentum taken by the parton j; and x_1 is the fraction of the projectile proton momentum taken by parton i. Furthermore we have the parton densities in the proton, f_i^{p}, and the corresponding densities in the Pomeron, $f_j^{\mathbb{P}}$. Finally we have

[10] Normal diffractive interactions between projectile and target nucleons are treated by the usual PYTHIA8 diffraction set-up.

JHEP10(2018)134

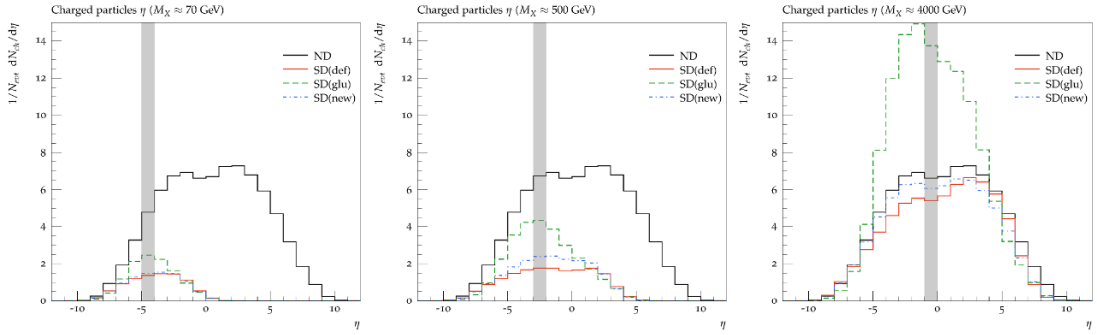

Figure 6. Pseudo-rapidity distribution of charged particles for different diffractive masses for the default single diffraction in PYTHIA8 (red solid lines), the modifications made in [9] (green dashed lines) and the new modifications presented here (blue dash-dotted lines). Left, centre and right histograms correspond to M_X values of ≈ 70, 500, and 4000 GeV respectively. For comparison the results from non-diffractive PYTHIA events at $\sqrt{s} = 5$ TeV is shown as the solid black line. The shaded areas in the figure indicate the pseudo rapidity intervals where the comparisons between SD and ND particle distributions in section 5.2 were studied.

the flux factor $F(x_{\mathbb{P}})$ controlling the diffractive mass given by $M_X^2 = x_{\mathbb{P}} s$. In the following we will assume a flat distribution in $\log(M_X^2)$, in which case $F(x_{\mathbb{P}})$ is just a constant.

The partonic cross section $d\hat{\sigma}_{ij}(p_\perp^2)$ diverges for small $p_\perp^2$, and although it is regularised as in eq. (3.2) the integrated partonic cross section may still exceed the total non-diffractive p$\mathbb{P}$ cross section for a given M_X. In the PYTHIA MPI model this is then interpreted as the possibility of having several sub-scatterings in each collision, with the average number of sub-scatterings given by

$$\langle N_{sc}^{\mathrm{p}\mathbb{P}}(M_X)\rangle = \frac{1}{\sigma_{\mathrm{ND}}^{\mathrm{p}\mathbb{P}}(M_X)} \int \frac{dx_1}{x_1} \int \frac{d\beta}{\beta} \int dp_\perp^2 \sum_{ij} x_1 f_i^{\mathrm{p}}(x_1, p_\perp^2) \beta f_j^{\mathbb{P}}(\beta, p_\perp^2) \frac{d\hat{\sigma}_{ij}}{dp_\perp^2}. \tag{5.2}$$

Here the default value of the of the non-diffractive p$\mathbb{P}$ cross section, $\sigma_{\mathrm{ND}}^{\mathrm{p}\mathbb{P}}(M_X)$, is just set to a constant 10 mb. The $p_\perp^2$ integral is over the full available phase space, all the way down to zero, but with the $\hat{\sigma}_{ij}$ regulated as in eq. (3.2). The parameter $p_{\perp 0}$ here varies as a small power of M_X^2, in the same way as the $p_{\perp 0}$ in normal pp scatterings varies with s.

In figure 6 we show the resulting pseudo-rapidity distribution of charged particles for different values of M_X for diffractive events from PYTHIA8 with $\sqrt{s} = 5$ TeV.[11] Here we see the expected behaviour with a large rapidity gap for smaller M_X, typical for diffraction. When we want to use the diffractive excitation in PYTHIA to model the secondary absorptive interactions, we want to make the event in the target proton direction to look as much as a normal non-diffractive pp event as possible, and in particular we want the whole event to look approximately the same in the limit $M_X^2 \to s$. From the figure we see that this is not quite the case for the default diffraction parameters in PYTHIA8. We also see that the modifications we presented in [9] seems to be a bit too forceful.

Looking at eqs. (5.1) and (5.2) it is easy to see that we can increase the multiplicity by either increasing the general activity by modifying the Pomeron parton densities (as is

[11] The kinematics is given by the LHC pPb run, giving a slightly tilted distribution in η.

JHEP10(2018)134

done in SD(glu) in figures 5 and 6), or we can try to increase the number of sub-scatterings by e.g. adjusting the free parameter $\sigma_{\mathrm{ND}}^{\mathrm{p}\mathbb{P}}(M_X)$. We will here look at both these options by studying eq. (5.2) more closely. Studying the average number of sub-scatterings for a fixed rapidity, $y = \log(x_1/\beta x_{\mathbb{P}})/2$, we get

$$\frac{d\langle N_{sc}^{\mathrm{p}\mathbb{P}}\rangle}{dy} = \frac{1}{\sigma_{\mathrm{ND}}^{\mathrm{p}\mathbb{P}}(M_X^2)} \int \frac{dx_1}{x_1} \int \frac{d\beta}{\beta} \int dp_\perp^2 \sum_{ij} x_1 f_i^{\mathrm{p}}(x_1, p_\perp^2) \beta f_j^{\mathbb{P}}(\beta, p_\perp^2) \times \frac{d\hat{\sigma}_{ij}}{dp_\perp^2} \delta\left(y - \log\frac{x_1}{\beta x_{\mathbb{P}}}\right). \tag{5.3}$$

If we now compare this to the same for standard non-diffractive pp events,

$$\frac{d\langle N_{sc}^{\mathrm{pp}}\rangle}{dy} = \frac{1}{\sigma_{\mathrm{ND}}^{\mathrm{pp}}(s)} \int \frac{dx_1}{x_1} \int \frac{dx_2}{x_2} \int dp_\perp^2 \sum_{ij} x_1 f_i^{\mathrm{p}}(x_1, p_\perp^2) x_2 f_j^{\mathrm{p}}(x_2, p_\perp^2) \times \frac{d\hat{\sigma}_{ij}}{dp_\perp^2} \delta\left(y - \log\frac{x_1}{x_2}\right), \tag{5.4}$$

we see immediately that if we modify the Pomeron parton density and make it $x_{\mathbb{P}}$-dependent, $\beta f_j^{\mathbb{P}}(\beta, p_\perp^2) \to x_{\mathbb{P}} \beta f_j^{\mathrm{p}}(x_{\mathbb{P}}\beta, p_\perp^2)$, and at the same time make the total non-diffractive p$\mathbb{P}$ cross section as well as the soft regulator, $p_{\perp 0}$, independent of M_X, i.e., $\sigma_{\mathrm{ND}}^{\mathrm{p}\mathbb{P}}(M_X^2) \to \sigma_{\mathrm{ND}}^{\mathrm{pp}}(s)$ and $p_{\perp 0}(M_X^2) \to p_{\perp 0}(s)$, we will get very similar expressions. They will not be exactly the same, since the kinematical limits $p_\perp$ will differ, especially for small M_X. Also, for technical reasons, Pythia8 will adjust the selected $p_{\perp 0}$ for each M_X value to ensure that the average number of scatterings is always larger than one, effectively making low M_X events softer.

The resulting modification is shown in figure 6 as the lines labelled SD(new), and we see that the multiplicity in the proton direction is not much improved at small M_X, but at large M_X it traces the non-diffractive quite well.

In the next section we will look in more detail on the particle distributions in the rapidity regions where we want the secondary absorptive sub-events to resemble normal non-diffractive events in Pythia.

5.2 Comparing primary and secondary absorptive sub-events

From figure 6 we see that SD final state particles only populate the rapidity region corresponding to the colour exchange between the Pomeron and the proton (cf. figure 3b). We will here investigate further to what extent the SD events generated by Pythia (with or without modifications) look the same as the ND events in this region. To do this we will study the distribution of particles in different pseudo-rapidity slices for different values of the diffractive mass, M_X. In these slices we have looked at standard minimum bias observables based on charged particles, such as average multiplicity (shown in figure 6), the distribution in multiplicity (N_{ch}), the transverse momentum distribution ($p_\perp$), the distribution in summed ($\sum p_\perp$) and average ($\langle p_\perp \rangle$) transverse momentum for particles within one unit of η, and average transverse momentum as a function of multiplicity ($\langle p_\perp(N_{ch})\rangle$).

JHEP10(2018)134

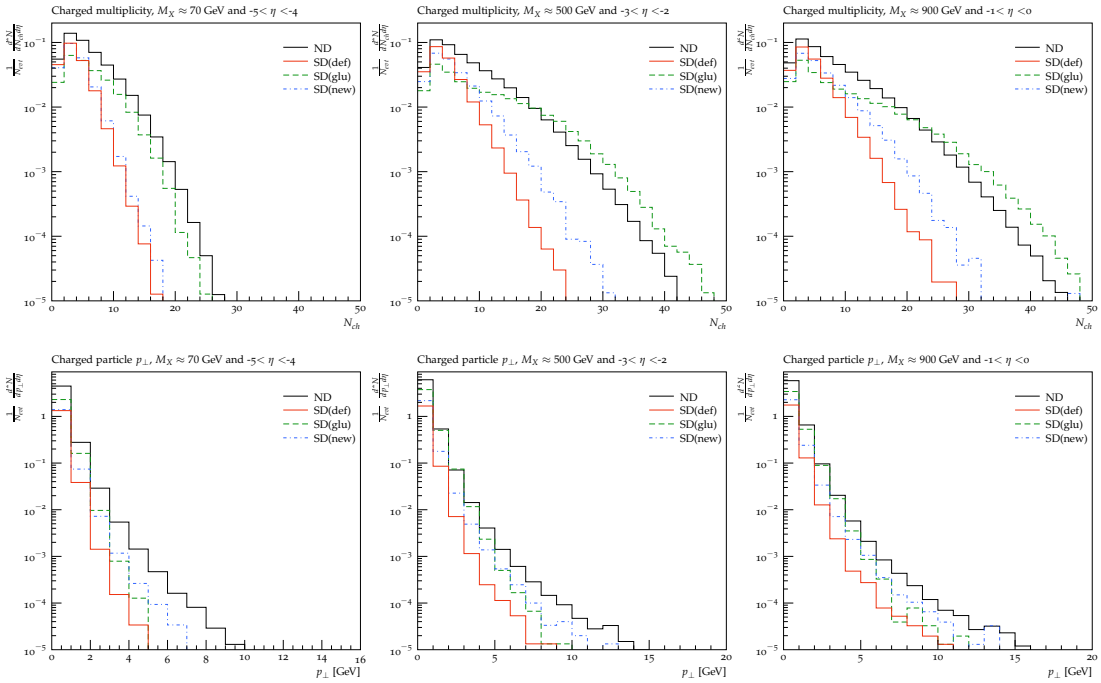

Figure 7. Charged particle distributions in non-diffractive events (black lines marked ND) compared to different options (SD(def): red lines, SD(glu): green dashed lines, and SD(new): blue dash-dotted lines) for single diffractive excitation events in different rapidity slices and different excitation masses, M_X. The top panel shows the multiplicity of charged particles, and the bottom panel their transverse momentum distribution.

Naturally, we do not expect these observables to look the same for a diffractively excited system and a full non-diffractive event. Close to the rapidity gap, we are in the fragmentation region of the Pomeron remnant, and here the transverse momentum of final state particles are severely restricted by the kinematics. Also close to the proton fragmentation region, the transverse momenta are limited by kinematics, but here we expect the SD and ND events to look very similar, and indeed we find that they do.

Here we will concentrate on the rapidity regions around the plateau of each M_X, and in figures 7 and 8 we show some distributions in the slices $\eta \in [-5,-4]$, $[-3,-2]$ and $[-1,-0]$ (the shaded regions in figure 6) for mass bins with $M_X \approx 70$, 500 and 900 GeV respectively. As for the overall multiplicity we find that the default SD machinery, (SD(def)), is quite far from the ND observables in the same rapidity slice. The SD(glu) modification is much closer, but overshoots quite significantly at large M_X in the multiplicity distribution (figure 7) and $\sum p_\perp$ (figure 8). The SD(new) curve gives a slightly better description of $p_\perp$ in figure 7 and the average $p_\perp$ observables in figure 8, but no improvement — or even a slightly worse performance — in the two remaining observables. The choice of which option to use can therefore only be based on an assessment of what types of observables are deemed most important to reproduce correctly. In particular the dependence of the average transverse momentum on the multiplicity is known to be very sensitive to the handling of the multi-parton interactions [12], and here we see that SD(new) is quite close to the ND curves here, as may be expected from comparing eqs. (5.4) and (5.3).

JHEP10(2018)134

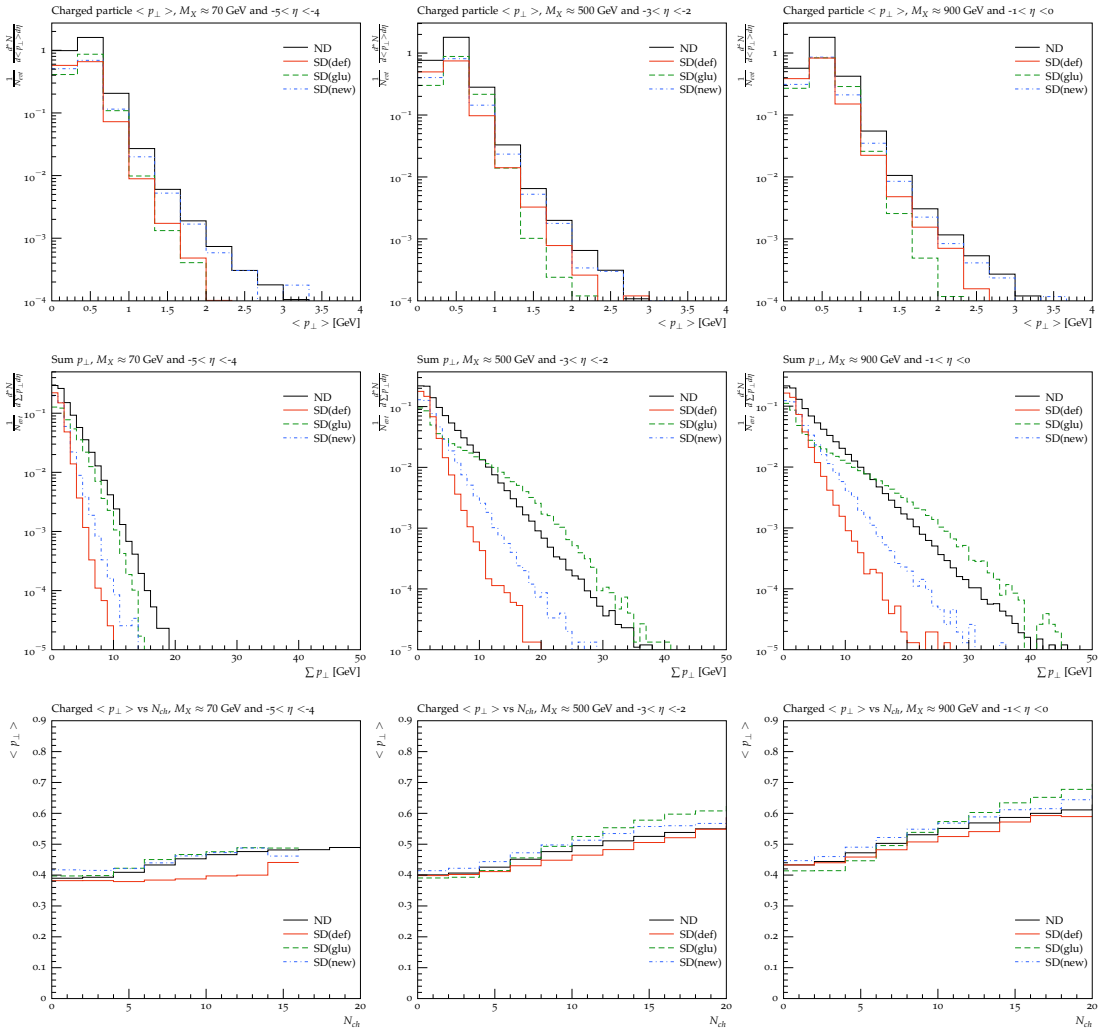

Figure 8. As figure 7, but different observables. The top panel shows the average transverse momentum, while the middle one shows the summed transverse momentum and the bottom panel the average transverse momentum as a function of the multiplicity.

The fact that the $\sum p_\perp$ distributions in SD(glu) in figure 8 is much harder than in standard ND events would be a problem for the description of the centrality observables used in pA and AA, which are often based on the total transverse activity in the forward/backward region (see section 6.2).

It is, however, clear that we could have put more emphasis on charged multiplicity and $\sum p_\perp$ in the regions where the SD(glu) option outperforms SD(new), and thereby made another choice of recommended option. In section 7 we will compare the three different choices against each other for pA results.

In section 4.1 we explained how the impact parameter obtained for each NN subcollision is used as input to PYTHIA8. Here small impact parameters will lead to more multiple scatterings for primary absorptive sub-events. The same impact parameter dependence is also used for secondary absorptive sub-events. It is therefore interesting to

JHEP10(2018)134

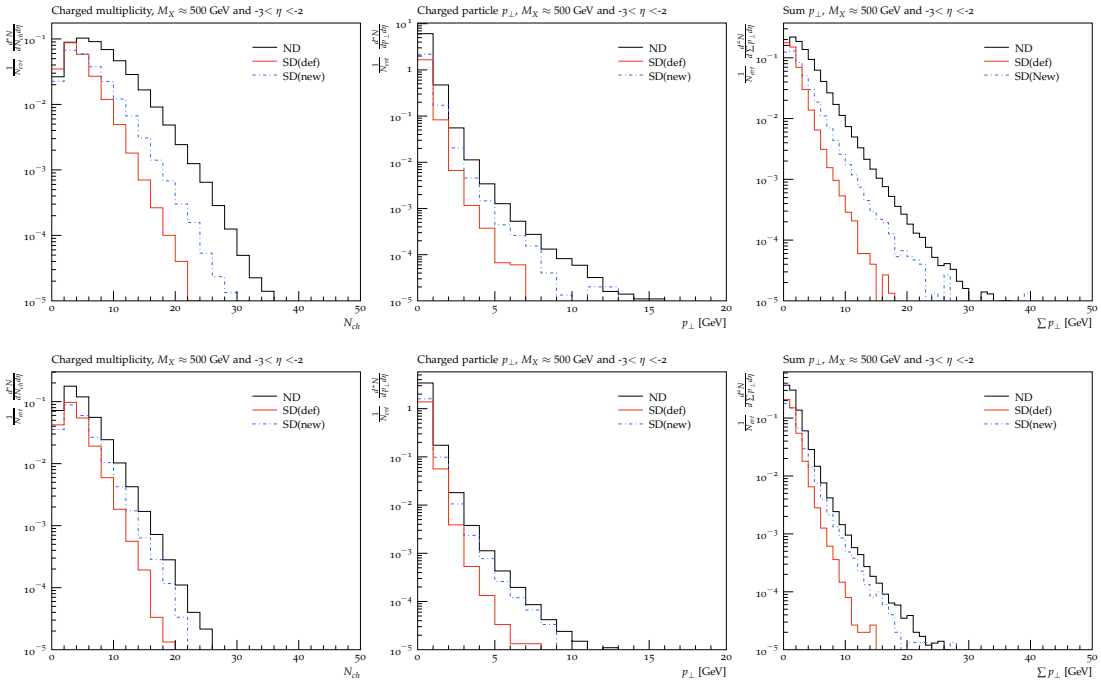

Figure 9. Multiplicity, $p_\perp$ and $\sum p_\perp$ of charged particles for different modifications of SD events with $M_X \approx 500$ GeV compared to ND events in the pseudo-rapidity interval $-3 < \eta < -2$. All events were generated at fixed impact parameter, $b/\langle b \rangle = 0.9$ (top panel) and 1.3 (bottom panel). The lines are as in figure 7.

compare the SD events with ND events for a specific impact parameter. In figure 9 we show typical examples of such comparisons for impact parameters slightly smaller and larger than average. Comparing with the corresponding distributions in figures 7 and 8, we see that the difference between the SD and ND curves tend to diminish with increasing impact parameter, which is good, since by construction the secondary absorptive interactions are at larger impact parameter than the primary ones.

In figure 9 we did not show curves for SD(glu), and in the following we will disregard this option completely. The modifications there are too severe and somewhat ad-hoc, resulting in far too large effects especially on particle production at high M_X (figure 6). We will also disregard the SD(def) option, as it produces too few particles in the nucleus' fragmentation region in pA collisions [9]. SD(new) does not give a perfect reproduction of the ND distributions, and we do not expect any SD model to do that, due to phase space constraints.

The conclusion from the analyses in this section is that SD(new) provides an overall fair description, as well as being more theoretically appealing than the other variations. The SD(new) is therefore, since version 8.235 of PYTHIA, the default model for secondary absorptive sub-events in Angantyr.

JHEP10(2018)134

6 Sample results

All results presented here are generated with PYTHIA8 version 8.235 using default settings.[12] This means in particular that:

- the nucleon distributions in the nuclei are generated according to the formulae in [15] using the hard-core option, where parameters are tuned to low-energy eA data;
- the impact parameter is sampled using a Gaussian distribution with a width large enough to have fairly uniform weights;
- the fluctuations in the nucleons were modelled according eqs. (2.11)–(2.13), fitted the default parameterisation of semi-inclusive cross sections in PYTHIA8;
- the different NN interactions were classified using the procedure described in sections 2.5 and 4;
- the sub-events were generated with the default PYTHIA8 minimum-bias machinery, except for the secondary absorptive ones, where the modifications in section 5 was used.

As with most things in PYTHIA8, there are many options beyond the default behaviour in Angantyr, and there are also so-called user hooks where the user can implement alternative models for e.g. the nucleon distribution, impact-parameter sampling and modelling of fluctuations. There are also a number of parameters in Angantyr that influences the generation of collisions involving nuclei, but most of these can be fitted to pp data. In fact, there are only two parameters that clearly influences the results presented here, which cannot be tuned to pp data. One is the distribution of diffractive masses used in the generation of secondary absorptive sub-events. Here we have assumed a distribution $\propto dM_X^2/M_X^{2(1+\Delta)}$ where we have simply chosen $\Delta = 0$ as in the original wounded nucleon model as implemented in Fritiof. The other was mentioned in section 4.2 and is related to energy-momentum conservation when adding secondary sub-events. The default is to simply veto a secondary NN interaction if there is not enough energy left in the corresponding remnant nucleon in the primary sub-event. An alternative is to instead generate a new secondary sub-event (regenerating M_X) to see if that one can be included.[13] Below in section 7 we will study the effects of these choices.

6.1 pp results

We begin by using the Angantyr generation for the simplest of nuclei, i.e. for pp collisions. Since we actually use the PYTHIA8 minimum bias machinery, we need to make sure that typical minimum-bias observables are reproduced as well when using Angantyr. We expect some differences since all semi-inclusive cross sections are not exactly reproduced in the generation, as explained in section 2.5. Furthermore the distribution in impact parameter

[12] Since Angantyr is the default heavy-ion model in PYTHIA, it suffices to specify suitable nuclei as beam particles to reproduce the results presented here.

[13] The number of attempts allowed for this is governed by the parameter `Angantyr:SDTries`.

JHEP10(2018)134

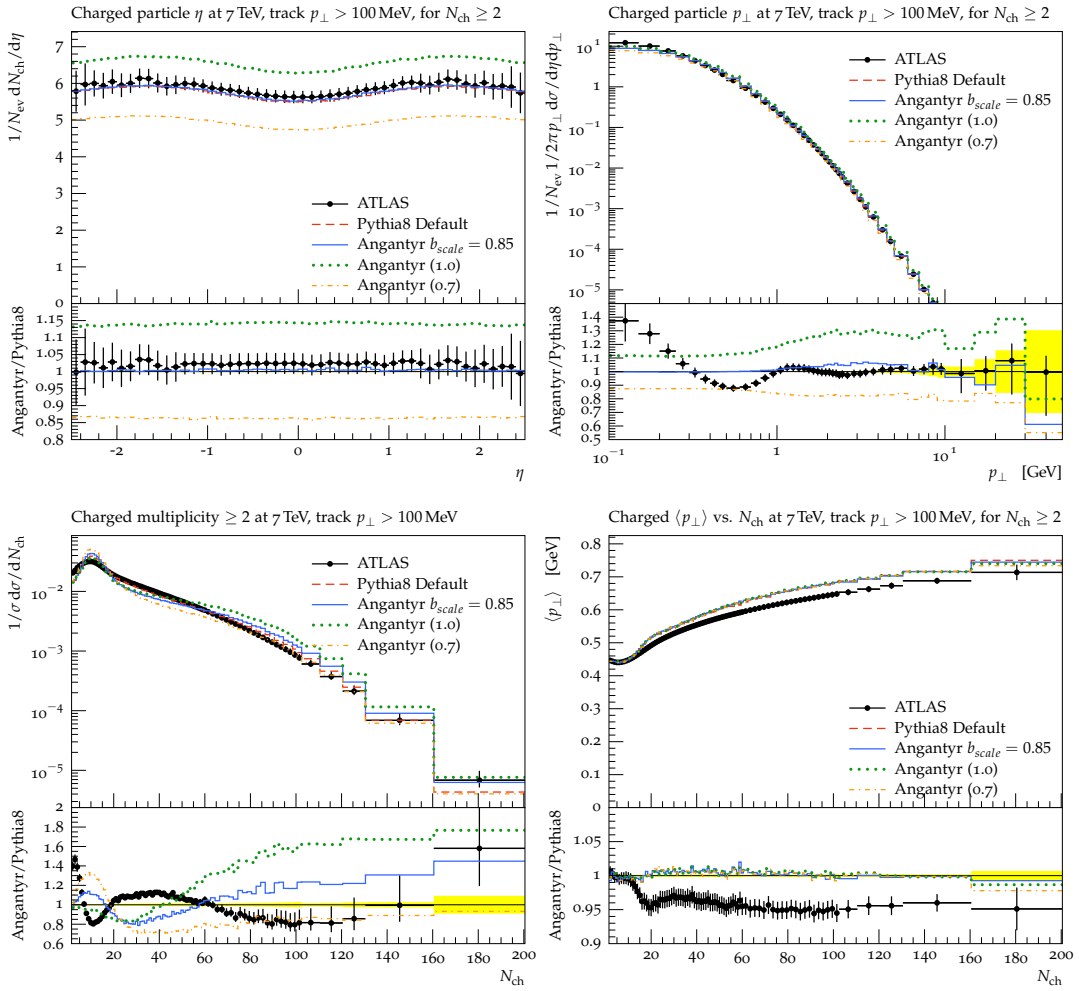

Figure 10. The default PYTHIA8 description of some typical minimum-bias observables in pp, compared to the description using the Angantyr machinery. The latter is given for a range of values of b_{scale} (as quoted in parenthesis in the figure legend). For comparison we show data from ATLAS [51] as implemented in Rivet [52].

is not the same, and since this directly affects the amount of MPI it is important to make sure that the translation between the two works, at least on average.

In PYTHIA8, the impact parameter is by default chosen according to an exponentially falling overlap function, while in Angantyr it is determined by the fluctuations and opacity functions in eqs. (2.11)–(2.13), and it is not straight forward to translate directly between the two. In principle one could try to implement the Angantyr distribution as an option in the PYTHIA8 MPI machinery, which then would require a full retuning to pp data. Here we have decided to instead implement a simple scaling factor, b_{scale}, so that for absorptive (non-diffractive) events,

$$b_{\text{Pyt}} = \frac{\langle b_{\text{Pyt}} \rangle}{\langle b_{\text{Ang}} \rangle} \frac{b_{\text{Ang}}}{b_{\text{scale}}}, \tag{6.1}$$

which is set to a value ensuring that Angantyr gives approximately the same results as

JHEP10(2018)134

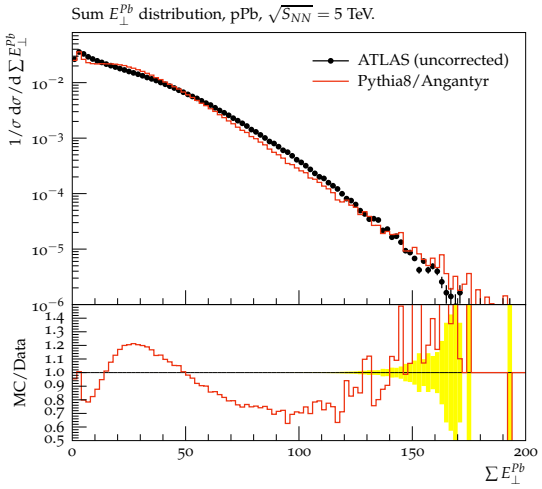

percentile (%)	ATLAS (GeV)	Angantyr (GeV)
0–1	90	87
1–5	66	62
5–10	53	51
10–20	41	39
20–30	32	32
30–40	24	26
40–60	13	16
60–90	6	3

Figure 11. The summed transverse energy in the lead direction ($-4.9 < \eta < -3.2$) for pPb collisions at $\sqrt{s_{NN}}$=5 TeV. Data from ATLAS [26] is compared to results from Angantyr. The table shows the resulting bin edges when dividing up in percentiles for the experimental and generated data respectively.

PYTHIA8 for typical pp minimum-bias observables. In figure 10 we see that our tuned value of $b_{\text{scale}} = 0.85$ fairly well reproduces the PYTHIA8 results and gives approximately the same level of agreement with data. For comparison, the figure also shows the effect of varying this scale to $b_{\text{scale}} = 1.0$ and 0.7, as indicated in the parenthesis in the figure legend.

6.2 p*A* results

Comparing to pA data means that we need to consider the concept of *centrality*, which is used in almost all published experimental heavy ion results. Centrality is based on a final-state observable that is assumed to be correlated with the overall impact parameter of a collision. Typically, this observable involves the activity (multiplicity, transverse energy) close to the direction of the nuclei, and other observables are then conventionally presented in bins of percentiles of this centrality observable.

We will here use the centrality observable defined by ATLAS in [26], which is based on the summed transverse energy in the pseudo-rapidity interval $[-4.9, -3.2]$. As seen in figure 11, Angantyr is able to reproduce fairly well the measured distribution. However, it should be noted that the experimental distribution has not been corrected for detector effects, so it is difficult to draw firm conclusions about the performance of the model.

When we want to use this centrality measure we now have the option to divide it into percentile bins using the measured distribution or the generated distribution, and since they do not exactly agree we will get somewhat different bins, as is shown in table in figure 11.

In figure 12(a) we show the average charged particle multiplicity as a function of pseudo-rapidity measured in the centrality bins defined in figure 11. It is important to remember that even if this is presented as the centrality dependence of the pseudo-rapidity distribution, what is in fact measured is the correlation between the transverse energy flow

JHEP10(2018)134

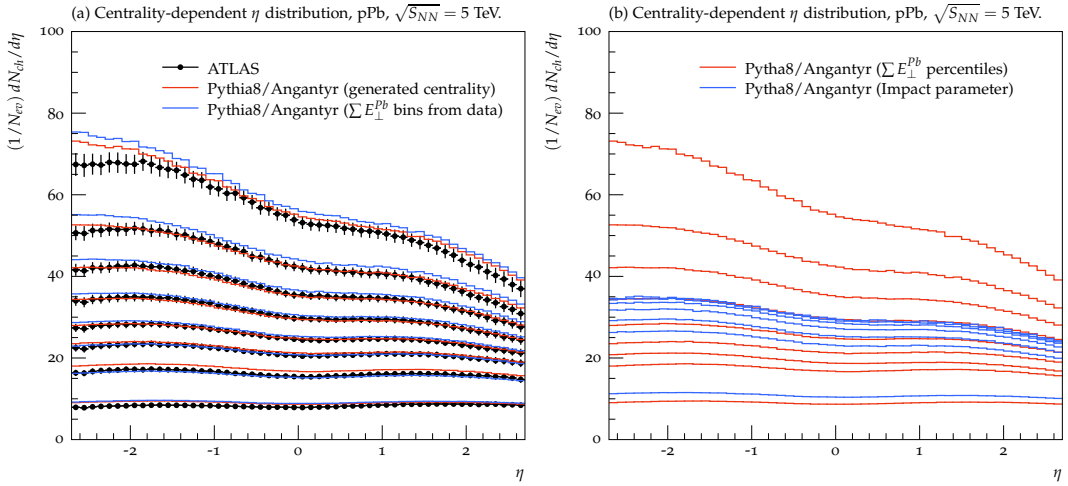

Figure 12. Comparison between the average charged multiplicity as a function of pseudo rapidity in percentile bins of centrality for pPb collisions at $\sqrt{s_{NN}} = 5$ TeV. In (a) data from ATLAS [26] is compared to results from Angantyr. The lines correspond to the percentile bins in figure 11 (from top to bottom: 0–1%, 1–5%, ..., 60–90%). The red line is binned using percentiles of the generated $\sum E_{\perp}^{Pb}$, and the blue line according to the experimental distribution (cf. the table in figure 11). In (b) the red line is the same as in (a), but here the blue line uses percentile bins based on the generated impact parameter in Angantyr.

in the direction of the nuclei and the central multiplicity. In the figure we therefore show two sets of lines generated with Angantyr with the two different binnings presented in figure 11. Clearly the difference between the two is not significant, which is an indication that Angantyr fairly well reproduces the centrality measure. And the fact that neither curve is far from the experimental data[14] gives a strong indication that the Angantyr is a reasonable way of extrapolating pp final states to pA.

Comparing to the results we presented in [9], the description of data has been much improved. The main reason for this is the more careful treatment of secondary absorptive sub-events, but the new handling of the impact-parameter dependence in the primary absorptive events has also somewhat improved the description of data.

Within our model it is possible to look at the actual centrality of an event in terms of the generated impact parameter, and in figure 12(b) we show a comparison between the pseudo-rapidity distribution when binned in percentiles of the generated impact parameter and when binned in the generated $\sum E_{\perp}^{Pb}$ distribution. Clearly, in the Angantyr model, the binning in $\sum E_{\perp}^{Pb}$ is not very strongly correlated with the actual centrality in impact parameter. This is especially the case for the most central collisions. The reason for this is the fluctuations modelled in Angantyr, both in the number of wounded nucleons and in the correlation between the number of wounded nucleons and the activity in the direction of the nucleus.

To study the fluctuations further we show in figure 13 the average number of wounded nucleons as a function of $\sum E_{\perp}^{Pb}$-centrality, both for Angantyr and for three Glauber-model

[14]The η-distributions in figure 12(a) has been corrected for detector effects.

JHEP10(2018)134

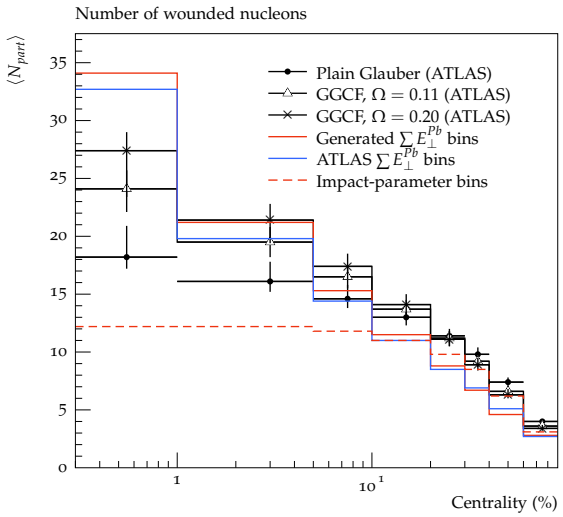

Figure 13. Average number of wounded nucleons as a function centrality for pPb collisions at $\sqrt{s_{NN}} = 5$ TeV. The point are taken from [26] where the numbers were calculated using three different Glauber calculations: filled circles used a standard calculation without fluctuations, while triangles and crosses used the model in eq. (2.8) with fluctuations controlled by $\Omega = 0.11$ and $\Omega = 0.20$ respectively. The solid lines are generated with Angantyr binned in generated (red) and experimental (blue) $\sum E_\perp^{Pb}$ percentiles. The dashed line is also from Angantyr, but binned in impact-parameter percentiles.

fits performed by ATLAS in [26]: one using standard calculation without fluctuations, and two using the fluctuating cross sections in eq. (2.8) with different Ω-parameters. Clearly we see that Angantyr has larger fluctuations than these standard calculations. In figure 13 we also show the number of wounded nucleons in percentile bins of generated impact parameter. As expected the dependence is very weak for the most central bins $(0 - 30\%)$, confirming here that the ATLAS centrality measure mainly picks up the fluctuations in the number of wounded nucleons in this region, and does not correlate very well with the actual impact parameter. The number of participant nucleons is a thus highly model dependent quantity, especially considering pA collisions.

Another way of studying possible nuclear effects in pA is to study particle production as a function of $p_\perp$. In figure 14 we show a comparison to CMS data. The model is clearly not perfect, but nevertheless gives a fair description of the shape over the ten orders of magnitudes shown. Comparing to the results in ref. [9] we again see an increased agreement due to the more careful treatment of secondary absorptive sub-events.

6.3 *AA* results

When we now turn to AA collisions, we expect the fluctuations to have less influence on the centrality measure, since at small impact parameters there are so many NN sub-collisions that most fluctuations will average out. It is therefore reasonable to assume that basically any centrality observable based on multiplicity or energy flow in the nuclei directions will be well correlated with the number of wounded nucleons and the actual impact parameter. Since we will now compare simulation to results from the ALICE experiment, we must in

JHEP10(2018)134

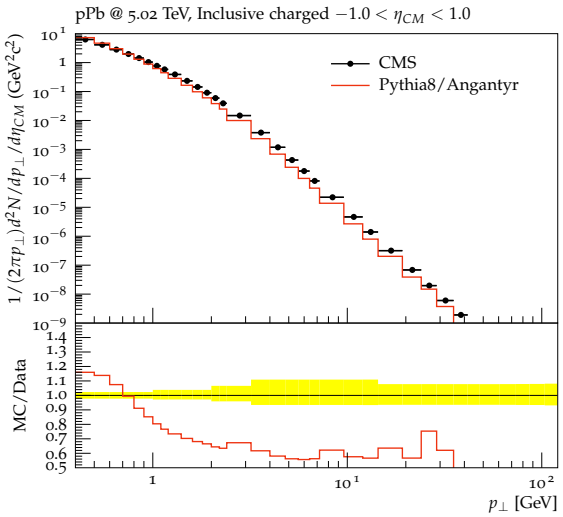

Figure 14. The transverse momentum distribution of charged particles in the central pseudo-rapidity region in inclusive pPb events.

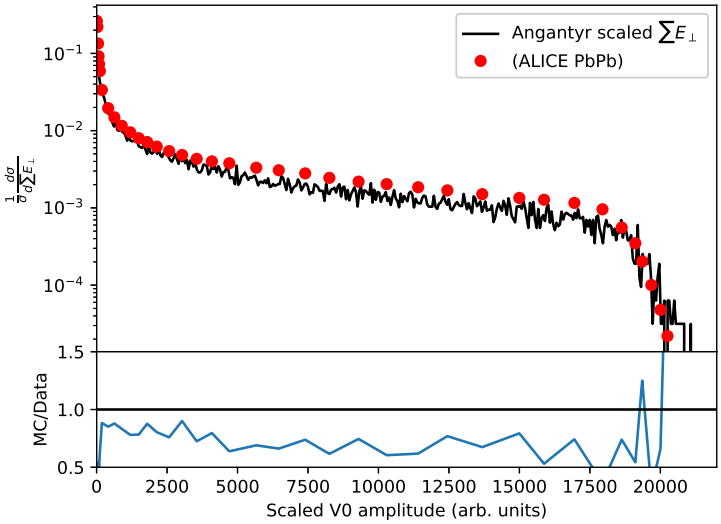

Figure 15. Scaled $\sum E_\perp$ of charged particles at $-3.7 < \eta < -1.7$ and $2.8 < \eta < 5.1$ from Angantyr, compared with the ALICE V0 amplitude, data taken from ref. [53].

principle use the ALICE experimental definition of centrality, rather than the one from ATLAS used in the previous section. In ALICE centrality is defined as percentiles of the amplitude distribution obtained in the two V0 detectors, placed at $-3.7 < \eta < -1.7$ and $2.8 < \eta < 5.1$. Since this amplitude is not unfolded to particle level, and cannot be reproduced by Angantyr without realistic detector simulation, we instead construct a reasonable particle level substitute for this measure. We assume that the V0 amplitude is proportional to the total $\sum E_\perp$ from charged particles with $p_\perp > 100$ MeV in that region.

In figure 15 we compare the measured V0 amplitude [53] with the substitute observable, scaled to match the bin just before the distribution drops sharply at high amplitudes. The

JHEP10(2018)134

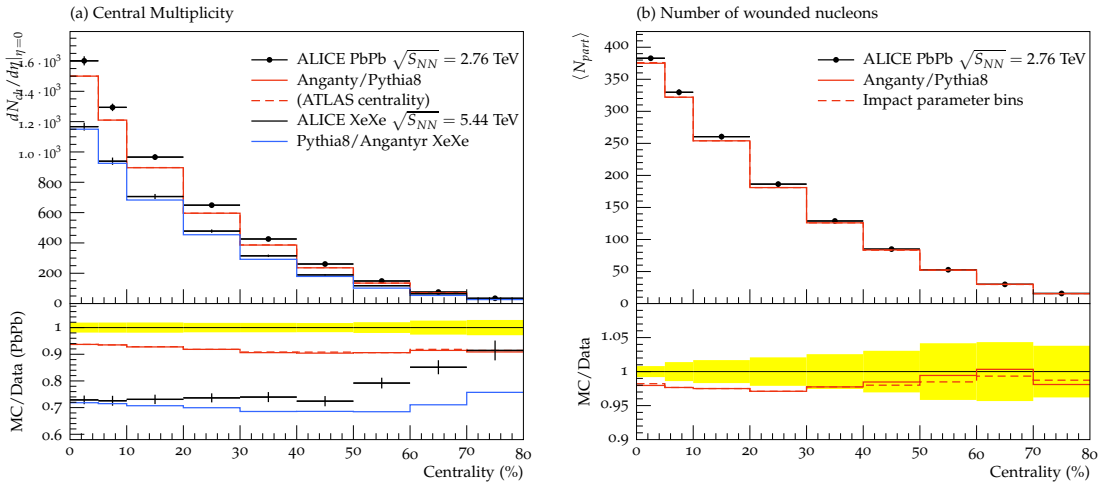

Figure 16. (a) The centrality dependence of the average charged multiplicity in the central pseudo-rapidity bin for PbPb collisions at $\sqrt{s_{NN}} = 2.76$ TeV and XeXe collisions at $\sqrt{s_{NN}} = 5.44$ TeV. Data points (for PbPb) are from ALICE [53], while red (PbPb) and blue (XeXe) lines are from Angantyr. (b) Shows the averaged number of wounded nucleons as a function of centrality. The points are from a Glauber-model calculations from ALICE [53], while the red line is the result from Angantyr. For comparison the dashed line shows the number of wounded nucleons as a function of percentiles in generated impact parameter in Angantyr.

shape of the distribution is described quite well, while the normalisation is a bit off. This is likely due to difficulties extracting the data for very low amplitudes. We will throughout this section use this as a centrality observable, combined with the trigger setup described in ref. [53]. Furthermore, all experiments have some definition of what a primary particle is. In figure 12 we used the ATLAS definition where all particles with $c\tau > 10$ mm are considered as primary.[15] The ALICE definition is at its heart very similar, but has been described in more detail in ref. [54]. This definition has been conveniently implemented in Rivet [54], and we use this definition instead of a cut on $c\tau$.

In order to finish the discussion on the centrality measure, we show in figure 16(a) the ALICE results on the centrality dependence of the average charged multiplicity in the central pseudo-rapidity bin for PbPb collisions at $\sqrt{s_{NN}} = 2.76$ TeV [53] using the measured centrality, and in figure 16(b) with impact parameter bins. The agreement between these two results are clearly much better in PbPb than for pPb, confirming the initial statement in this section.

In figure 16(a) we also show our predictions[16] for Xenon-Xenon collisions at $\sqrt{s_{NN}} =$ 5.44 TeV compared to the ALICE data that were published in [55].

In figure 17 we show the charged multiplicity compared to ALICE data [56–58] over a much wider η range, for both $\sqrt{s_{NN}} = 2.76$ TeV and $\sqrt{s_{NN}} = 5.02$ TeV. The trend, also visible in figure 16, is that Angantyr produces somewhat too few particles at central

[15] This means e.g., that a pair of $\pi^+\pi^-$ which comes from the decay of a K^0_S, will not be included in the charged multiplicity.

[16] Although we present this after the data was published we still consider it a prediction, as the program was released before the data was analysed.

JHEP10(2018)134

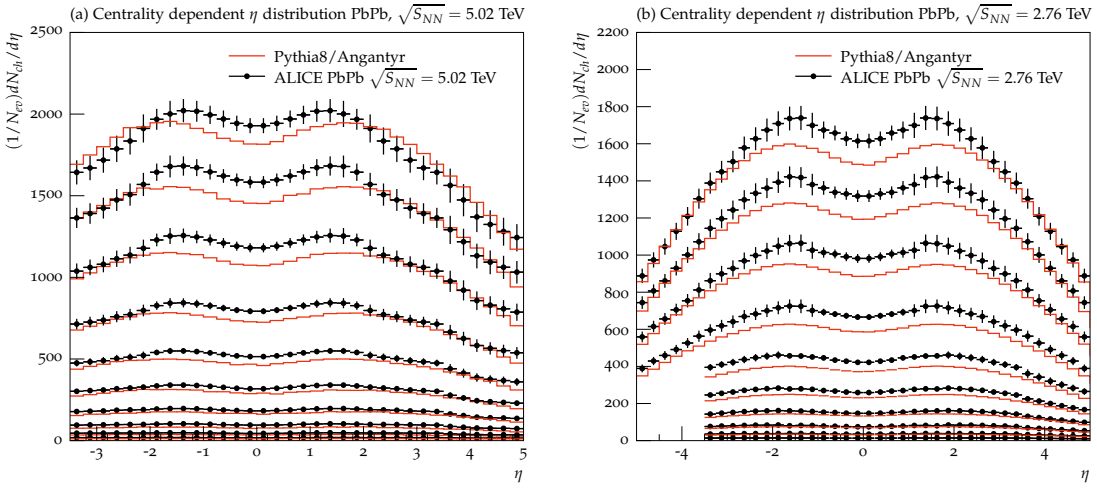

Figure 17. The centrality dependence charged multiplicity over a wide η range in PbPb collisions at $\sqrt{s_{NN}} = 5.02$ TeV (a) and $\sqrt{s_{NN}} = 2.76$ TeV (b). Both for centralities 0–5%, 5–10%, 10–20%, 20–30%...80–90%. Data from ALICE [56–58].

η; the multiplicity is systematically 5–10% too low. We regard this as surprisingly good, considered that no tuning of any kind to AA data has been done.

We now turn to transverse momentum spectra in AA collisions. In figure 18 we show results from ATLAS [59] compared to our model. The published $p_\perp$ spectra was scaled with the average number of wounded nucleons, calculated using a black disk Glauber model. We have not used the number of wounded nucleons as input to Angantyr, just scaled our result with the same number (as published in the article) to obtain comparable spectra. Hence, the results are not scaled to match, as both are simply scaled with the same number.

Finally we want to add a comment about the low multiplicity in the central region, shown in figures 16(a) and 17. One of the main features of Angantyr is that tuning of MPI model, shower and hadronisation should only be carried out using e^+e^-, ep and pp data. However, looking at the comparison to pp in figure 10, we see that even the pp model undershoots the multiplicity at very low $p_\perp$ (below 500 MeV). Since ALICE measures charged particle multiplicity all the way down to zero transverse momentum,[17] it is not clear if the default PYTHIA8 behaviour should even be applicable here. The transverse momentum of such low-$p_\perp$ particles does not origin in the (perturbative) parton shower, but rather in the dynamics of string breakings. As seen from the comparison to pp this is not yet fully understood. The validity of this point is underlined by comparing to the ATLAS data shown in figure 18, where multiplicity is measured with low-$p_\perp$ cut-off of 500 MeV. In figure 19 we show the multiplicity distribution obtained by integrating the distributions measured by ATLAS, and see that the description improves.

We want to make clear that (part of) this discrepancy could of course be due to a faulty comparison to data, where triggers, centrality measure etc. is not implemented in exactly the way as it is done by experiments. But if it is not, it points to an interesting

[17] The multiplicity below 50 MeV is extrapolated, but this does not contribute to the total multiplicity by more than a few percent.

JHEP10(2018)134

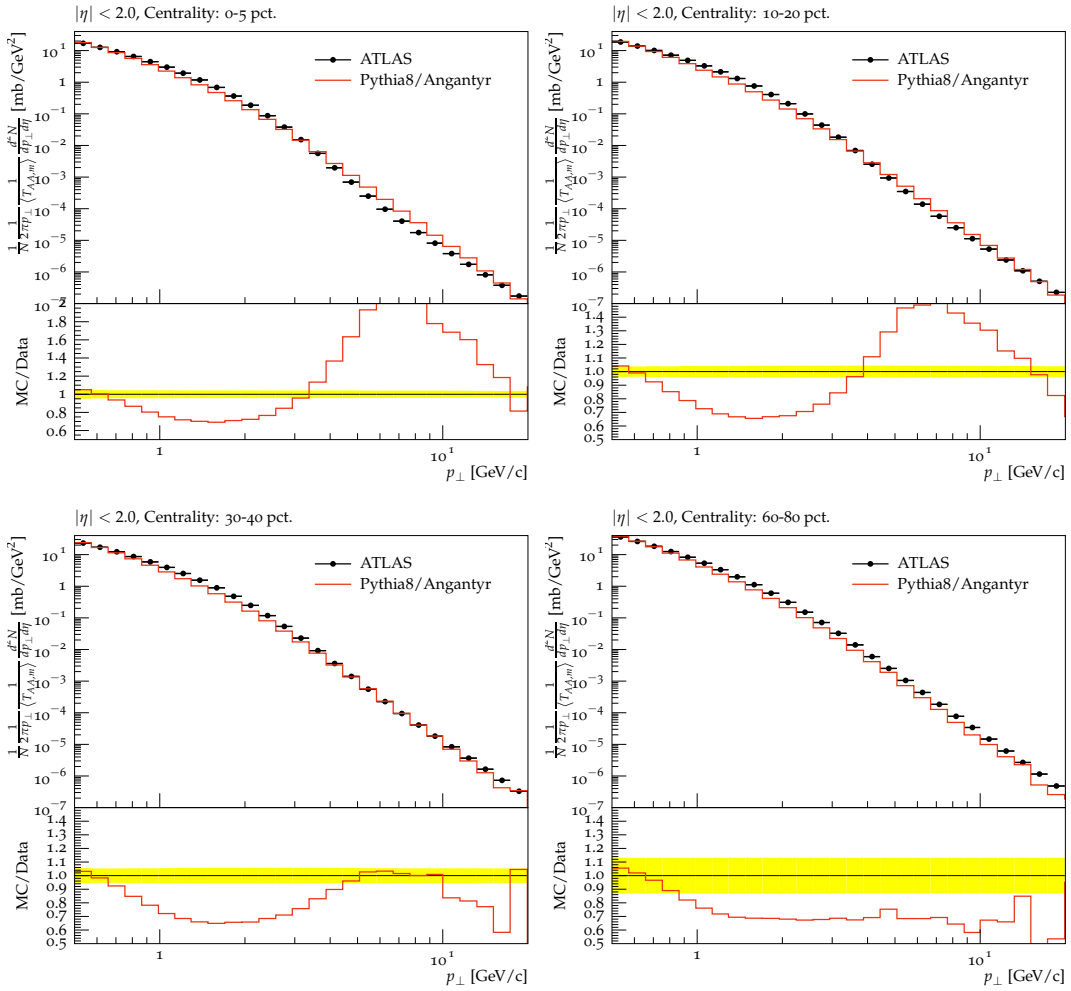

Figure 18. Transverse momentum distributions of charged particles in PbPb collisions at $\sqrt{s_{NN}} = 2.76$ TeV in four centrality bins, compared to Angantyr. Data from ATLAS [59].

point for improvement of the underlying model for soft particle production, also in pp. We will return to this subject in a future paper, but meanwhile we note that it would be interesting if experiments like ALICE, who can measure very near zero $p_\perp$, will extend their publications to also include data with a minimum $p_\perp$ cut-off, which could serve as an important aide in further understanding.

6.4 Collectivity and non-flow estimation

One of the primary goals of the heavy ion programs at RHIC and LHC, is to investigate the collective behaviour of final state particles produced in collisions of nuclei accelerated to relativistic energies. The anisotropic flow measures the momentum anisotropy of the final state particles. As such, it is sensitive to both the initial geometry of the nuclear overlap region, as well as the transport properties of the final state before hadronisation.

The anisotropic flow is quantified in flow coefficients v_n and corresponding symmetry planes Ψ_n, defined by a Fourier series decomposition of the azimuthal distribution of final

JHEP10(2018)134

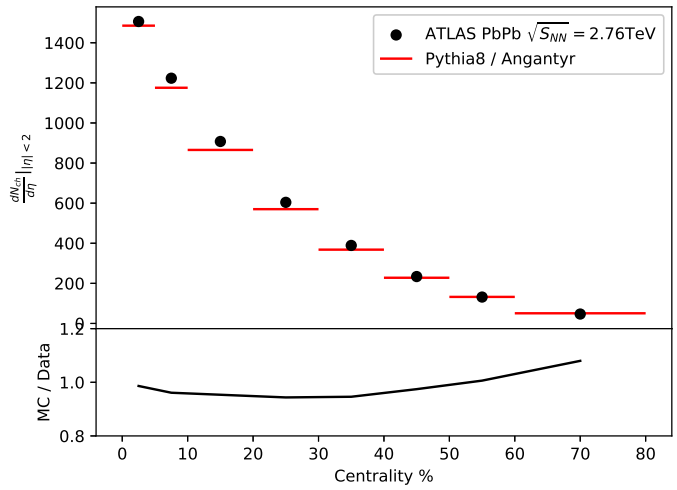

Figure 19. Comparison to total multiplicity at mid-rapidity in PbPb collisions at $\sqrt{s_{NN}} = 2.76$ TeV, with a minimum $p_\perp$ cut of 500 MeV, obtained by integrating the $p_\perp$ distributions measured by ATLAS [59].

state particles:

$$\frac{dN}{d\phi} \propto 1 + 2\sum_{n=1}^{\infty} v_n \cos\left[n(\phi - \Psi_n)\right]. \tag{6.2}$$

In practise, the flow coefficients are calculated using cumulants [60–62], which we also employ here. When flow coefficients are calculated using two-particle cumulants, the calculated coefficient also picks up azimuthal correlations not related to collectivity, but from e.g. resonance decays and intra-jet correlations. Such "non-flow" effects can be suppressed by requiring a gap in η between particle pairs.

In figure 20 we show $v_2\{2\}$ as function of centrality[18] measured with and without a $\Delta\eta$ gap of 1.0, by ALICE [64, 65] and CMS [63] respectively. Since Angantyr produces a full final state, it allows for the construction of the same observable, even in the absence of collective effects, giving an estimate of the non-flow present. We see that the non-flow contribution in the most central collisions is negligible (as one would expect), but rise to about 40% of the measured result for $v_2\{2\}$ without gap for peripheral collisions. This number falls to 20% when a gap is included, indicating that the method of applying a gap can remove some non-flow effects, but not all.

We want to emphasise that at this point, Angantyr does not make any attempt at modelling collective effects, and can therefore be used to estimate the contribution of non-flow. It is our plan to introduce a microscopic model for collectivity, based on string-string interactions to Angantyr, which has shown promising results in pp. The increased energy density from overlapping strings would here give a transverse pressure, leading to strings "shoving" each other before hadronisation [34, 66].

[18] Using the aforementioned adapted version of ALICE centrality.

JHEP10(2018)134

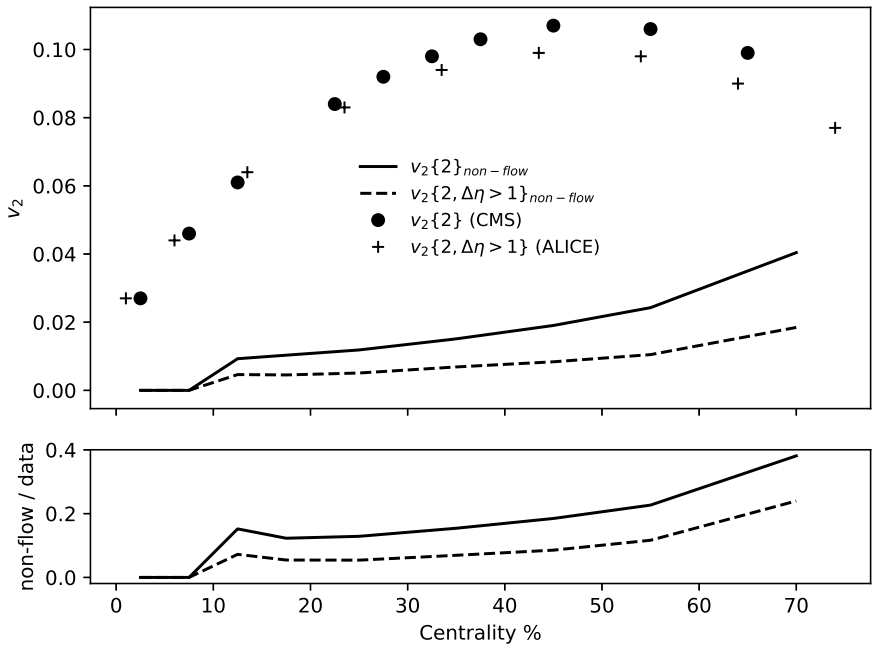

Figure 20. The elliptic flow coefficient $v_2\{2\}$ at $\sqrt{s_{NN}} = 2.76$ TeV, as measured by CMS [63] (without $\Delta\eta$-gap) and ALICE [64, 65] (with $\Delta\eta = 1$), compared to the non-flow contribution calculated by Angantyr. In the ratio plot it is seen that the non-flow contribution without $\Delta\eta$-gap is nearly 40%. This is reduced to 20% when applying a gap.

7 Model uncertainties

The main idea behind Angantyr is to extrapolate pp dynamics, as described by the model for MPIs/underlying event in the PYTHIA8 MC, to heavy ion collisions, retaining as much as possible from pp. This principle was outlined already in the introduction, especially figure 1, but as the model has now been presented, as well as results from pA and AA collisions, we will here also discuss the model uncertainties related to this extrapolation procedure.

Primary interactions correspond directly to inelastic non-diffractive pp collisions. Here PYTHIA8, is known to reproduce most features of both soft and hard pp collisions at LHC fairly well, and the extrapolation to primary interactions in a heavy ion collision is therefore mainly a source of model uncertainty up to PYTHIA8's shortcomings in describing such collisions in pp. We already discussed some of those shortcomings in the previous section, but as they are not uncertainties directly related to the Angantyr model (but rather the underlying PYTHIA8 model) we will not discuss them further here.

The largest uncertainty comes instead from our treatment of secondary absorbed nucleons. The main reason is that secondary absorption has no pp equivalent. In section 5 we outlined the procedure of modifying single diffractive collisions to describe secondary absorbed nucleons, and we will investigate uncertainties related to this treatment in section 7.1.

Diffractively excited nucleons give a comparatively small contribution in collisions with nuclei, especially in central AA collisions, as illustrated in figure 21. Diffractive excitation

JHEP10(2018)134

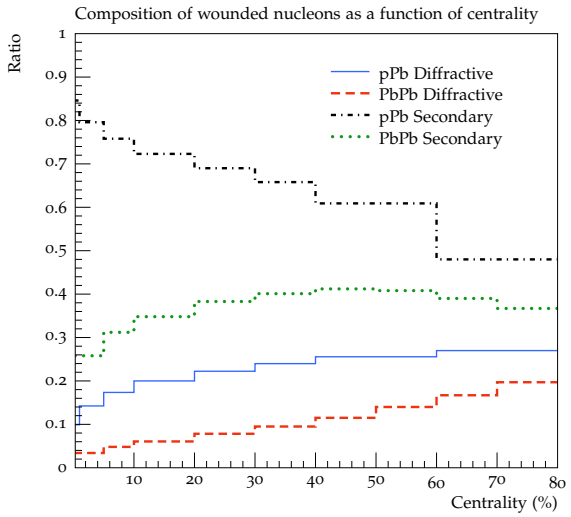

Figure 21. The fraction of the wounded nucleons in the Angantyr model that are diffractively excited as a function of centrality for pPb at $\sqrt{s_{NN}} = 5$ TeV (blue line) and PbPb at $\sqrt{s_{NN}} = 2.76$ TeV (red dashed line). Also shown is the fraction of wounded nucleons that come from secondary absorptive interactions in pPb (black dash-dotted line) and PbPb (green dotted line).

of nucleons can in principle be determined from pp collisions, but as we will discuss in section 7.2, this is not straight forward.

7.1 Uncertainties in treating secondary wounded nucleons

A core feature of the Angantyr model, is that the contribution from a secondary absorbed nucleon is similar to the contribution from an excited nucleon in a single diffraction event. This corresponds to the black pieces in figures 3a and 3b respectively. This assumption has two components:

(i) The distributions in the rapidity range covered, Δy, and the corresponding mass, $M \approx \exp(\Delta y/2) \times (1\text{GeV})$, are similar.

(ii) The distribution of partons from the projectile nucleon, involved in the interaction with the secondary absorbed nucleon in figure 3a, is similar to the partons in the Pomeron in figure 3b.

Naturally none of these assumed similarities can be exact. Extracting the relevant properties in diffractive excitation in pp collisions from data at LHC has also large uncertainties, as we will discuss further in section 7.2. We also note that:

(iii) Energy-momentum conservation has generally important effects in high energy reactions, and has to be satisfied when nucleons suffer multiple NN sub-collisions.

Also this point is associated with some model uncertainty, as discussed in section 4.2 and in section 7.1.3 below.

In the following we will discuss the uncertainties associated with all three choices in the treatment of secondary wounded nucleons, and their impact on model predictions. We

JHEP10(2018)134

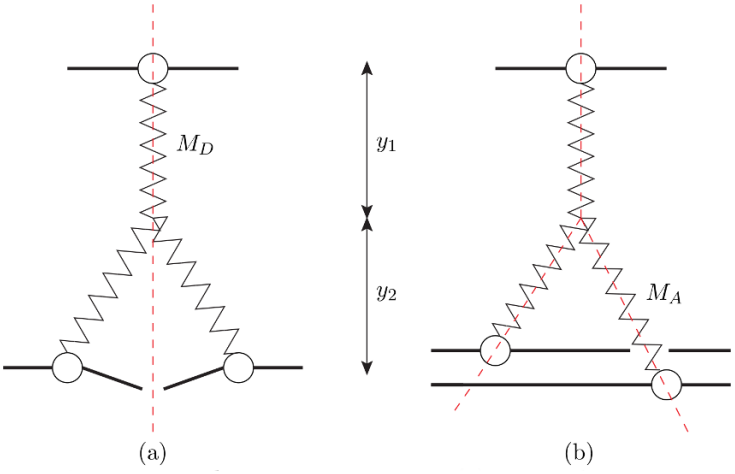

Figure 22. Pomeron diagrams with cuts indicated for (a) single diffractive excitation in proton-proton and (b) doubly absorptive proton-deuteron scattering.

will focus on pA collisions, where there can at most be a single primary interaction, and the treatment of secondary interactions consequently has a relatively larger effect. This is illustrated in figure 21, where we see that secondary absorbed nucleons correspond to about 80% of all wounded nucleons in central pPb collisions, but only about 25% in central PbPb collisions.

7.1.1 Mass distribution

We begin by discussing point (i), the mass distribution of secondary wounded nucleons. The picture in figure 3a has the structure of a triple-Pomeron diagram. This similarity is somewhat symbolic, as each chain in this figure includes the multiple parton scatterings in figure 2, which correspond to Pomeron loops in a Reggeon field theoretical approach (see e.g. refs. [67–69]). The triple-Pomeron diagrams shown in figure 22 would have a weight proportional to:

$$\begin{aligned} dy_1 dy_2 \delta(y_1 + y_2 - Y) \exp(\Delta(y_1 + 2y_2)) = \\ = \frac{ds}{s^{(1-2\Delta)}} \frac{dM_D^2}{(M_D^2)^{(1+\Delta)}} \quad \text{for diffractive excitation,} \\ = \frac{ds}{s^{(1-\Delta)}} \frac{dM_A^2}{(M_A^2)^{(1-\Delta)}} \quad \text{for secondary absorption.} \end{aligned} \tag{7.1}$$

Here y_1 and y_2 are the rapidities indicated in the figure, and $Y = y_1 + y_2 \propto \ln(s)$ is the total allowed rapidity range. The quantity $M_D \propto \exp(y_1/2)$ is the diffractively excited mass to the left, and $M_A \propto \exp(y_2/2)$ is the mass of the secondary absorbed nucleon to the right. Finally the expression $1 + \Delta = \alpha_{\mathbb{P}}(0)$ is the intercept of the Pomeron trajectory.

As discussed above, in the default version of Angantyr we assume a mass distribution $\propto dM^2/M^2$ for both diffractively excited and secondary absorbed nucleons, corresponding to a critical Pomeron with $\Delta = 0$. With a hard BFKL-like Pomeron one could imagine a positive Δ in the range $0 < \Delta < 0.2$. In figure 23 we show the result of generating the

JHEP10(2018)134

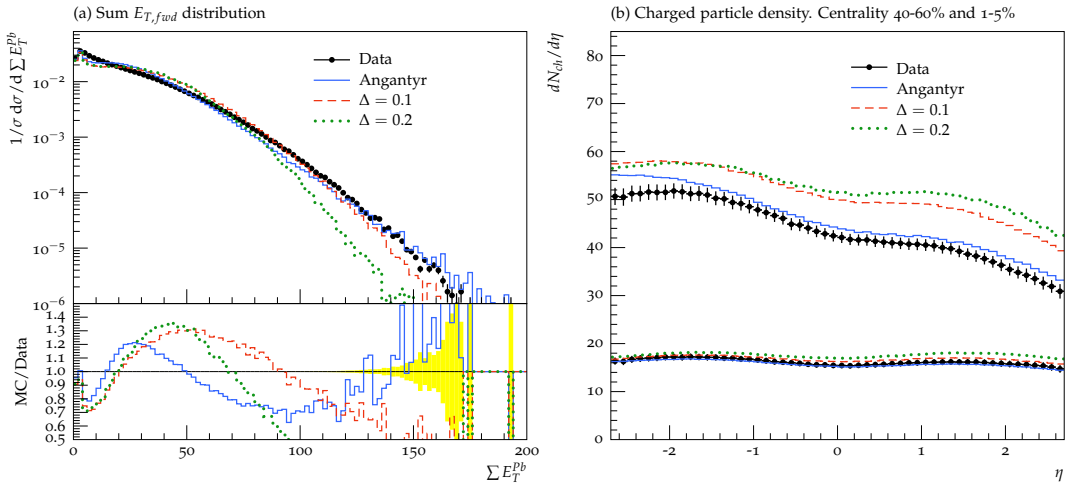

Figure 23. Comparison between different choices of Δ for generation of secondary absorptive sub-events. Variations shown for (a) the summed transverse energy in the Pb direction ($-4.9 < \eta < -3.2$) and (b) the average charged multiplicity as a function of pseudo-rapidity for pPb collisions at $\sqrt{s_{NN}} = 5.02$ TeV. Data points are from ATLAS [26]. Full blue line is the default choice of $\Delta = 0$, while the red dashed and green dotted lines corresponds to $\Delta = 0.1$ and 0.2 respectively. In (b) the lines on the bottom and top corresponds to the 40–60% and 1–5% centrality bins respectively, using the experimentally defined bin limits in $\sum E_\perp^{Pb}$.

secondary absorptive sub-events with $\Delta = 0$, 0.1, and 0.2. From the $\sum E_\perp^{Pb}$ distribution in pPb at $\sqrt{s_{NN}} = 5.02$ TeV (used by ATLAS as centrality measure) shown in figure 23a, we see a noticeable effect already below 50 GeV. The effect follows the expectation that a larger Δ will give larger M_A values and thus more activity. However, we also see that above 50 GeV the distributions for larger Δ seem to run out of steam, which we attribute to the fact that higher M_A values mean that the energy available from the projectile proton is used up faster. This means that fewer secondary absorptive interactions are accepted. In figure 23b we also show the resulting pseudo-rapidity distribution of charged particles for two centrality bins (using the experimentally determined bin edges in $\sum E_\perp^{Pb}$). The larger values of M_A are also reflected in the η-distributions, where the effect is that the distribution becomes too flat to describe data, especially for central events.

7.1.2 Parton distribution in the projectile

As discussed in section 5, the secondary absorptive interaction in figure 3a may involve several partons coming from the projectile nucleon, in a way similar to how diffractive excitation is described by a Pomeron PDF in the Ingelman-Schlein model. Point (ii) concerns the distribution of these partons. In section 5 we studied three different distributions, SD(new) (which is the default for secondary absorption), SD(def) (which is the PYTHIA8 default for diffractive excitation), and SD(glu) (which is the modified PDF for increased gluon activity introduced in ref. [9]). In figure 24a we show the effect on the $\sum E_\perp^{Pb}$ distribution. Below 50 GeV, where the bulk of the events are found, all three options are reasonably close to each other, but the tail of the distributions diverges considerably, in a way consistent with

JHEP10(2018)134

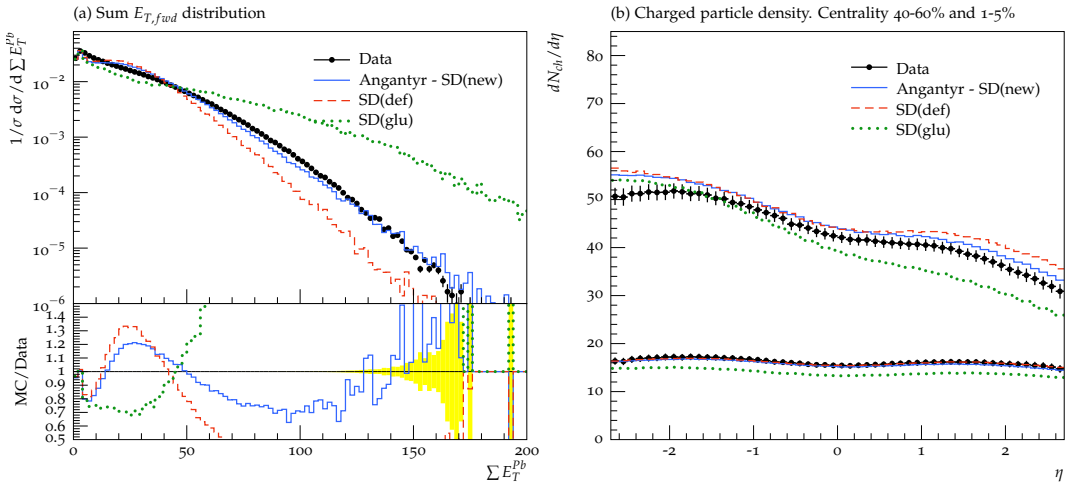

Figure 24. Same as figure 23, but comparing different choices in the treatment of secondary absorptive interactions. The lines corresponds to the models in figure 6.

the differences found in section 5. The resulting pseudo-rapidity distributions shown in figure 24b do not show so dramatic differences. It is, however, clear that our default choice gives the best description of data. As discussed in section 5 our default choice is the one that makes most sense on theoretical grounds, and it is satisfying to see that it also makes sense in comparison to data.

7.1.3 Energy-momentum conservation

Energy-momentum conservation is frequently seen to have a very large impact in high energy reactions. Here its effect could be seen in figure 23a. It is not clear from first principles if energy-momentum conservation should prohibit a sub-collision, if a single sampling of the M_A distribution turns out to require more than what is available, or if it is possible to simply try again. To further study the effects of this ambiguity, we show in figure 25, what happens if we allow Angantyr to retry adding secondary sub-events, which fail due to energy-momentum conservation (as discussed in section 4.2). We see that it does have an impact on the most central collisions in the $\sum E_{\perp}^{Pb}$ centrality measure, while the effect on the resulting η-distribution is barely visible. It is interesting to note that the effect of allowing more attempts seem to saturate quickly, and going from 2 to 4 attempts makes a much smaller change than allowing two attempts instead of one (which is the default).

7.2 Diffractively excited nucleons

In contrast to the secondary absorbed nucleons, a positive Δ in eq. (7.1) means lower masses for diffractively excited nucleons. In principle the M_D-distribution could be measured in pp collisions at LHC, but it is quite challenging to isolate single diffraction from the experimental distribution in the size of a gap in rapidity (see refs. [70, 71]).

In collisions with nuclei, multiple NN interactions imply that, the probability for absorption is enhanced and, as a consequence, the probability for diffractive excitation is

JHEP10(2018)134

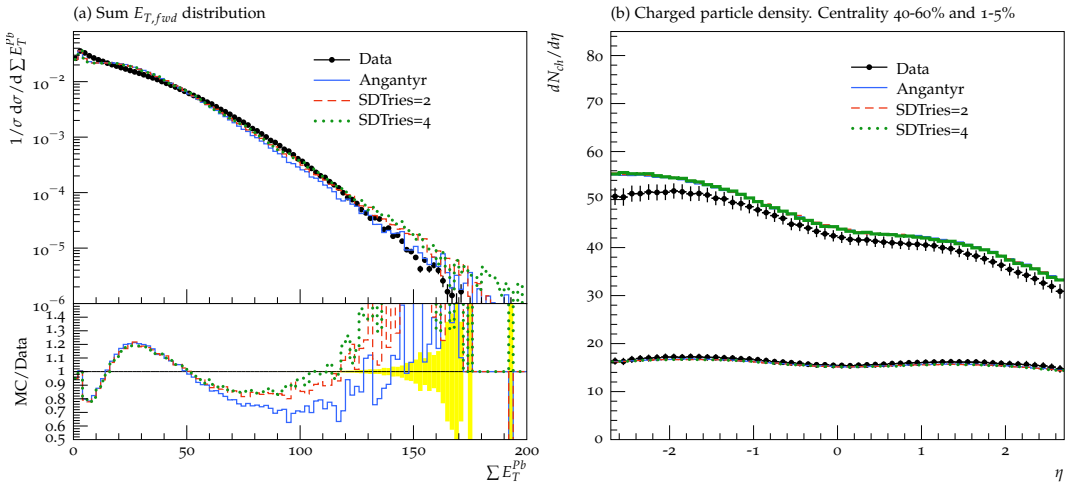

Figure 25. Same as figure 23, but now varying the number of attempts (parameter `Angantyr:SDTries`) allowed to generate secondary sub-events that can be added without violating energy-momentum conservation before giving up and vetoing the secondary interaction. The default version allows only a single attempt and is shown as the blue lines, while allowing two or four attempts is shown as dashed red and dotted green lines respectively.

reduced. From figure 21 we see that in pA collisions about 20% of the wounded nucleons are diffractively excited, dropping to 10% in central pPb collisions. In AA collisions this fraction is further reduced to an average about 10%, and below 4% for central PbPb collisions. This implies that a reasonable variation of the diffractive component will have comparatively small effect. For this reason we have here chosen to keep the default setting in the PYTHIA8 MC, with a distribution $\propto dM_D^2/M_D^2$.

One could here also imagine including a Reggeon contribution $\propto dM_D^2/(M_D^2)^{1.5}$. This contribution is concentrated to low masses, and would not affect the results in most of the rapidity range, including the forward detectors used to measure the centrality. It could, however, give a contribution in the very forward region, and thus it might be of importance e.g. for interactions with cosmic rays.

7.3 Uncertainties in AA collisions

Above we have discussed model uncertainties in pA collisions. We have also pointed out that the corresponding uncertainties are significantly smaller in AA collisions, in particular in central AA collisions. In figure 21 we showed that the fraction of wounded nucleons which are secondary absorbed is about 70% in pPb but about 35% in PbPb collisions. For central collisions these ratios are about 80% in pPb and only about 25% in PbPb. We have checked that a corresponding reduction of the uncertainties is obtained in the MC results for AA collisions.

8 Relation to other models

As Angantyr is a new model, it is instructive to compare it to existing models, and we here discuss the most commonly used ones, also mentioned in the introduction, HIJING [6],

JHEP10(2018)134

AMPT [5], and EPOS-LHC [4]. Here HIJING is most similar to Angantyr. Like Angantyr it is constructed as an extrapolation of pp dynamics, with the explicit motivation that differences between the model and experimental results may indicate effects of collective behaviour. In contrast AMPT and EPOS are both assuming collective expansion of a thermalised medium.

The HIJING generator is built with a similar starting point as Angantyr, thus it is inspired by the Fritiof model, using PYTHIA for generating multiple hard partonic sub-collisions and the Lund string model in PYTHIA for the hadronisation. Similarly to Angantyr, HIJING relies on a Glauber calculation to determine the number of inelastic sub-collisions, which are of two types: soft nucleon-nucleon collisions treated as in Fritiof, and hard parton-parton collisions treated as in PYTHIA. A new version written in C++ was recently presented [72].

In contrast to Fritiof the interacting nucleons are in HIJING excited to higher masses, covering most of the available rapidity range, but just as in the later Fritiof version [29, 73], gluon radiation is added using the soft radiation scheme [74] implemented in Ariadne [75]. The hard partonic scatterings are determined via nucleus PDFs, where the parton density is suppressed by a shadowing factor $R_{a/A}$, compared to A independent nucleon PDFs. To avoid double counting, emitted gluons in the soft component is allowed only for $p_\perp$ below a scale p_0 (chosen to be ≈ 2 GeV), while the hard partonic collisions have a lower cut at $p_\perp = p_0$.

Another difference between Angantyr and HIJING is that in HIJING fluctuations are neglected both in the initial states of the individual nucleons and in the position of nucleons within the nuclei. The soft NN amplitude is then chosen to reproduce the inelastic cross section including diffraction. The probability for multiple scattering is determined by the nuclear overlap function in impact parameter space. In Angantyr we find that fluctuations plus the distinction between primary and secondary absorptively wounded nucleons, have a quite significant effect for the final state multiplicity. In HIJING, the same effect may partly be due to the introduction of the shadowing factor $R_{a/A}$. The shadowing factor is a geometry dependent "k-factor", which accounts for nucleons shadowing for each other during the collision, thus reducing to nucleon-nucleon cross section from the result obtained from pp collisions, to a lower, effective cross section. This suppresses the hard partonic cross section with up to 50% in AuAu collisions at $\sqrt{s_{NN}} = 200$ GeV [6]. In the end all partons are in HIJING connected by strings, and hadronised with PYTHIA. As an option it is possible to include a model for jet quenching, and also a jet trigger, enhancing the rate for events with high-$p_\perp$ jets.

As mentioned above, AMPT presumes that a hot dense medium is formed. It uses the parton state obtained in HIJING as initial conditions. The partons then evolve in a partonic cascade up to freeze-out. After freeze-out the partons are connected in strings, which hadronise according to the Lund model in PYTHIA. Finally the obtained hadrons form a secondary cascade until the density is low enough, when they continue as free particles. As an option the hadronisation can also be calculated via quark-antiquark coalescence.

Finally the EPOS model works on different principles than the other two, as no explicit Glauber calculation is performed. Instead partonic sub-collisions are calculated using

JHEP10(2018)134

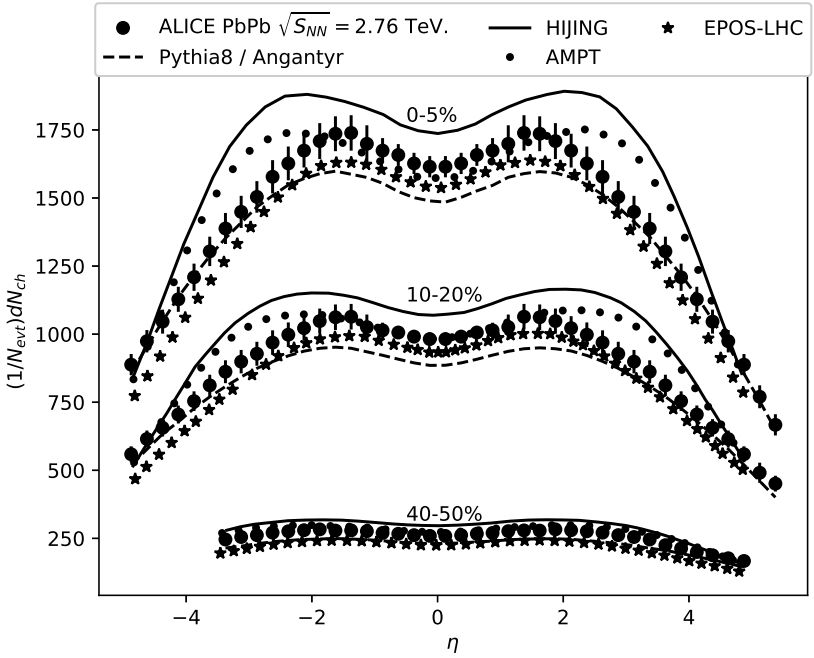

Figure 26. Comparison of Angantyr to the generators EPOS-LHC, AMPT and HIJING. The figure shows charged particle production as function of pseudo-rapidity in PbPb at $\sqrt{s_{NN}} = 2.76$ TeV as measured by ALICE [57].

parton-based Gribov-Regge theory [76]. An elementary scattering is here represented by a cut Pomeron or "parton ladder". This ladder is interpreted as a flux tube, or a string, where the intermediate gluons provide a transverse motion. The strings then break up into segments by quark-antiquark pair production. In the central region with high density, the "core", the segments within a bin in η form a cluster, which expands longitudinally and radially until freeze-out. In regions of low density, called the "corona", the strings fragment instead directly to hadrons. This is mainly the case in the fragmentation regions. In a recent version, called EPOS LHC [4], a new flow parametrisation is introduced, which does not take advantage of the complete hydrodynamical calculation followed by the hadronic cascade as in EPOS2 [77] or EPOS3 [78]. One consequence is here that the time for one PbPb event is reduced from one hour to a few tenths of a second. According to the authors, this also implies that this version should not be used for a precise study of $p_\perp$ distributions or particle correlations in HI collisions.

In figure 26 we compare the multiplicity spectra at $\sqrt{s_{NN}} = 2.76$ TeV from figure 17(b) with Angantyr and the three generators discussed above. (For HIJING jet quenching is disabled in figure 26, but this should not have a major impact on the result.)

We note that with all differences mentioned above, all four generators produce quite similar results for the centrality dependence of the charged particle distribution.

Comparing first HIJING to Angantyr, we see that while Angantyr undershoots at mid-η, HIJING overshoots on the full interval, and produces a too wide shape for the distribution. The likely source of this difference is the different way of handling secondary

JHEP10(2018)134

absorptive events, as described in section 3. HIJING treats all absorptive events on a similar footing, but the nuclear shadowing included in HIJING implies that it produces an overall lower amount of hard sub-collisions.

AMPT uses HIJING for initial conditions, but compared to HIJING the overall multiplicity is reduced by the partonic and the hadronic cascades. However, although the central density agrees with data, the distribution is too wide. We also note that AMPT reproduces multiplicity at mid-η better than Angantyr, and refer to our discussion about possible retuning of Angantyr to low-$p_\perp$ pp data in section 6.3. Finally EPOS-LHC also does a better job than Angantyr at mid-η, but worse away from the central region. We note that AMPT and EPOS-LHC, which both include the hydrodynamic expansion of a hot medium, do not describe data better than Angantyr over the full η-range.

It is, however, clear that if one wants to pin down the physics of a possible plasma phase, more exclusive observables than particle production must be used. This is indeed also the case in contemporary studies at the LHC and RHIC. Considering the precision obtained by the current tools, we see that there is a need for improved tools for comparing theory to data in heavy ion physics. To account for the final 10% discrepancy shown by all four generators, analysis specific effects like choice of centrality measure, trigger selection, primary particle definition etc. all play a major role. In the present paper all comparisons of Angantyr to data are carried out using the Rivet tool [52], which has proved highly successful for this task in pp. This has, however, been done using our own implementation of the experimental analyses. It is crucial for the further development of Monte Carlo event generators for heavy ion physics, that present and future heavy ion data is released using Rivet (or a similar tool), and we are pleased to note that experiments are now starting to commit to this task, also in heavy ion physics.

9 Conclusion and outlook

We have introduced a new model called Angantyr for generating exclusive final states in proton-nucleus and nucleus-nucleus collisions. It extrapolates pp dynamics with a minimum of free parameters, and in this way it bridges the gap between heavy ion and high energy physics phenomenology. It does not assume a hot thermalised medium, and the aim is to see how well such an extrapolation can reproduce experimental data, thus exposing effects of collective behaviour. The model is a generalisation of the model for pA collisions in ref. [9], and is based on the following points:

- The basic pp interaction is described by the Pythia8 event generator, based on multiple partonic sub-collisions and string hadronisation.
- The generalisation to nucleus collisions is inspired by the Fritiof model, and the notion of "wounded" or "participating" nucleons.
- The number of wounded nucleons is calculated from the Glauber model in impact parameter space, including "Gribov corrections" due to diffractive excitation of individual nucleons.

JHEP10(2018)134

- The Glauber model is formulated in impact parameter space. Diffractive excitation is then most conveniently described by the Good-Walker formalism, as the result of fluctuations in the nucleon substructure. We here for the fist time account for fluctuations in both the projectile and the target nucleons, in a Glauber calculation. (As frequently in MC simulations, fluctuations in the position of nucleons in the nuclei are also included.)

The model is implemented in an event generator, which generates exclusive final states. It is included in the PYTHIA8 package, where the user simply specifies a nucleus instead of a hadron as projectile and/or target. The possibility to add a signal process (of electroweak or other origin) is also included, enabling the user to study every process one could normally study in a pp collision.

We have shown that Angantyr gives a good description of general final state properties. This includes not only multiplicity and transverse momentum distributions both in pPb and PbPb collisions, but also its dependence on centrality. We note, however, that this dependence is very sensitive to the experimental definition of centrality. Thus we see that for low centrality the correlation between central multiplicity and "centrality" is more a correlation between central and forward activity, rather than between central activity and impact parameter. The model predictions for XeXe collisions are also in good agreement with ALICE data published later.

The model underestimates somewhat central particle production, when $p_\perp$ is integrated down to $p_\perp = 0$. This may be not surprising, as it is an extrapolation of PYTHIA's description of pp dynamics, which is too low for small $p_\perp$ below 200 MeV. Future work is needed to improve the hadronisation models in this region, including their interface to the perturbative shower.

The description of data is quite sensitive to the handling of, in particular, secondary absorptive sub-events. We have investigated several different choices relating to this treatment, relating to (i) the distributions in the covered rapidity ranges, (ii) distributions of partons in the projectile nucleon, and (iii) energy-momentum conservation. For visualization we performed this investigation in pPb collisions, noting that they will be significantly smaller in PbPb collisions. Although our final choices may not be based on completely solid theoretical grounds, the fact that alternatives investigated give a poorer description of data tells us, that the choices are reasonable. Certainly there are other variations to investigate, but we postpone such studies to a future publication.

In PYTHIA8 all strings decay into hadrons independently. Thus it does not include a mechanism to reproduce the collective effects seen in pp collisions. Such effects are therefore also not reproduced by the present version of Angantyr, and the model should be thought of as a baseline for understanding the non-collective background to observables sensitive to collective behaviour.

Also in high energy pp collisions the number of strings is quite large, in particular in events with high multiplicity. In ref. [33] we showed that overlapping strings forming "ropes" can qualitatively reproduce the increased strangeness in pp [7], as well as in pPb and PbPb [79] collisions. In ref. [34] we further showed that the transverse pressure due to

JHEP10(2018)134

the increased energy density provides a transverse expansion and a qualitative description of the "ridge" observed in pp collisions. An important future direction will be to fully include these models in Angantyr, and test to what degree they provide a description of the observed collective effects in nucleus collisions. Besides the angular correlations, the transverse expansion may affect the $p_\perp$ distributions, which are less accurately reproduced in pPb and PbPb collisions.

To conclude we think that it is notable that a direct extrapolation of pp dynamics can reproduce general features of inclusive particle production in AA collisions to better than 10%. This emphasises the importance of correlation studies, and in a future version of Angantyr we plan to include the collective effects from string-string interactions in the description of collisions with nuclei. In the future we also want to find observables sensitive to the fluctuations related to diffractive excitation and the internal substructure of nucleons. This is an essential feature which distinguishes Angantyr from other event generators available for nucleus-nucleus collisions.

Acknowledgments

CB wants to thank C. H. Christensen for assistance in comparing to ALICE data. This work was funded in part by the Swedish Research Council, contracts number 2016-03291, 2016-05996 and 2017-0034, in part by the European Research Council (ERC) under the European Union's Horizon 2020 research and innovation programme, grant agreement No 668679, and in part by the MCnetITN3 H2020 Marie Curie Initial Training Network, contract 722104.

A Generating absorptively and diffractively wounded nucleons

Here we will go through the technicalities of choosing the interactions between projectile and target nucleons. In [9] we showed that for a fixed nucleon-nucleon impact parameter, b, and a fixed projectile state, the cross section for the target nucleon to be wounded is given by the average of the fluctuations in the target nucleon. Writing the imaginary part of the scattering amplitude for given projectile and target states, p and t, in terms of the corresponding S-matrix, $T_{pt}(b) \equiv 1 - S_{pt}(b)$, we have

$$d\sigma_{\mathrm{Wt}} = \left(1 - \left\langle \langle S_{pt} \rangle_t^2 \right\rangle_p\right) d^2b. \tag{A.1}$$

This works well for pA collisions, but for AA we also want to look at the probability for the projectile nucleon being wounded, and on top of this we want to be able to separate between absorptively and diffractively wounded nucleons.

A.1 Absorptively wounded nucleons

We expect the absorptively wounded nucleons will give the most important contributions to the final state particle production, and we therefore want to take special care to capture

JHEP10(2018)134

cross section fluctuations in this case and at the same time make sure we correctly reproduce the absorptive nucleon-nucleon cross section,

$$d\sigma_{\text{abs}} = \left(1 - \left\langle S_{pt}^2(b)\right\rangle_{pt}\right) d^2b. \tag{A.2}$$

The procedure will therefore be to generate one state for each nucleon in the projectile and target nuclei and for each pair of nucleons calculate

$$P_{\text{abs}} = 1 - S_{pt}^2(b), \tag{A.3}$$

and declare the nucleon-nucleon interaction absorptive with this probability. This will clearly give the correct absorptive nucleon-nucleon cross section.

If we find the interaction is not absorptive we want to go on and check if either the target or the projectile or both are diffractively wounded, but this will then require us to consider averages over the possible states of the projectile or target or both. In the following we will consider a diffractively wounded target, but the corresponding treatment of the projectile is completely analogous.

A.2 Diffractively wounded nucleons

In general it is not necessarily straight forward to analytically calculate the average $\langle S_{pt}^2(b)\rangle_t$ needed to get the correct cross section for diffractive excitation. Instead we will estimate the fluctuations by generating a secondary, or auxiliary state for each projectile (p') and target (t') nucleon. We will still calculate the probability for absorptive interaction using only the primary states, but to get the probability of the target nucleon to be wounded we note that the product $S_{pt}(b)S_{pt'}(b)$ will on average yield the correct value for $\langle\langle S_{pt}^2(b)\rangle_t\rangle_p$, so naively we could use the probability $P_{\text{Wt}} = 1 - S_{pt}(b)S_{pt'}$. However, it is clear that we will then have a negative probability for having a diffractively wounded target $P_{\text{Wt}} - P_{\text{abs}} < 0$, for $S_{pt} < S_{pt'}$. Therefore we also need to consider the statistically equivalent situation where the absorptive interaction probability is given by

$$P'_{\text{abs}} = 1 - S_{pt'}^2(b), \tag{A.4}$$

while the corresponding wounded probability is still

$$P'_{\text{Wt}} = 1 - S_{pt}(b)S_{pt'}(b) = P_{\text{Wt}}, \tag{A.5}$$

where the probability for a diffractively wounded target is then positive.

The procedure we have chosen to handle this, is to shuffle probabilities between the two situations so that we always get non-negative probabilities for diffractively wounded nucleons according to

$$\tilde{P}_{\text{Wt}} = \begin{cases} S_{tp} < S_{pt'} : 0 \\ S_{pt} > S_{pt'} : P_{\text{Wt}} + P'_{\text{Wt}} - P'_{\text{abs}} = 1 - 2S_{pt}(b)S_{pt'}(b) + S_{pt'}^2(b) \end{cases} \tag{A.6}$$

$$\tilde{P}'_{\text{Wt}} = \begin{cases} S_{tp} < S_{pt'} : P'_{\text{Wt}} + P_{\text{Wt}} - P_{\text{abs}} = 1 - 2S_{pt}(b)S_{pt'}(b) + S_{pt}^2(b) \\ S_{pt} > S_{pt'} : 0 \end{cases} \tag{A.7}$$

which will give the correct cross section for the target nucleon being wounded.

JHEP10(2018)134

By considering the auxiliary state for the projectile, p', we can then also find the probability for the projectile being diffractively wounded. And if both are wounded we say that the interaction is a double diffractive excitation.[19]

References

[1] T. Gleisberg et al., *Event generation with SHERPA 1.1*, *JHEP* **02** (2009) 007 [arXiv:0811.4622] [INSPIRE].

[2] J. Bellm et al., *HERWIG 7.0/HERWIG++ 3.0 release note*, *Eur. Phys. J.* **C 76** (2016) 196 [arXiv:1512.01178] [INSPIRE].

[3] T. Sjöstrand et al., *An introduction to PYTHIA 8.2*, *Comput. Phys. Commun.* **191** (2015) 159 [arXiv:1410.3012] [INSPIRE].

[4] T. Pierog et al., *EPOS LHC: test of collective hadronization with data measured at the CERN Large Hadron Collider*, *Phys. Rev.* **C 92** (2015) 034906 [arXiv:1306.0121] [INSPIRE].

[5] Z.-W. Lin et al., *A multi-phase transport model for relativistic heavy ion collisions*, *Phys. Rev.* **C 72** (2005) 064901 [nucl-th/0411110] [INSPIRE].

[6] X.-N. Wang and M. Gyulassy, *HIJING: a Monte Carlo model for multiple jet production in pp, pA and AA collisions*, *Phys. Rev.* **D 44** (1991) 3501 [INSPIRE].

[7] ALICE collaboration, *Enhanced production of multi-strange hadrons in high-multiplicity proton-proton collisions*, *Nature Phys.* **13** (2017) 535 [arXiv:1606.07424] [INSPIRE].

[8] CMS collaboration, *Evidence for collectivity in pp collisions at the LHC*, *Phys. Lett.* **B 765** (2017) 193 [arXiv:1606.06198] [INSPIRE].

[9] C. Bierlich, G. Gustafson and L. Lönnblad, *Diffractive and non-diffractive wounded nucleons and final states in pA collisions*, *JHEP* **10** (2016) 139 [arXiv:1607.04434] [INSPIRE].

[10] Y. Hatta et al., *Diffusive scaling and the high-energy limit of deep inelastic scattering in QCD at large N_c*, *Nucl. Phys.* **A 773** (2006) 95 [hep-ph/0601150] [INSPIRE].

[11] E. Avsar, G. Gustafson and L. Lönnblad, *Small-x dipole evolution beyond the large-N_c imit*, *JHEP* **01** (2007) 012 [hep-ph/0610157] [INSPIRE].

[12] T. Sjöstrand and M. van Zijl, *A multiple interaction model for the event structure in hadron collisions*, *Phys. Rev.* **D 36** (1987) 2019 [INSPIRE].

[13] G. Ingelman and P.E. Schlein, *Jet structure in high mass diffractive scattering*, *Phys. Lett.* **B 152** (1985) 256.

[14] W. Broniowski, M. Rybczynski and P. Bozek, *GLISSANDO: Glauber initial-state simulation and more..*, *Comput. Phys. Commun.* **180** (2009) 69 [arXiv:0710.5731] [INSPIRE].

[19] This will actually not give the correct double diffraction cross section, but as we are mainly concerned with the number of wounded nucleons, we postpone the detailed treatment of double diffraction to future improvements.

JHEP10(2018)134

[15] M. Rybczynski, G. Stefanek, W. Broniowski and P. Bozek, *GLISSANDO 2: GLauber Initial-State Simulation AND mOre..., ver. 2*, *Comput. Phys. Commun.* **185** (2014) 1759 [arXiv:1310.5475] [INSPIRE].

[16] M. Alvioli, H.J. Drescher and M. Strikman, *A Monte Carlo generator of nucleon configurations in complex nuclei including Nucleon-Nucleon correlations*, *Phys. Lett.* **B 680** (2009) 225 [arXiv:0905.2670] [INSPIRE].

[17] M. Alvioli, H. Holopainen, K.J. Eskola and M. Strikman, *Initial state anisotropies and their uncertainties in ultrarelativistic heavy-ion collisions from the Monte Carlo Glauber model*, *Phys. Rev.* **C 85** (2012) 034902 [arXiv:1112.5306] [INSPIRE].

[18] R.J. Glauber, *Cross-sections in deuterium at high-energies*, *Phys. Rev.* **100** (1955) 242 [INSPIRE].

[19] M.L. Miller, K. Reygers, S.J. Sanders and P. Steinberg, *Glauber modeling in high energy nuclear collisions*, *Ann. Rev. Nucl. Part. Sci.* **57** (2007) 205 [nucl-ex/0701025] [INSPIRE].

[20] V.N. Gribov, *Glauber corrections and the interaction between high-energy hadrons and nuclei*, *Sov. Phys. JETP* **29** (1969) 483 [INSPIRE].

[21] H. Heiselberg et al., *Color transparency, color opacity and fluctuations in nuclear collisions*, *Phys. Rev. Lett.* **67** (1991) 2946 [INSPIRE].

[22] B. Blaettel et al., *Hadronic cross-section fluctuations*, *Phys. Rev.* **D 47** (1993) 2761 [INSPIRE].

[23] M. Alvioli and M. Strikman, *Color fluctuation effects in proton-nucleus collisions*, *Phys. Lett.* **B 722** (2013) 347 [arXiv:1301.0728] [INSPIRE].

[24] M. Alvioli, L. Frankfurt, V. Guzey and M. Strikman, *Revealing "flickering" of the interaction strength in pA collisions at the CERN LHC*, *Phys. Rev.* **C 90** (2014) 034914 [arXiv:1402.2868] [INSPIRE].

[25] M. Alvioli et al., *Evidence for x-dependent proton color fluctuations in pA collisions at the CERN Large Hadron Collider*, *Phys. Rev.* **C 93** (2016) 011902 [arXiv:1409.7381] [INSPIRE].

[26] ATLAS collaboration, *Measurement of the centrality dependence of the charged-particle pseudorapidity distribution in proton–lead collisions at* $\sqrt{s_{NN}} = 5.02$ *TeV with the ATLAS detector*, *Eur. Phys. J.* **C 76** (2016) 199 [arXiv:1508.00848] [INSPIRE].

[27] ALICE collaboration, *Centrality dependence of particle production in p-Pb collisions at* $\sqrt{s_{\rm NN}} = 5.02$ *TeV*, *Phys. Rev.* **C 91** (2015) 064905 [arXiv:1412.6828] [INSPIRE].

[28] B. Andersson, G. Gustafson and B. Nilsson-Almqvist, *A model for low* p_T *hadronic reactions, with generalizations to hadron-nucleus and nucleus-nucleus collisions*, *Nucl. Phys.* **B 281** (1987) 289 [INSPIRE].

[29] H. Pi, *An event generator for interactions between hadrons and nuclei: FRITIOF version 7.0*, *Comput. Phys. Commun.* **71** (1992) 173 [INSPIRE].

[30] A. Bialas, M. Bleszynski and W. Czyz, *Multiplicity distributions in nucleus-nucleus collisions at high-energies*, *Nucl. Phys.* **B 111** (1976) 461 [INSPIRE].

[31] A. Bialas and W. Czyz, *Wounded nucleon model and Deuteron-Gold collisions at RHIC*, *Acta Phys. Polon.* **B 36** (2005) 905 [hep-ph/0410265] [INSPIRE].

[32] C. Bierlich and J.R. Christiansen, *Effects of color reconnection on hadron flavor observables*, *Phys. Rev.* **D 92** (2015) 094010 [arXiv:1507.02091] [INSPIRE].

JHEP10(2018)134

[33] C. Bierlich, G. Gustafson, L. Lönnblad and A. Tarasov, *Effects of overlapping strings in pp collisions*, *JHEP* **03** (2015) 148 [arXiv:1412.6259] [INSPIRE].

[34] C. Bierlich, G. Gustafson and L. Lönnblad, *Collectivity without plasma in hadronic collisions*, *Phys. Lett.* **B 779** (2018) 58 [arXiv:1710.09725] [INSPIRE].

[35] M.L. Good and W.D. Walker, *Diffraction dissociation of beam particles*, *Phys. Rev.* **120** (1960) 1857 [INSPIRE].

[36] A.H. Mueller, *Soft gluons in the infinite momentum wave function and the BFKL Pomeron*, *Nucl. Phys.* **B 415** (1994) 373 [INSPIRE].

[37] A.H. Mueller and B. Patel, *Single and double BFKL Pomeron exchange and a dipole picture of high-energy hard processes*, *Nucl. Phys.* **B 425** (1994) 471 [hep-ph/9403256] [INSPIRE].

[38] E. Avsar, G. Gustafson and L. Lönnblad, *Energy conservation and saturation in small-x evolution*, *JHEP* **07** (2005) 062 [hep-ph/0503181] [INSPIRE].

[39] C. Flensburg, G. Gustafson and L. Lönnblad, *Inclusive and exclusive observables from dipoles in high energy collisions*, *JHEP* **08** (2011) 103 [arXiv:1103.4321] [INSPIRE].

[40] E. Iancu, A.H. Mueller and S. Munier, *Universal behavior of QCD amplitudes at high energy from general tools of statistical physics*, *Phys. Lett.* **B 606** (2005) 342 [hep-ph/0410018] [INSPIRE].

[41] G.A. Schuler and T. Sjöstrand, *Hadronic diffractive cross-sections and the rise of the total cross-section*, *Phys. Rev.* **D 49** (1994) 2257 [INSPIRE].

[42] A. Donnachie and P.V. Landshoff, *Total cross-sections*, *Phys. Lett.* **B 296** (1992) 227 [hep-ph/9209205] [INSPIRE].

[43] C.O. Rasmussen and T. Sjöstrand, *Models for total, elastic and diffractive cross sections*, *Eur. Phys. J.* **C 78** (2018) 461 [arXiv:1804.10373] [INSPIRE].

[44] M. Barej, A. Bzdak and P. Gutowski, *Wounded-quark emission function at the top energy available at the BNL Relativistic Heavy Ion Collider*, *Phys. Rev.* **C 97** (2018) 034901 [arXiv:1712.02618] [INSPIRE].

[45] CMS collaboration, *Study of jet quenching with $Z+jet$ correlations in PbPb and pp Collisions at $\sqrt{s_{NN}} = 5.02$ TeV*, *Phys. Rev. Lett.* **119** (2017) 082301 [arXiv:1702.01060] [INSPIRE].

[46] CMS collaboration, *Observation of top quark production in proton-nucleus collisions*, *Phys. Rev. Lett.* **119** (2017) 242001 [arXiv:1709.07411] [INSPIRE].

[47] C.M. Tarbert et al., *Neutron skin of ^{208}Pb from coherent pion photoproduction*, *Phys. Rev. Lett.* **112** (2014) 242502 [arXiv:1311.0168] [INSPIRE].

[48] I. Helenius, H. Paukkunen and K.J. Eskola, *Neutron-skin effect in direct-photon and charged hadron-production in Pb+Pb collisions at the LHC*, *Eur. Phys. J.* **C 77** (2017) 148 [arXiv:1606.06910] [INSPIRE].

[49] H. Paukkunen, *Neutron skin and centrality classification in high-energy heavy-ion collisions at the LHC*, *Phys. Lett.* **B 745** (2015) 73 [arXiv:1503.02448] [INSPIRE].

[50] C. Loizides, J. Kamin and D. d'Enterria, *Improved Monte Carlo Glauber predictions at present and future nuclear colliders*, *Phys. Rev.* **C 97** (2018) 054910 [arXiv:1710.07098] [INSPIRE].

JHEP10(2018)134

[51] ATLAS collaboration, *Charged-particle multiplicities in pp interactions measured with the ATLAS detector at the LHC*, *New J. Phys.* **13** (2011) 053033 [arXiv:1012.5104] [INSPIRE].

[52] A. Buckley et al., *Rivet user manual*, *Comput. Phys. Commun.* **184** (2013) 2803 [arXiv:1003.0694] [INSPIRE].

[53] ALICE collaboration, *Centrality dependence of the charged-particle multiplicity density at mid-rapidity in Pb-Pb collisions at* $\sqrt{s_{NN}} = 2.76$ *TeV*, *Phys. Rev. Lett.* **106** (2011) 032301 [arXiv:1012.1657] [INSPIRE].

[54] ALICE collaboration, *The ALICE definition of primary particles*, ALICE-PUBLIC-2017-005 (2017).

[55] ALICE collaboration, *Centrality and pseudorapidity dependence of the charged-particle multiplicity density in Xe-Xe collisions at* $\sqrt{s_{NN}} = 5.44$ *TeV*, arXiv:1805.04432 [INSPIRE].

[56] ALICE collaboration, *Centrality dependence of the pseudorapidity density distribution for charged particles in Pb-Pb collisions at* $\sqrt{s_{NN}} = 2.76$ *TeV*, *Phys. Lett.* **B 726** (2013) 610 [arXiv:1304.0347] [INSPIRE].

[57] ALICE collaboration, *Centrality evolution of the charged-particle pseudorapidity density over a broad pseudorapidity range in Pb-Pb collisions at* $\sqrt{s_{NN}} = 2.76$ *TeV*, *Phys. Lett.* **B 754** (2016) 373 [arXiv:1509.07299] [INSPIRE].

[58] ALICE collaboration, *Centrality dependence of the pseudorapidity density distribution for charged particles in Pb-Pb collisions at* $\sqrt{s_{NN}} = 5.02$ *TeV*, *Phys. Lett.* **B 772** (2017) 567 [arXiv:1612.08966] [INSPIRE].

[59] ATLAS collaboration, *Measurement of charged-particle spectra in Pb+Pb collisions at* $\sqrt{s_{NN}} = 2.76$ *TeV with the ATLAS detector at the LHC*, *JHEP* **09** (2015) 050 [arXiv:1504.04337] [INSPIRE].

[60] Y. Zhou, X. Zhu, P. Li and H. Song, *Investigation of possible hadronic flow in* $\sqrt{s_{NN}} = 5.02$ *TeV* $p-Pb$ *collisions*, *Phys. Rev.* **C 91** (2015) 064908 [arXiv:1503.06986] [INSPIRE].

[61] A. Bilandzic, R. Snellings and S. Voloshin, *Flow analysis with cumulants: direct calculations*, *Phys. Rev.* **C 83** (2011) 044913 [arXiv:1010.0233] [INSPIRE].

[62] A. Bilandzic et al., *Generic framework for anisotropic flow analyses with multiparticle azimuthal correlations*, *Phys. Rev.* **C 89** (2014) 064904 [arXiv:1312.3572] [INSPIRE].

[63] CMS collaboration, *Measurement of the elliptic anisotropy of charged particles produced in PbPb collisions at* $\sqrt{s}_{NN} = 2.76$ *TeV*, *Phys. Rev.* **C 87** (2013) 014902 [arXiv:1204.1409] [INSPIRE].

[64] ALICE collaboration, *Higher harmonic anisotropic flow measurements of charged particles in Pb-Pb collisions at* $\sqrt{s_{NN}} = 2.76$ *TeV*, *Phys. Rev. Lett.* **107** (2011) 032301 [arXiv:1105.3865] [INSPIRE].

[65] ALICE collaboration, *Anisotropic flow of charged particles in Pb-Pb collisions at* $\sqrt{s_{NN}} = 5.02$ *TeV*, *Phys. Rev. Lett.* **116** (2016) 132302 [arXiv:1602.01119] [INSPIRE].

[66] C. Bierlich, G. Gustafson and L. Lönnblad, *A shoving model for collectivity in hadronic collisions*, arXiv:1612.05132 [INSPIRE].

[67] E. Gotsman, E. Levin and U. Maor, *A comprehensive model of soft interactions in the LHC era*, *Int. J. Mod. Phys.* **A 30** (2015) 1542005 [arXiv:1403.4531] [INSPIRE].

JHEP10(2018)134

[68] V.A. Khoze, A.D. Martin and M.G. Ryskin, *Elastic scattering and Diffractive dissociation in the light of LHC data*, *Int. J. Mod. Phys.* **A 30** (2015) 1542004 [arXiv:1402.2778] [INSPIRE].

[69] S. Ostapchenko, *Monte Carlo treatment of hadronic interactions in enhanced Pomeron scheme: I. QGSJET-II model*, *Phys. Rev.* **D 83** (2011) 014018 [arXiv:1010.1869] [INSPIRE].

[70] ATLAS collaboration, *Rapidity gap cross sections measured with the ATLAS detector in pp collisions at* $\sqrt{s} = 7$ *TeV*, *Eur. Phys. J.* **C 72** (2012) 1926 [arXiv:1201.2808] [INSPIRE].

[71] CMS collaboration, *Measurement of diffraction dissociation cross sections in pp collisions at* $\sqrt{s} = 7$ *TeV*, *Phys. Rev.* **D 92** (2015) 012003 [arXiv:1503.08689] [INSPIRE].

[72] G.G. Barnaföldi et al., *First results with HIJING++ in high-energy heavy-ion collisions*, *Nucl. Part. Phys. Proc.* **289-290** (2017) 373 [arXiv:1701.08496] [INSPIRE].

[73] B. Andersson, G. Gustafson and H. Pi, *FRITIOF extended*, in the proceedings of 27th *Rencontres de Moriond, Perturbative QCD and hadronic interactions*, March 22–28, Les Arcs, France (1992).

[74] B. Andersson, G. Gustafson, L. Lönnblad and U. Pettersson, *Coherence effects in deep inelastic scattering*, *Z. Phys.* **C 43** (1989) 625 [INSPIRE].

[75] L. Lönnblad, *ARIADNE version 4: a program for simulation of QCD cascades implementing the color dipole model*, *Comput. Phys. Commun.* **71** (1992) 15 [INSPIRE].

[76] H.J. Drescher et al., *Parton based Gribov-Regge theory*, *Phys. Rept.* **350** (2001) 93 [hep-ph/0007198] [INSPIRE].

[77] K. Werner et al., *Event-by-event simulation of the three-dimensional hydrodynamic evolution from flux tube initial conditions in ultrarelativistic heavy ion collisions*, *Phys. Rev.* **C 82** (2010) 044904 [arXiv:1004.0805] [INSPIRE].

[78] K. Werner, B. Guiot, I. Karpenko and T. Pierog, *Analysing radial flow features in p-Pb and p-p collisions at several TeV by studying identified particle production in EPOS3*, *Phys. Rev.* **C 89** (2014) 064903 [arXiv:1312.1233] [INSPIRE].

[79] C. Bierlich, *Rope hadronization and strange particle production*, *EPJ Web Conf.* **171** (2018) 14003 [arXiv:1710.04464] [INSPIRE].

JHEP10(2018)134